

The following revised manuscript is based on two reviewers' comments during two iterations. The red shades are revisions, adjustments and corrections based on the comments of Reviewer #1 and the blue shades are based on the comments of Reviewer #2.

First iteration: Major revision

Response to Reviewer #1:

(1) Reviewer Comment:

I suggest to provide more context / justification / details about the calibration procedure – for example, how do you make sure your calibrated best-fits were not local best-fits but globe ones. The best-fit results of different implementations (such as IM-SAS-L and IM-SAS-D) were similar, but that does not mean the modelled results such as MTT was true. This generally requires an analysis of the potential uncertainty. While I understand a full uncertainty analysis may be unfeasible, the impact of choices done in the calibration need to be better discussed.

Reply:

We completely agree with this point. We have therefore done an uncertainty analysis to quantify the effects of parameter uncertainty on the modelled TTDs by randomly sampling from the posterior parameter distributions for both, IM-SAS-L and IM-SAS-D models. While parameter uncertainty can cause some variability in TTDs and thus in the actual magnitudes of water ages, this variability is consistently within similar age ranges for ^{18}O and ^3H , respectively. It does therefore not affect the overall interpretation of the results and the rejection of the hypothesis that ^{18}O underestimates water ages, as shown for scenarios 19-21 in Figure FR1 here below. We will add these results in the revised manuscript. (In the track-changed revised manuscript: Table 7)

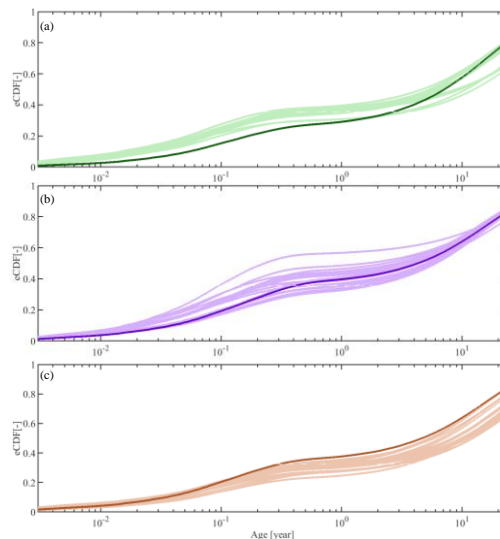


Figure FR1. Stream flow TTDs derived from the 6 model scenarios based on IM-SAS models with the different associated calibration strategies (scenarios 10-12). Each line represents the volume weighted average daily TTDs during the modelling period 01/10/2001 – 31/12/2016, generated from parameters randomly sampled from the posterior distribution (light shades) and the most balanced solution of each scenario (dark shades). (a) TTDs inferred from $\delta^{18}\text{O}$ in scenario 19; (b) TTDs inferred from ^3H in scenario 20; (c) The TTDs inferred from combined $\delta^{18}\text{O}$ and ^3H in scenario 21.

(2) Reviewer Comment:

I do agree with the authors that the ^3H and $\delta^{18}\text{O}$ tracers both are informative for the flow systems, what is needed is just a model good enough to resolve such information in a meaningful way. Especially for the catchments with strong seasonality. However, I am not sure if the model has to use combined data sets of hydrological and tracer as the author argued that “only the combined information using hydrological and tracer data and the consideration of transient flow conditions gives similar MTT, independent of the used tracer”. I think the important thing is that the flow model can represent the reality in a good way, such that the tracer transport can be well reproduced. Using hydrological data in calibration may not a key control for that.

Reply:

We agree with this point. We will therefore reformulate that sentence on P.20, l.620, “only the combined information using hydrological and tracer data and the consideration of transient flow conditions gives similar MTT, independent of the used tracer” in the revised manuscript so that it better reflects that point. (In the track-changed revised manuscript: P.22, l.685ff)

(3) Reviewer Comment:

Line 160: What are E_p and P ?

Reply:

Thank you for pointing this out. While E_p represents potential evaporation, P represents precipitation. We will add the definitions in the revised manuscript. (In the track-changed revised manuscript: P.6, l.165ff)

(4) Reviewer Comment:

Line 368: perhaps say that the storage component is just locally full-mixed and those local full mixtures do not lead to an overall fully mixed system

Reply:

We completely agree with this suggestion. It was mentioned on P.12, L.368ff, but we will make it clearer in the revised manuscript. (In the track-changed revised manuscript: P.13, l.405ff)

(5) Reviewer Comment:

I don't think that to reduce computational time and computer memory requirements is good reason for using uniform SAS functions rather than other shapes of SAS function. I think the right way should be describing the model of reduced complexity (parameters) was already enough for your modelling targets.

Reply:

We agree with the argument that reduced complexity here already allows to draw robust conclusions. We will reformulate the statement and add this aspect. However, we would also like to explicitly re-iterate here that computational capacity imposes major practical obstacles to testing other SAS function shapes: in contrast to uniform distributions, the sampling process then requires an explicit generation of RTDs and TTDs for each time step and to “carry” all RTDs and TTDs of all model components through the entire model period, including the warm-up period (here: 46 years). This entails for a daily modelling time-step the simultaneous handling of multiple matrices > 16.800x16.800 elements in floating number format (i.e. 8B each), which corresponds to >2 GB/matrix. With a working memory of common but good computers (i.e. 16-32 GB) this means that the generation of RTDs and TTDs alone will use (if not exceed) the memory of these computers, not to speak of other processes required.

(6) Reviewer Comment:

Line 378: could you explain in more detail how was the tracer sampled from the passive and active volumes? Also random sampling from $S_{s,tot}$?

Reply:

The tracer and age composition of that outflow is indeed randomly sampled from the total groundwater storage volume $S_{s,tot}$. We will clarify this in the revised manuscript. (In the track-changed revised manuscript: P.14, l.420ff)

(7) Reviewer Comment:

Line 393-395: maybe simply say the lumped implementation used a single HUR to represent the entire basin. Is that what you mean? In this case the precipitation zones were not used any more, right? Maybe clarify this.

Reply:

Indeed, the lumped implementation used a single HRU (equivalent to the forest HRU described in distributed model, Fig.2) to represent the entire catchment and the precipitation zones were not used any more in this lumped case. We will clarify this in the revised manuscript. (In the track-changed revised manuscript: P.14, l.438ff)

(8) Reviewer Comment:

Equation 14: what are $E_{mse,Q,n}$ and $E_{mse,tracer,m}$?

Reply:

Thank you for pointing this out. We will add the missing definitions in the revised manuscript. (In the track-changed revised manuscript: P.16, l.483ff)

(9) Reviewer Comment:

Line 473: it looks like that when using all the data, the lumped model (scenario 9) was even better than the distributed model (scenario 12) that has more parameters, does that mean the high model complexity is not essential for a better model performance in your case, could you clarify that.

Reply:

This is an interesting aspect. However, while the distributed implementation IM-SAS-D can indeed not be considered to outperform the lumped IM-SAS-L implementation, the opposite cannot be concluded either: as can be seen in Table 4, considering the most balanced solution, some signatures were indeed captured better by IM-SAS-L than by IM-SAS-D. Yet, others were much better reproduced by IM-SAS-D. In addition, it can be seen that the full set of pareto front solutions of IM-SAS-L includes a considerable number with poorer performance metrics (i.e. upper limit of performance ranges shown in Table S5 in the Supplementary Material).

(10) Reviewer Comment:

Line 508: Table 3?

Reply:

Indeed. We will correct that.

Response to Reviewer #2:

(1) Reviewer Comment:

The study fits the scope of HESS and makes a valuable contribution to the field of transit time modelling and tracer hydrology. Illustrating the capacity of stable water isotopes to quantify older water will open up new opportunities for TT modelling in catchments that are assumed to show comparably large MTTs. Hence, I support the general motivation and objectives of the study.

Reply:

We highly appreciate this positive overall assessment of our work and we thank the reviewer for her interest in our work as well as for the thoughtful and detailed comments that helped to strengthen our analysis. Below, we provide clarifications and our perspectives to respond in detail to the individual reviewer comments.

(2) Reviewer Comment:

First, I am not sure whether a catchment (river basin) of 13,000 km² with at the same time limited availability of tracer data is the best choice for the study objectives. While individual controls on TTs remains largely elusive, it has been shown that TTs (or their metrics) vary widely depending on catchment characteristics such as elevation, topography or climate (e.g., Jasecko et al., 2016, Kumar et al., 2020). Modelling TTs in a river basin that shows a gradient of more than 800 mm yr⁻¹ in annual precipitation, an elevation gradient of around 900 meters and varying land use types adds a lot of complexity that could have been avoided when using a much smaller and more homogeneous catchment. At the same time, the study relies on only one precipitation station for both stable water isotopes and tritium (within the basin) providing monthly composite samples. Hence, the tracer data are rather sparse both temporally and spatially, which adds another layer of uncertainty to the modelling. An alternative might be to compile data from previous TT modelling approaches that have been conducted in smaller catchments with more highly-resolved (space and/or time) stable water isotope and tritium data (e.g., Rodriguez et al., 2021 – reference already in manuscript).

Reply:

Choice of study region

We agree that it remains a defining challenge in hydrology to fully account for heterogeneities in larger systems. Unfortunately, there is no “silver bullet” to solve that problem. This is also explicitly discussed in the Discussion section of our manuscript (p.21, l.658ff). While we share the reviewer’s view that studies at smaller scales are very important, these types of studies typically suffer from other limitations. Specifically for the case of stable isotope and tritium comparisons and apart from the fact that there are hardly any catchments world-wide in which data for both tracers are available, the study cited by the Reviewer (Rodriguez et al., 2021) is indeed conducted in a smaller catchment with higher tracer sampling frequency. *However*, and as explicitly mentioned in the manuscript (p.4, l.132-150), it relies on much shorter time series, i.e. 2 years, and only a handful of tritium

samples, i.e. 24. In addition, conclusions from that study on the ability of stable isotopes to see older water may be hampered by the potential *absence* of older water. In other words, if there is no older water present in a catchment, stable isotopes can also not see it, as recently pointed out by Stewart et al. (2021). We therefore believe, that in spite of potential uncertainties arising from the size of the system, our study allows us to explore aspects of the research question that could not (or not fully) be addressed by Rodriguez et al. (2021).

Role of heterogeneity for older water ages – catchment as low-pass filter

It is also important to note that in our study we are mostly interested in older water ages. As catchments act as low-pass filters, they already smooth out much of short time-scale and small spatial-scale hydro-climatic variability. The remaining higher-frequency components in the response, e.g. responses to individual rain events, then mostly affect water ages at the younger side of the spectrum. These can indeed be sensitive to spatial-temporal heterogeneities. In contrast, older water ages are mostly controlled by low frequency components of the system and thus variabilities at much larger spatial and longer temporal scales, e.g. seasonal or inter-annual changes in groundwater tables, and are thus much less sensitive to small-scale heterogeneities. This can for example be seen in the significant differences between the power spectra of stream tracer concentrations of fast responding parts of the system (i.e. short time-scales, high-frequency components and thus younger water ages) and groundwater tracer concentrations (i.e. much longer time-scales, low-frequency components of the system and older water ages), as for example demonstrated by Hrachowitz et al. (2015; Figure 8 therein) and which define the recurrently described, very characteristic $1/f$ scaling of stream tracer responses across many system in contrasting environmental settings across the world (e.g. Kirchner et al., 2001; Godsey et al., 2009; Hrachowitz et al., 2009; Aubert et al., 2013; Kirchner and Neal, 2013). Another piece of evidence for the lower sensitivity of older water to heterogeneity is the higher sensitivity of high-frequency components and younger water ages to hydro-climatic variability (e.g. Figure 9 in our original manuscript) as compared to the almost complete lack sensitivity to hydro-climatic in low-frequency components and thus older water (e.g. Figure 10), which has also been reported in many other studies (e.g. Hrachowitz et al., 2013, 2015; Soulsby et al., 2016). Overall, this means that while the pattern and dynamics of young water ages may indeed to some degree be affected by heterogeneities within our study basin, it is plausible to assume that they have only minor impact on the estimation of older water ages.

Spatial representation of hydro-climatic and tracer input heterogeneity in the study

Notwithstanding the above and to limit adverse effects of a coarser data resolution, we here invested considerable effort into spatial adjustments of hydro-meteorological input data as well as tracer data, according to the best available information in our distributed model implementation. While the major spatial differences in precipitation are accounted for by the identification and use of four individual precipitation zones, major spatial differences in temperature (and thus also in EP) are accounted for by the additional stratification into 100m elevation zones as described in Sections 3.2.1 and 4.2.2. Similarly and more importantly, the tracer input signals were spatially adjusted, as described in Sections 3.2.2 and 3.2.3 as well as in the Supplement, following the

method recently developed by Allan et al. (2018, 2019). This method identified strong relationships between multiple catchment characteristics and seasonal stable isotope signals in precipitation. These relationships thus allow a robust estimation of the spatial differences in stable isotope input, both globally (Allan et al., 2019) and perhaps more importantly, also regionally, as demonstrated in Allan et al. (2018) who quantified spatial stable isotope input for Switzerland, which is just across the border from our study basin in Southern Germany. A comparable approach was applied for precipitation tritium concentrations, which in any case do not exhibit major spatial differences (e.g. Schmidt et al., 2020). The same applies also to water stable isotopes in precipitation for monthly sampling resolution as indicated by the similarity to isotopes for stations close by, i.e. Karlsruhe (Stumpp et al. 2014).

Ability of the model to represent the response and spatial heterogeneity therein

To reduce the potential of misrepresentations of the system and its heterogeneities by the model we have deliberately chosen to expose the model to a rigorous calibration and post-calibration evaluation procedure that goes far beyond what is done in the vast majority of studies in scientific hydrology. The use of eight different performance indicators, that describe the models' ability to simultaneously reproduce distinct signatures and thus distinct aspects of the system response, allowed to identify and discard solutions that in traditional model calibration/evaluation procedures, based on one or two performance metrics, would have been falsely accepted as feasible. This leads to a robust representation of the system, as can be seen by the models' ability to relatively well and simultaneously reproduce these multiple signatures – both, in the calibration as well as and more importantly in the post-calibration evaluation ("validation") periods as illustrated by Figures 3-5 and Table 4 in the original manuscript and also illustrated here below in Figure FR1, for the example of stream flow Q in Scenario 12.

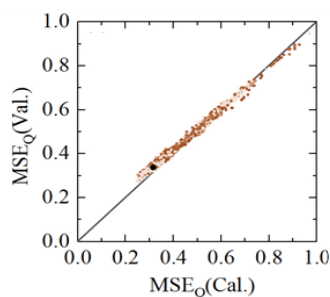


Figure FR1. Model performance of all Pareto-optimal solutions accepted as feasible against to reproduce stream flow Q in model calibration vs. model evaluation periods based on the mean squared error (MSE_Q). The dark dot indicates the most balanced Pareto-optimal solution. The fact that all solutions plot very close to the 1:1 line suggests that the model does reproduce Q in the model post-calibration evaluation period ("validation") almost as good as in the calibration period. This is a strong indicator of the model being a plausible representation of the system response.

However and in addition to the strict model evaluation procedure in our original manuscript, we have taken this concern of the reviewer very serious and decided to confront the model with additional observations to further

test its ability to meaningfully represent spatial differences in the response. To do so, we have now also evaluated the model outputs against streamflow observations in three sub-catchments (C1: Kirchentellinsfurt, C2: Calw, and C3: Untergriesheim) within the Neckar basin, whereby each one of them largely represents the response from one of the precipitation zones (Figure FR2 here below).

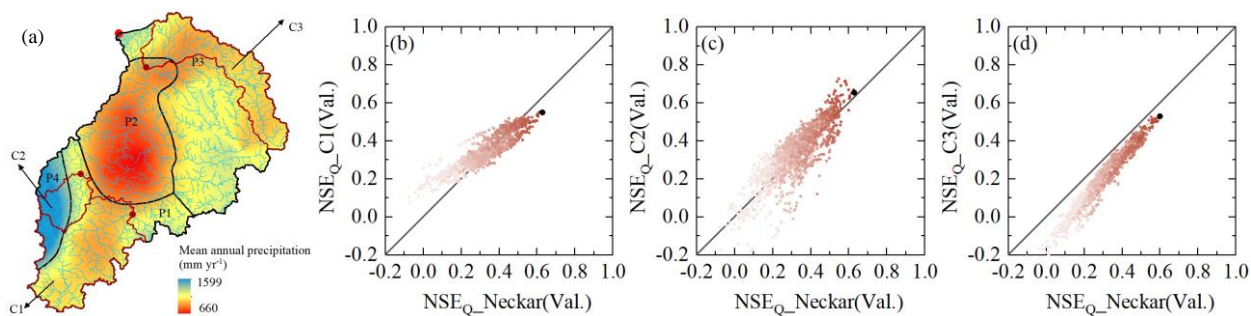


Figure FR2: (a) Sub-catchments C1 – C3 within the Neckar basin used to evaluate the model performance, (b) model performance in the Neckar basin vs. sub-catchment C1, (c) Neckar vs. C2 and (d) Neckar vs. C3, based on Scenario 10. The dots indicate all Pareto-optimal solutions in the multi-objective model performance space. The shades from dark to light indicate the overall model performance based on the Euclidean Distance D_E , with the darker solutions representing the overall better solutions (i.e. smaller D_E)

It can be seen, that the model calibrated on stream flow of the entire Neckar basin can reproduce stream flow in the 3 sub-catchments similarly well, with C1 and C2 even better reproduced with many of the solutions than the calibrated Neckar stream flow. These results suggest that the model does indeed pick up the major differences in response types due to hydro-climatic heterogeneities throughout the Neckar basin. Together with the spatial adjustments of the tracer inputs as described above, this is further evidence that the model provides an adequate representation of the major features of the hydrological response even at the larger scale of the Neckar basin and therefore also a meaningful spatial representation of the tracer circulation. We will add these additional model tests to the manuscript to better demonstrate the suitability of the model for our study.

Overall, we can and do not claim that our models generate the best possible TTD estimates. Rather, our intention in this analysis is to show the consistency between TTD estimates derived from stable isotopes and tritium, i.e. that both contain enough and comparable information which can be exploited to estimate water ages. In other words, even if TTD estimates of both tracers are subject to uncertainties, the fact that they provide similar TTD estimates when used in the same model type is evidence for a similar information content, supporting the notion that stable isotopes have indeed the potential to see older water, if used in conjunction with suitable modelling approaches. This is explicitly discussed in the text (p.19, l.600ff in the original manuscript).

(3) Reviewer Comment:

Secondly, there is a remarkably great difference in model complexities between the individual TT modelling approaches. On the one hand, simple CO models with only one compartment, no temporal/seasonal variation and two pre-defined shape parameters for the TTs have been used, while on the other hand, the SAS model consists of three hydrological response units with multiple storage volumes each, has 11 calibration parameters and is also tested in a spatially distributed implementation. As the authors are clearly aware of, time-variant concepts of CO models (see Hrachowitz et al., 2010; and references cited therein) as well as multi-compartment models representing fast and slow flow routes have been used; using especially the latter is a common approach in CO modelling. Moreover, the SAS model with its comparably large number of parameters is calibrated simultaneously to discharge and at least one of the two tracers, while the CO models are calibrated to only one tracer. I am thus wondering to what extent results from these TT models can be compared at all. I understand that the objective of this paper is not to dismiss a specific model type, but rather to analyse the flexibility of stable water isotopes as TT model tracers. However, this requires to use model setups and data similar to those used in the papers that have demonstrated the truncation of TT distributions by calibration to stable water isotopes. To address this concern, one could think of (i) focussing on a smaller (or even headwater) catchment with preferably daily tracer data, (ii) using established CO models such as the more complex ones in Stewart et al. (2010), and (iii) using measured and modelled P, ET, storage and Q data as input for SAS modelling (potentially with non-random sampling) with one or a maximum of two SAS function compartments, as commonly done in more recent SAS modelling studies (e.g., Benettin et al., 2017; Harman, 2015; Nguyen et al., 2021).

Reply:

We agree with the reviewer that the model approaches are different and we also agree that comparisons need to be consistent and systematic to be meaningful.

However, we also want to point out here – as correctly mentioned by the reviewer – that the objective of our analysis is to analyse the potential of stable isotopes to see older water and not a full-fledged comparison of different model approaches. This is explicitly stated in the research hypothesis “[...] that ^{18}O as tracer generally and systematically cannot detect tails in water age distributions and that this truncation leads to systematically younger water age estimates than the use of ^3H ” (p.5, l.151-152)

Please note that therefore what is actually compared here are models of the same type (and same complexity) run with stable isotopes and subsequently with tritium. The comparison is not made between models of different types and/or complexities. In other words, we compare water age estimates obtained from e.g. a CO model with exponential TTD run with ^{18}O with those obtained from the same model but run with ^3H . In contrast, we do not compare water ages from that CO model with ages estimated from another model, e.g. IM-SAS. This is also emphasized by the last four columns of table 5.

To further clarify, we have estimated water ages based on CO models to check if we would find differences in water ages between ^{18}O - and ^3H -based model runs in the study basin, using the same types of lumped, time-invariant models that Stewart et al. (2010) based their argument on. The fact that we found significant differences

between these estimates, would, without further analysis, further support the observation of Stewart et al. (2010) that ^{18}O generally truncates water ages.

Our intention is *not* to show that CO models are generally not capable to estimate older ages. Perhaps, time-variant implementations can do that very well, but exploring this was not the objective of our study. Also the combined use of ^{18}O and ^3H in CO models has previously been shown to be useful to estimate older ages. But this is outside the scope of our study. Instead, as clearly stated in the research hypothesis, we test if ^{18}O can generally be considered to be useless for the determination of ages older than ~ 4 years. Our results then further suggest, that, if used in combination with IM-SAS models, the hypothesis needs to be rejected, as these models produce similar water ages with ^{18}O and ^3H that are much older than 4 years. Given that the results of Stewart et al. (2010) as well as our own CO scenarios are based on lumped, time-invariant CO model implementations, our results eventually also allow the observation that the perceived failure of ^{18}O to see older ages is not a general limitation of that tracer, but rather a consequence of its use in *lumped, time-invariant* CO models.

However, we agree with the reviewer that we have not tested the more complex CO model implementations from Stewart et al. (2010) in our original manuscript. We therefore took up this advice of the reviewer and did additional model runs, with full calibrations (and evaluations) of a wider range of common time-invariant implementations of CO models, also including more complex ones. Our analysis now includes in addition to exponential (EM) and gamma (GM) models also two parallel reservoir (2EM; scenarios X1-2), three parallel reservoir (3EM; scenarios X3-4) and exponential piston flow (EPM, scenarios X5-6) implementations. The TTD estimates from these additional model implementations are consistent with those in the original analysis: for all tested lumped, time-invariant CO models, the TTDs derived from ^{18}O indicated with MTTs ~ 1 -2 yrs significantly younger water than those derived from ^3H , which suggest MTTs ~ 10 yrs throughout (see Table TR1 and Figure FR3 below). This further strengthens our previous results, suggesting that ^{18}O when used in lumped, time-invariant CO models underestimates water ages, as suggested by Stewart et al. (2010).

Table TR1. Metrics of stream flow TTDs derived from the 10 model scenarios with the different associated calibration strategies based on different CO models, where $\text{C}_{\delta^{18}\text{O}}$ indicates calibration to $\delta^{18}\text{O}$, $\text{C}_{^3\text{H}}$ calibration to ^3H . The TTD metrics represent the best fits of the respective time-invariant TTD. The water fractions are shown as the fractions of below a specific age T. The columns with absolute difference Δ illustrate the differences in TTDs from the same models calibrated to $\delta^{18}\text{O}$ and ^3H , respectively. The subscripts indicate the scenarios that are compared (e.g., $\Delta_{3,4}$ compares scenarios 3 and 4).

Scenario	3	4	5	6	X1	X2	X3	X4	X5	X6	$\Delta_{3,4}$	$\Delta_{5,6}$	$\Delta_{X1,X2}$	$\Delta_{X3,X4}$	$\Delta_{X5,X6}$
Model	CO-EM		CO-GM		CO-2EM		CO-3EM		CO-EPM		Absolute difference				
Calibration strategy \rightarrow TTD metrics \downarrow	$\text{C}_{\delta^{18}\text{O}}$	$\text{C}_{^3\text{H}}$	$\text{C}_{\delta^{18}\text{O}}$	$\text{C}_{^3\text{H}}$	$\text{C}_{\delta^{18}\text{O}}$	$\text{C}_{^3\text{H}}$	$\text{C}_{\delta^{18}\text{O}}$	$\text{C}_{^3\text{H}}$	$\text{C}_{\delta^{18}\text{O}}$	$\text{C}_{^3\text{H}}$	$\Delta\text{TT}_{\delta^{18}\text{O},^3\text{H}}$	$\Delta\text{F}(\text{T}<\text{X})_{\delta^{18}\text{O},^3\text{H}}$			
Mean (yr)	1.4	10.4	2.4	9.7	1.9	9.5	2.1	9.4	1.8	10	-9.0	-7.3	-7.6	-7.3	-8.2
10 th	0.1	1.1	<0.1	0.3	<0.1	<0.1	<0.1	0.9	1.0	1.1	-1.0	-0.2	0.0	-0.8	-0.1
25 th	0.4	3.0	0.2	1.3	0.2	0.3	0.2	2.8	1.1	2.9	-2.6	-1.1	-0.1	-2.6	-1.8
50 th (median)	1.0	7.2	1.0	5.0	1.1	3.6	1.3	7.3	1.5	7	-6.2	-4.0	-2.5	-6.0	-5.5
75 th	1.9	14.4	3.2	13.1	2.7	13.8	3.1	15.0	2.2	13.9	-12.5	-9.9	-11.1	-11.9	-11.7
90 th	3.2	26.3	6.8	25.4	4.8	27.3	5.6	25.6	3.0	23.1	-23.1	-18.6	-22.5	-20.0	-20.1
F(T<3 m)*	16	2	28	10	26	25	25	3	0	2	14	18	1	22	-2
F(T<6 m)	30	5	38	14	34	34	32	6	0	5	25	24	0	26	-5
F(T<1 yr)	51	9	50	21	47	40	44	10	13	9	42	29	7	34	4
F(T<3 yr)	88	25	74	39	78	48	74	26	90	26	63	35	30	48	64
F(T<5 yr)	97	38	85	50	91	55	88	38	99	39	59	35	36	50	60
F(T<10 yr)	100	62	95	68	99	68	98	60	100	63	38	27	31	38	37
F(T<20 yr)	100	85	100	85	100	84	100	84	100	86	15	15	16	16	14

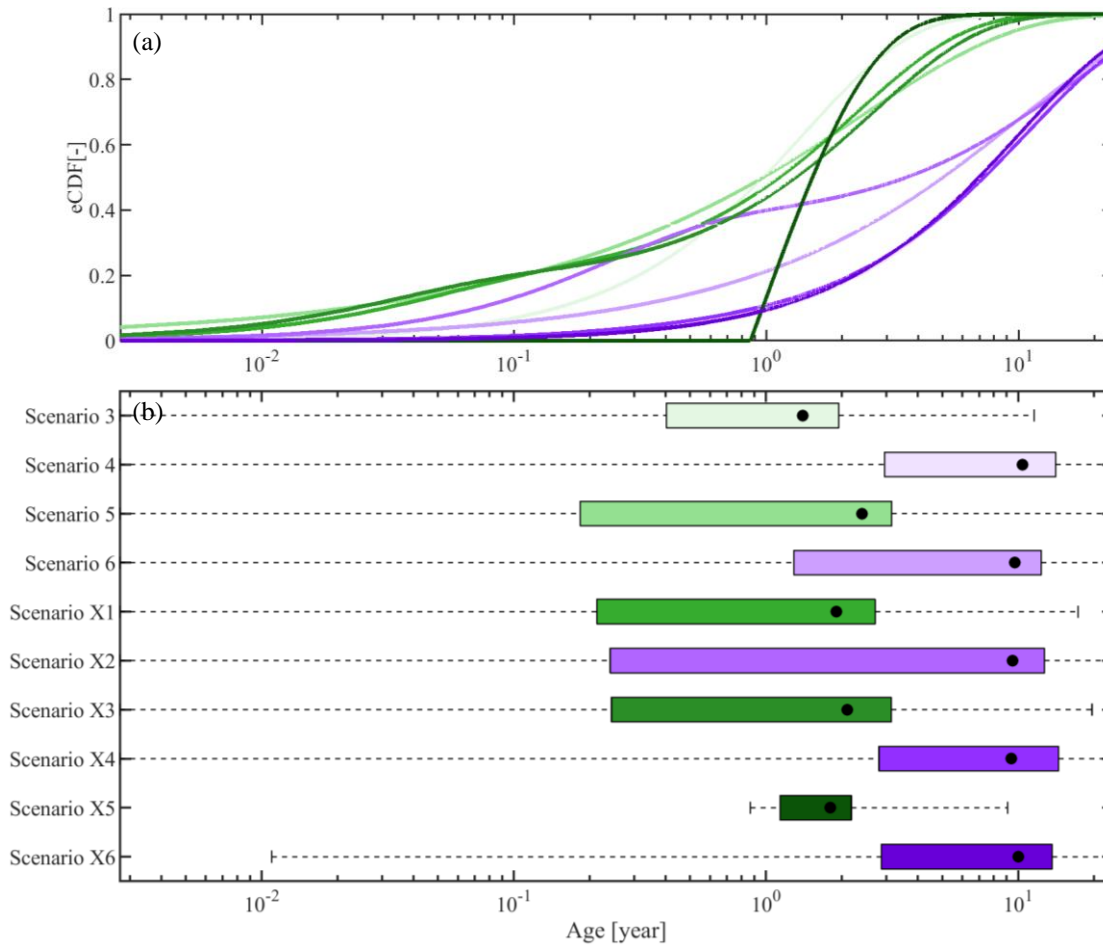


Figure FR3. Stream flow TTDs derived from the 10 model scenarios with the different associated calibration strategies based on different CO models. The TTDs represent the best fits of the respective time-invariant TTD. Green shades represent the TTDs inferred from $\delta^{18}\text{O}$ based on different CO models (from lighter to darker for scenarios 3, 5, X1, X3 and X5) in (a) and (b); the purple shades represent TTDs inferred from ^3H based on different CO models (from lighter to darker for scenario 4, 6, X2, X4 and X6); the black dots in (b) indicate the mean transit time for each model scenario.

In addition, and as requested by the reviewer, we have also included a “pure” SAS scenario (scenarios X7-9) with one compartment as described in Benettin et al. (2017), using observed Q to account for storage variations (as opposed to modelled Q in the IM-SAS implementations in scenarios 7-12) and one power-law shaped SAS function to route tracers through the system. Also, the results from this model implementation supports our original interpretation: the SAS model, similar to all other IM-SAS implementations (scenarios 7-12), provides similar TTDs for ^{18}O and ^3H . Both estimates are with MTT ~ 11 yrs also broadly consistent with the higher MTTs obtained from the other IM-SAS implementations (see Figure FR4 and Table TR2 here below).

Overall, all results and TTD estimates from additional model implementations are highly consistent with our previous results and considerably strengthen our conclusions to reject the hypothesis that stable isotopes underestimate water ages. We will add all additional model scenarios in the revised manuscript.

Table TR2. Metrics of stream flow TTDs derived from the 9 model scenarios with the different associated calibration strategies based on different SAS models, where $C_{\delta^{18}O}$ indicates calibration to $\delta^{18}O$, C^3H calibration to 3H , while $C_{\delta^{18}O,Q}$, C^3H,Q and $C_{\delta^{18}O,^3H,Q}$ indicate multi-objective, i.e. simultaneous calibration to combinations of $\delta^{18}O$, 3H and stream flow. The TTD metrics represent the mean and standard deviations of all daily streamflow TTDs during the modelling period 01/10/2001 – 31/12/2016 are given. The mean transit time was estimated by fitting Gamma distributions to the volume-weighted mean TTDs of each individual scenario. The water fractions are shown as the fractions of below a specific age T. The columns with absolute difference Δ illustrate the differences in TTDs from the same models calibrated to $\delta^{18}O$ and 3H , respectively. The subscripts indicate the scenarios that are compared (e.g., $\Delta_{7,8}$ compares scenarios 7 and 8). *Note that the fraction of water younger than 3 months is comparable to the fraction of young water as suggested by Kirchner (2016).

Scenario	7	8	9	10	11	12	X7	X8	X9	$\Delta_{7,8}$	$\Delta_{10,11}$	$\Delta_{X7,X8}$
Model	IM-SAS-L			IM-SAS-D			P-SAS			Absolute difference		
Calibration strategy → TTD metrics ↓	$C_{\delta^{18}O,Q}$	C^3H,Q	$C_{\delta^{18}O,^3H,Q}$	$C_{\delta^{18}O,Q}$	C^3H,Q	$C_{\delta^{18}O,^3H,Q}$	$C_{\delta^{18}O}$	C^3H	$C_{\delta^{18}O,^3H}$	$\Delta TT_{\delta^{18}O,^3H}$	$\Delta F(T<X)_{\delta^{18}O,^3H}$	
Mean (yr)	17.4	11.9	11.2	15.6	13.2	12.8	11.4	11.0	11.0	5.5	2.4	0.4
10 th	0.5±0.7	0.5±0.8	0.4±0.6	0.3±0.5	0.3±0.5	0.3±0.4	0.04±0.03	0.02±0.02	0.02±0.02	0.0	0.0	0.02
25 th	2.1±2.1	1.9±2.1	1.5±1.8	2.1±1.7	1.5±1.7	1.4±1.5	0.4±0.1	0.2±0.1	0.2±0.1	0.2	0.6	0.2
50 th (median)	9.0±3.3	6.5±4.8	5.7±4.3	8.6±2.6	6.7±3.7	6.6±3.5	3.2±0.2	2.4±0.2	2.5±0.2	2.5	1.9	0.7
75 th	22.2±3.3	17.6±6.5	16.3±6.2	20.8±2.8	18.8±4.6	17.8±4.2	13.7±0.3	12.5±0.4	12.5±0.3	4.6	2.0	1.2
90 th	31.3±4.3	29.2±5.0	28.6±5.1	31.1±4.2	30.4±4.3	29.9±4.2	33.4±0.4	33.4±0.4	32.7±0.2	2.1	0.7	0.0
F(T<3 m)*	18±12	23±19	21±15	16±10	22±13	23±15	22±3	26±3	26±2	-5	-6	-5
F(T<6 m)	21±13	29±22	30±19	20±11	27±16	27±16	27±2	32±2	32±2	-8	-7	-5
F(T<1 yr)	24±13	32±22	35±21	22±11	30±16	29±15	34±2	39±2	39±1	-8	-8	-5
F(T<3 yr)	31±11	39±20	42±19	30±10	37±14	37±14	49±1	53±1	52±1	-8	-7	-4
F(T<5 yr)	38±10	46±18	49±17	38±9	44±13	44±12	57±1	60±1	60±1	-8	-6	-3
F(T<10 yr)	52±8	59±13	62±12	53±7	58±10	58±9	69±1	71±1	71±1	-7	-5	-2
F(T<20 yr)	71±5	77±7	79±7	74±4	76±5	77±5	82±0	83±0	83±0	-6	-2	-1

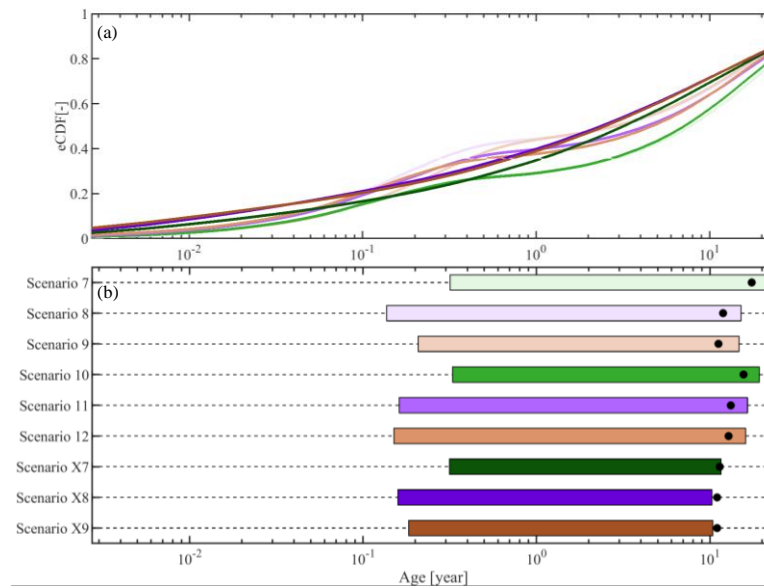


Figure FR4. Stream flow TTDs derived from the 9 model scenarios with the different associated calibration strategies based on different SAS models (i.e., scenarios 7-9 based on model IM-SAS-L, scenarios 10-12 based on model IM-SAS-D, scenarios X7-X9 based on model P-SAS which is same as that described in Benettin et al. (2017)). The TTDs represent the volume weighted average daily TTDs during the modelling period 01/10/2001 – 31/12/2016 are given. Green shades represent the TTDs inferred from $\delta^{18}O$ based on different SAS models (from lighter to darker for scenario 7, 10, X7) in (a) and (b); the purple shades represent TTDs inferred from 3H based on different models (from lighter to darker for scenario 8, 11, X8), the brown lines represent TTDs inferred from combined $\delta^{18}O$ and 3H based on different models (brown shades from lighter to darker for scenario 9, 12, X9); the black dots in (b) indicate the mean transit time for each model scenario. Note that the mean transit time was estimated by fitting Gamma distributions to the volume-weighted mean TTDs of each individual scenario.

(4) Reviewer Comment:

Thirdly, the fact that spatial aggregation introduces bias in CO model-based MTTs, as stated also by the authors, raises the question to what extent comparison of MTT estimates is meaningful. I understand that the authors would like to test the validity of stable water isotopes in TT modelling particularly of older water ages, and that MTT has been a metric commonly reported for CO models. Nonetheless, according to Kirchner (2016 – reference already in manuscript), sine-wave fitting to seasonal isotope data does give robust estimates of the young water fraction F_{yw} . Hence, it might be more meaningful to compare F_{yw} estimates by the different TT model approaches, or, even better, to add this as further TT metric in the comparison.

Reply:

We agree, that MTT estimates from stable isotopes may be less robust than previously assumed *if* they are estimated using CO-type of models and *if* there is a large contrast in MTTs from sub-parts of the system (which we do not know in reality), as demonstrated by Kirchner (2016). This, however, can at this point not (yet) be generalized as it does not imply that MTT estimates obtained from different model approaches and/or systems with little internal contrast in MTTs suffer similar uncertainties.

But we also completely agree with the reviewer that the exclusive comparison of MTT has the potential to conceal interesting pattern. In that sense there seems to be a misunderstanding: our analysis was never limited to MTTs. Instead, throughout the experiment and the reporting of the results, we always analyse the full range of TTDs, i.e. percentiles and fractions of water of different ages. This can be seen in Table 5, as well as Figures 7 – 10 in the original manuscript but also in Figures FR3-4 and Tables TR1-2 here above. As water ages throughout all percentiles show similar pattern between the individual scenarios, we used the MTT for communicative purposes in the text (note that the use of any other percentile would have resulted in equivalent descriptions) as this has traditionally been the most commonly used metric. For the purpose of our analysis we believe that the emphasis on MTT in the text instead of using multiple metrics improves the readability of the manuscript. In addition, we think that MTT is more suitable here than the fraction of young water, because the core of the analysis is older water instead of young water. In any case, the young water fractions F_{yw} are of course also part of the analysis in the original manuscript (Table 5, Figures 7 – 10) but also here above (Tables TR1-2, Figures FR3-4). Please note that we used a different symbol to represent it – $F(T<3m)$ (see p.17, l.536) – to remain consistent with the notation of other metrics throughout the manuscript. We will clarify this in the text.

(5) Reviewer Comment:

Finally, I would highly appreciate if the authors could increase traceability of their results and provide the underlying tracer data as well as model codes. Traceability is one of the main criteria for HESS nowadays and given that the authors address such a fundamental claim in tracer hydrology and TT modelling, I find it necessary for the entire TT community to benefit from this study not only via the paper, but also in terms of data and code accessibility.

Reply:

We agree, and we will upload the model code to an open access repository. Most tracer data are available via open access databases as explicitly highlighted in text and the Data availability section. The water stable isotopes in stream samples will be available soon, together with other stream data from Germany, as those data are currently prepared for publication in a data paper. Still, the data from the Neckar can be shared upon request.

Minor Comments

(6) Reviewer Comment:

Lines 35—37: if this refers to the findings by Kirchner (2016), one could be more precise by specifying that the MTT (as commonly reported metric) derived from CO models is affected by spatial aggregation errors.

Reply:

Agreed. We will adjust that in the revised manuscript.

(7) Reviewer Comment:

Line 59: in what sense is there more coherence?

Reply:

There is more coherence in the sense that tracer circulation is explicitly linked to and described by the movement of water (i.e. storage and release), which is the actual agent of physical transport in terrestrial hydrological systems.

(8) Reviewer Comment:

Line 70: does Cl⁻ have a clear seasonal cycle? I assume both weathering and anthropogenic effects (e.g., application of road salt) govern its concentrations. Another possible distinction would be radioactive vs. conservative tracers.

Reply:

The chloride ion has a pronounced seasonal cycle, in particular in coastal and maritime influenced climates. It has been successfully applied as age tracer in many previous studies (e.g. Kirchner et al., 2001, 2010; Page et al., 2007; Shaw et al., 2008; Hrachowitz et al., 2009; Soulsby et al., 2010; McMillan et al., 2012; Benettin et al., 2015; Harman, 2015; Wilusz et al., 2017; Cain et al., 2019; Kaandorp et al., 2021; Meira Neto et al., 2022). Anthropogenic effects,

such as road gritting, can indeed influence the chloride concentrations. That is why the above studies are limited to catchments with minor human influence.

(9) Reviewer Comment:

Lines 80—98: the focus on the amplitude ratio for the “traditional” TT approaches is fine for simple one-compartment gamma (and thus also exponential) models, but is this also relevant for multiple-compartment CO models and other pre-defined TT shapes such as the dispersion model? This suggests that CO models are exclusively based on the amplitude ratio and shift in seasonal isotope ratios.

Reply:

We are not entirely sure what the reviewer wants to express here. The concept of seasonal tracers as means to estimate stream water ages is rooted in the attenuation of seasonal tracer precipitation amplitudes in the stream water. This is independent of the model application. Any model that aims to represent the movement of such a seasonal tracer through a catchment will have to reproduce these observed attenuation between precipitation stream tracer amplitudes, i.e. the amplitude ratio.

(10) Reviewer Comment:

Lines 84—85: “practically” and “feasibly” twice?

Reply:

Indeed. We will correct that.

(11) Reviewer Comment:

Lines 97: to what extent could a spatial aggregation bias also affect spatially lumped (one-compartment) SAS models?

Reply:

This is unknown and to some extent also investigated here, as explicitly mentioned in the original manuscript (e.g. p.5, l.147ff; p.21, l.636ff; p.22, l.698ff).

(12) Reviewer Comment:

Lines 197: you used the CORINE dataset from 2018. To what extent has land use remained stable since 2001?

Reply:

There was no significant change between the here defined land use classes over the 2001-2018 period, as shown in Table TR3 below.

Table TR3: Landuse in the Neckar basin between 1990 and 2018 based on CORINE landcover data.

Landcover percentage	1990	2000	2006	2012	2018
Forest (%)	35	35	35	36	36
Grass/Crop (%)	53	53	52	50	50
Urban (%)	11	12	13	14	14
Water (%)	1	~0	~0	~0	~0

(13) Reviewer Comment:

Line 374: we do not necessarily see passive storage volumes in the most recent SAS model studies.

Reply:

This seems to be a misunderstanding. Indeed, studies based on the “pure” SAS approach that do not model Q , typically define a mixing/sampling storage S_{tot} , although the symbols and terminology vary between individual papers (e.g. Benettin et al., 2017). This S_{tot} represents the total storage available for mixing/sampling in a component and is thereby fully equivalent with our $S_{S,tot}$. The difference is that we have to distinguish a hydraulically active part S_s of that storage that represents the hydraulic head above the river bed to generate Q in our model as visualized in e.g. Zuber (1986, Figure 1 – “dynamic” and “minimum” volume) or Hrachowitz et al. (2016; Figure 2), so that $S_{S,tot}=S_s+S_{S,p}$. As “pure” SAS models do not generate Q they also do not need this distinction. Besides that, two definitions of storage are completely identical.

(14) Reviewer Comment:

Lines 398—414: I am wondering to what extent we can trust the spatially distributed implementation, given that there is only one calibration gauge at the outlet of the entire catchment. This also relates to my general comment about the considerable size and few data for the study basin.

Reply:

This is indeed an important comment. To further test the IM-SAS implementations for their ability to reflect the spatial differences in the study basin, we have now evaluated the models' ability to reproduce observed stream flow in several sub-catchments within the Neckar river basin. As described in detail in reply to Comment (2) above and as can be seen in Figure FR2, the results suggest that the model provides a rather robust representation of the hydrological response and its spatial variability throughout the Neckar basin. We will add this analysis to the revised version of the manuscript.

(15) Reviewer Comment:

Line 411: could you specify what the distributed moisture accounting approach is?

Reply:

This type of model implementation, elsewhere also referred to as “data-gridded” or “semi-lumped” as in detail described by Ajami et al. (2004), runs a model with spatially distributed forcing data but using the same model parameters. For example, here, each precipitation zone receives different precipitation, but the model parameters are the same in all four precipitation zones. This approach has in past been shown to be very effective for improving the representation of spatially variable response dynamics while limiting the amount of necessary model parameters (e.g. Fenicia et al., 2008; Euser et al., 2015).

(16) Reviewer Comment:

Lines 420—421: why have the authors not applied a multi-objective calibration to the CO models?

Reply:

We are not sure what the reviewer intends to express here. The CO models in our study exclusively model the tracer circulation in the basin. They generate only one single output variable, i.e. the tracer concentration in the stream. We therefore cannot perform the same multi-objective calibration as for the IM-SAS models that besides tracer concentrations also reproduce streamflow Q. If the reviewer had a simultaneous calibration of ^{18}O and ^3H in mind, we would like to emphasize that the objective of this paper is to test if the *exclusive* use of ^{18}O underestimates water ages. A simultaneous calibration to both tracers in CO models will not add any additional information to answer this question. Please also note that the simultaneous calibration to ^{18}O and ^3H in the IM-SAS models was only done to test if/how it affects parameters that control water fluxes in the model. Major differences in model parameters between the different calibration approaches would have been an indication for differences of how the individual models route water and tracers through the system and thus a source of potential uncertainty in the interpretation.

(17) Reviewer Comment:

Line 424: this is interesting but I think, as stated in my general comments, that TTs should be obtained from a SAS model with storage, input and output fluxes defined a priori (as if they were “real” data), rather than computing TTs from simultaneous calibration against flow and tracers. I think that this would be a more straightforward methodology given the scope of TT modelling and tracers. As presented here, we do not know to what extent simulated TTs are affected by equifinality in the hydrological model parameters.

Reply:

Please see above: as replied to Comment (3) we have now added such a model implementation (scenario X7-8; Figure FR4 and Table TR2). The results lead to the same conclusions as the IM-SAS model implementations: ^{18}O and ^3H lead to similar TTDs, and there is no indication for ^{18}O truncating water ages. This further strengthens our original conclusions. We will add this model implementation to the revised manuscript.

(18) Reviewer Comment:

Lines 553—555: not a complete sentence

Reply:

We will correct this.

(19) Reviewer Comment:

Line 571: not only, but also...?

Reply:

We will correct this.

(20) Reviewer Comment:

Lines 577—578: I think you could easily implement the multi-objective calibration for the CO models as well.

Reply:

Indeed. It would be easy to implement that, but as explained in response to Comment (16) it does not add any additional information to test the research hypothesis.

(21) Reviewer Comment:

Lines 619—620: so here one could at least test how time-variant/seasonal CO models perform

Reply:

This would indeed be an interesting analysis. However, it is outside the scope of this study as explained in response to Comment (3) above.

(22) Reviewer Comment:

Lines 642—644: could this not be an indication of the fact that there are too many degrees of freedom and the model always succeeds to fit the tracer data, regardless of whether it is spatially lumped or semi-distributed?

Reply:

As shown in Figure FR1 above, there is little indication of model overfitting that could result from “too many degrees of freedom”. One explanation of the observed similarity between the lumped and distributed models could be that much of the climatic and topographic heterogeneity within the catchment is filtered out in the response (see also reply to Comment (2) above), so that a lumped representation may be sufficient to pick up the major features of the hydrological response in the study basin.

(23) Reviewer Comment:

Lines 656—657: see, e.g., Nguyen et al. (2022) who found substantial differences in SAS-based transport models between spatially lumped and semi-distributed setup.

Reply:

We will refer to that study as an example of a setting where spatial differences seem to be more relevant.

Response to Editor:

Both the Referees agree about the great improvement of the revised manuscript, which now substantially meets the standards required for publication in HESS.

However, as pointed out by Referee #2, the manuscript would benefit if some of the results of the additional model simulations, carried out in response to some of the comments received during the peer review process, could find more room in the discussion of the results.

Hence, I ask you this final effort before considering the paper suitable for publication.

Reply:

We thank the Editor for the positive assessment of our work.

We have addressed the remaining comments of Reviewer #2 in the revisions attached. In particular we have added the results of the P-SAS model to Figures 3, 4 and 10 as requested by the reviewer. In addition, we emphasize P-SAS throughout the Results and Discussion Sections.

Second iteration: Minor revision

Response to Editor:

Both the Referees agree about the great improvement of the revised manuscript, which now substantially meets the standards required for publication in HESS.

However, as pointed out by Referee #2, the manuscript would benefit if some of the results of the additional model simulations, carried out in response to some of the comments received during the peer review process, could find more room in the discussion of the results.

Hence, I ask you this final effort before considering the paper suitable for publication.

Reply:

We thank the Editor for the positive assessment of our work.

We have addressed the remaining comments of Reviewer #2 in the revisions attached. In particular we have added the results of the P-SAS model to Figures 3, 4 and 10 as requested by the reviewer. In addition, we emphasize P-SAS throughout the Results and Discussion Sections.

Response to Reviewer #2:

(1) Reviewer Comment:

Thank you for your detailed replies to all of my comments and for including additional simulations. I think that the manuscript is now much more balanced regarding the use of different modelling concepts.

Reply:

We thank the reviewer for the positive evaluation of our manuscript and thank her for the additional comments.

(2) Reviewer Comment:

As the P-SAS implementation has been added to the revised manuscript, most of the figures describing simulation results in the manuscript show IM-SAS results only (Figs. 3-7; 10-12) and there is a large emphasis on these model scenarios in the text (e.g., lines 516-537; 539-566; 590-598). Given both types of SAS models give comparably good

and matching results for d18O and 3H (with the absolute difference in TTs being smaller for P-SAS), would it be possible to show the results of both model types or replace some of the IM-SAS figures by P-SAS figures?

Reply:

We have now added the results of P-SAS to Figure 3, Figure 4 and to Figure 10. In addition, we emphasize P-SAS throughout the Results and Discussion Sections as highlighted in yellow in the revised manuscript (lines 514, 544, 547, 549, 551, 576, 579, 586, 608, 634, 637, 640, 643, 664, 667, 686, 688, 755, 759, 760)

Minor Comments

(3) Reviewer Comment:

- lines 463–468: mention calibration approach for P-SAS as well.

Reply:

Ok.

(4) Reviewer Comment:

- lines 640–641: "to a lesser degree" sounds to me as if P-SAS were not be able to represent all signatures that accurately. I assume that what you mean here is that it cannot represent all kinds of hydrological signatures as it does not simulate streamflow.

Reply:

That is correct.

(5) Reviewer Comment:

- lines 642–643: related to the previous comment - CO models could also be calibrated to two different tracers (as mentioned by the authors in the reply). Hence, P-SAS and CO are in that sense more similar than P-SAS and IM-SAS.

Reply:

Agreed.

Stable water isotopes and tritium tracers tell the same tale: No evidence for underestimation of catchment transit times inferred by stable isotopes in SAS function models.

Siyuan Wang¹, Markus Hrachowitz¹, Gerrit Schoups¹, Christine Stumpp²

5 ¹Department of Water Management, Faculty of Civil Engineering and Geosciences, Delft University of Technology, Stevinweg 1, 2628CN Delft, Netherlands

²Institute of Soil Physics and Rural Water Management, University of Natural Resources and Life Sciences Vienna, Muthgasse 18, 1190 Vienna, Austria

Correspondence to: Siyuan Wang (S.Wang-9@tudelft.nl)

10 **Abstract.** Stable isotopes ($\delta^{18}\text{O}$) and tritium (^3H) are frequently used as tracers in environmental sciences to estimate age distributions of water. However, it has previously been argued that seasonally variable tracers, such as $\delta^{18}\text{O}$, generally and systematically fail to detect the tails of water age distributions and therefore substantially underestimate water ages as compared to radioactive tracers, such as ^3H . In this study for the Neckar river basin in central Europe and based on a >20-year record of hydrological, $\delta^{18}\text{O}$ and ^3H data, we systematically scrutinized the above postulate together with the potential role of spatial aggregation effects to exacerbate the underestimation of water ages. This was done by comparing water age distributions inferred from $\delta^{18}\text{O}$ and ^3H with a total of 21 different model implementations, including time-invariant, lumped parameter sine-wave (SW) and convolution integral models (CO) as well as SAS-function models (P-SAS) and integrated hydrological models in combination with SAS-functions (IM-SAS).

We found that, indeed, water ages inferred from $\delta^{18}\text{O}$ with commonly used SW and CO models are with mean transit times (MTT) $\sim 1 - 2$ years substantially lower than those obtained from ^3H with the same models, reaching MTTs ~ 10 years. In contrast, several implementations of P-SAS and IM-SAS models did not only allow simultaneous representations of storage variations and stream flow as well as $\delta^{18}\text{O}$ and ^3H stream signals, but water ages inferred from $\delta^{18}\text{O}$ with these models were with MTTs $\sim 11 - 17$ years much higher and similar to those inferred from ^3H , which suggested MTTs $\sim 11 - 13$ years. Characterized by similar parameter posterior distributions, in particular for parameters that control water age, P-SAS and IM-SAS model implementations individually constrained with $\delta^{18}\text{O}$ or ^3H observations, exhibited only limited differences in the magnitudes of water ages in different parts of the models as well as in the temporal variability of TTDs in response to changing wetness conditions. This suggests that both tracers lead to comparable descriptions of how water is routed through the system. These findings provide evidence that allowed us to reject the hypothesis that $\delta^{18}\text{O}$ as a tracer generally and systematically “cannot see water older than about 4 years” and that it truncates the corresponding tails in water age distributions, leading to underestimations of water ages. Instead, our results provide evidence for a broad equivalence of $\delta^{18}\text{O}$ and ^3H as age tracers for systems characterized by MTTs of at least 15 – 20 years. The question to which degree aggregation of spatial heterogeneity can further adversely affect estimates of water ages remains unresolved as the lumped and distributed implementations of the IM-SAS model provided inconclusive results.

Overall, this study demonstrates that previously reported underestimations of water ages are most likely not a result of the use of $\delta^{18}\text{O}$ or other seasonally variable tracers *per se*. Rather, these underestimations can be largely attributed to choices of model approaches and complexity not considering transient hydrological conditions next to tracer aspects. Given the additional vulnerability of time-invariant, lumped SW and CO model approaches in combination with $\delta^{18}\text{O}$ to substantially underestimate water ages due to spatial aggregation and potentially other, still unknown effects, we therefore advocate to avoid the use of this model type in combination with seasonally variable tracers if possible, and to instead adopt SAS-based models or time-variant formulations of CO models.

1 Introduction

Age distributions of water fluxes (“transit time distributions”, TTD) and water stored in catchments (“residence time distributions”, RTD) are fundamental descriptors of hydrological functioning (Botter et al., 2011; Sprenger et al., 2019) and catchment storage (Birkel et al., 2015). They provide a way to quantitatively describe the physical link between the hydrological response of catchments and physical transport processes of conservative solutes. While the former is largely controlled by the celerities of pressure waves propagating through the system, the latter, in contrast, occur at velocities that can be up to several orders of magnitude lower (McDonnell and Beven, 2014; Hrachowitz et al., 2016).

Water age distributions cannot be directly observed. Instead, they can, in principle, be inferred from observed tracer breakthrough curves. While practically feasible at lysimeter (e.g. Asadollahi et al., 2020; Benettin et al., 2021) and small hillslope scales (e.g. Kim et al., 2022), lack of adequate observation technology together with logistical constraints make this problematic at scales larger than that. At the catchment-scale, estimates of water age distributions are therefore typically inferred from models that describe the relationships between time-series of observed tracer input and output signals.

Over the past decades a wide spectrum of such models has been developed. Early approaches often relied on simple lumped sine-wave (hereafter: SW) or lumped parameter convolution integral models (hereafter CO; Maloszewski and Zuber, 1982; Maloszewski et al., 1983; McGuire and McDonnell, 2006), originally developed for aquifers. In spite of their wide-spread application, these models feature multiple critical simplifying assumptions. Most importantly, the vast majority of these model implementations work under the assumption that water storage in catchments is at steady state and that, as a consequence, TTDs are time-invariant and can be *a priori* defined or calibrated. While the role of storage as first order control on water ages was described early in the general definition of mean turnover times (e.g. Eriksson, 1958; Bolin and Rodhe, 1973; Nir, 1973), the steady state assumption, i.e. constant storage, may have limited effect on TTDs in aquifers, as the fraction of transient water volumes in such systems is typically rather low. However, given the temporal variability in the hydro-meteorological system drivers (e.g. precipitation, atmospheric water demand) and the spatial heterogeneity in near-surface hydrological processes, this assumption is violated in most surface water systems world-wide and can lead to misinterpretations of the model results. This triggered the development of a more coherent framework to estimate water age distributions without the need of an *a priori* definition of time-invariant TTDs. Instead, probability distributions, referred to as StorAge Selection (SAS)

functions, are *a priori* defined or calibrated, and changes in water storage are explicitly accounted for. Thus, water fluxes within and released from the system are sampled from water volumes of different ages stored in the system according to these SAS functions (Botter et al., 2011; Rinaldo et al., 2015). The general concept is firmly rooted in the development of hydrochemical routing schemes for the Birkenes, HBV or similar models going back to at least the 1970s (e.g. Lundquist, 1977; Christophersen and Wright, 1981; Christophersen et al., 1982; Seip et al., 1985; de Groisbois et al., 1988; Hooper et al., 1988; Barnes and Bonell, 1996), as illustrated by Figure 1 in Bergström et al. (1985). Although functionally very similar to CO model implementations that allow for transient, i.e. time-variant TTDs (Nir, 1973; Niemi, 1977), the sampling procedure based on SAS functions has the advantage to explicitly track the history of water (and tracer) input to and output from the system through the water age balance. As such it does explicitly account for non-steady state conditions, which in turn leads to the emergence of time-variable TTDs and RTDs (see review Benettin et al., 2022).

Irrespective of the modelling approach, two types of environmental tracers have in the past been frequently used to estimate water age distributions with the above models. The first type are tracers that are characterized by distinct differences in their seasonal signals. They include stable isotopes of water (^2H , ^{18}O ; e.g. Maloszewski et al., 1983; Vitvar and Balderer, 1997; Fenicia et al., 2010) or solutes, such as Cl^- (e.g. Kirchner et al., 2001, 2010; Shaw et al., 2008; Hrachowitz et al., 2009a, 2015). With these tracers, water ages and (metrics of) their distributions can be estimated by the degree to which the seasonal amplitudes of the precipitation tracer concentrations are time-shifted and/or attenuated in the stream flow (McGuire and McDonnell, 2006; Kirchner, 2016). Broadly speaking, the stronger the attenuation of the seasonally variable tracer amplitude in stream flow (A_s) as compared to its amplitude in precipitation (A_p), i.e., the lower the amplitude ratio A_s/A_p , the older stream water is, on average. The second type of commonly used tracers are radioactive isotopes, such as tritium (^3H). Forming the basis for many water dating studies going back to the 1950s (e.g. Begemann and Libby, 1957; Eriksson, 1958; Dincer et al., 1970; Stewart et al., 2007; Morgenstern et al., 2010; Duvert et al., 2016; Gallart et al., 2016; Rank et al., 2018; Visser et al., 2019), water age can be estimated with radioactive tracers based on the level of radioactive decay experienced by precipitation input signals experience before they reach the stream.

The relationship between the tracer amplitude ratios A_s/A_p and water age that is exploited by seasonally variable tracers is highly non-linear. With increasing attenuation of the tracer signal in the stream, i.e., a lower A_s/A_p , water therefore does not only become older but the age estimates become more sensitive to changes in the amplitude ratio (Kirchner, 2016). This implies that the older the water, uncertainties in the observed amplitude ratios lead to increased uncertainties in water age estimates. As a consequence, there is an upper limit to the age of water which can be **practically and feasibly** determined with seasonally variable tracers. A rare attempt to quantify this potential upper detectable age limit was reported by DeWalle et al. (1997). With an observed $\delta^{18}\text{O}$ precipitation amplitude $A_p = 3.41\%$, an assumed lowest possible $\delta^{18}\text{O}$ stream water amplitude that equaled the observational error $A_s = 0.1\%$, and the use of a lumped, time-invariant exponential TTD (“complete mixing”) they determined a maximum detectable mean transit time (MTT) of around 5 years at their study site. Several authors subsequently emphasized that estimates of MTT and in particular of maximum detectable MTT such as reported by DeWalle et al. (1997) are specific to A_p at individual study sites (McGuire and McDonnell, 2006) and highly sensitive to choices in

100 the modelling process (Stewart et al., 2010; Seeger and Weiler, 2014; Kirchner, 2016). For example, multiple previous studies demonstrated that the use of gamma distributions with a shape parameter $\alpha \sim 0.5$ as TTD produces model results that are more consistent with observed tracer data than the use of exponential distributions (i.e. $\alpha = 1$) in a wide range of contrasting environments world-wide (Kirchner et al., 2001; Godsey et al. 2010; Hrachowitz et al., 2010a, b). Merely replacing the exponential distribution by a gamma distribution with $\alpha = 0.5$ as TTD at the study site of DeWalle et al. (1997) leads, in a quick back-of-the-envelope calculation, to a substantial increase of the maximum MTT from the reported 5 years to ~ 90 years. This is exacerbated by the potential presence of spatial aggregation bias in the lumped implementation of that model, which may cause further considerable underestimation of MTT as demonstrated by Kirchner (2016).

The relevance of the above assumptions is often overlooked and in spite of little additional quantitative evidence, it remains widely assumed that water ages in systems characterized by MTTs $> 4 - 5$ years cannot be meaningfully quantified with seasonally variable tracers. Most notably, Stewart et al. (2010, 2012) argued that water older than that remains *hidden* to stable water isotopes and other seasonally variable tracers, which inevitably results in a misleading truncation of water age distributions. Such a pronounced and systematic underestimation of water ages would have far reaching consequences for estimates of water storage (e.g. Birkel et al., 2015; Pfister et al., 2017) and the associated turnover times of nutrients and contaminants in catchments (e.g. Harman, 2015; Hrachowitz et al., 2015). Stewart et al. (2012), further argue that the use of radioactive tracers, such as ^3H , can largely avoid the truncation of the long tails of TTDs. This is mostly owed to the ^3H half-life of $T_{1/2} = 12.32$ years. Even with the current atmospheric ^3H concentrations that, after peaking in the early 1960s, have been converging back towards pre-nuclear bomb testing levels, precipitation ^3H signals can be detected in the system for several decades, making ^3H an effective tracer now and for the foreseeable future (Michel et al., 2015; Harms et al., 2016; Stewart and Morgenstern, 2016). Indeed, a range of studies, based on ^3H and often in conjunction with lumped parameter convolution integral approaches, suggest that many catchments and larger river basins world-wide are characterized by MTTs that are decadal or higher (e.g. Stewart et al., 2010 and references therein). It is further rather remarkable that such elevated water ages are largely absent in estimates derived from lumped parameter convolution integral studies based on seasonally variable tracers, which often indicate MTTs between 1 – 3 years (e.g. McGuire and McDonnell, 2006 and references therein; Hrachowitz et al., 2009b; Godsey et al., 2010), as correctly and importantly pointed out by Stewart et al. (2010). This in itself could be supporting evidence for the failure of seasonally variable tracers to detect long tails of TTDs, as postulated by Stewart et al. (2012). However, it could just as well be a mere artifact arising from a sample bias due to the different catchments analyzed or from choices in the modelling process. There are only a few studies that have directly and systematically compared estimates of water age derived from both, seasonally variable (^2H , ^{18}O) and radioactive tracers (^3H) at the same study site and based on (at least partly) comparable model approaches (Maloszewski et al., 1983; Uhlenbrook et al., 2002; Stewart et al., 2007; Stewart and Thomas, 2008). The MTT estimates derived from seasonally variable tracers in these comparative studies are consistently, but to varying degrees lower than estimates based on ^3H . However, these studies are nevertheless subject to limitations that may weaken the generality of the conclusion that seasonally variable tracers underestimate catchment water ages. More specifically, tracer data were available for only rather short time periods of about

2 – 3 years, including, for some studies, only a handful of ^3H data points. Many these studies relied on lumped parameter convolution integral approaches with time-invariant TTDs whose pre-defined functional form when applied with seasonally variable tracers was limited to shapes (e.g. exponential) that already *a priori* precluded the representation of heavy-tails and thus a meaningful representation of old ages. In addition, the models to estimate water ages in these studies were implemented in a spatially lumped way, which further exacerbates the potential for underestimating water ages due to spatial aggregation effects in environments that are likely subject to considerable heterogeneity in hydrological functioning (Kirchner, 2016).

Addressing some of the concerns above, a recent study by Rodriguez et al. (2021) compared catchment water ages inferred from two-year data records of a seasonally variable tracer (^2H ; 1088 data points) and ^3H (24 data points) using a spatially lumped implementation of a previously developed simple tracer circulation model based on the SAS approach, which generates time-variable TTDs (Rodriguez and Klaus., 2019). In spite of consistently higher age estimates obtained from ^3H , the absolute differences to ^2H inferred estimates were very minor. While the difference in mean transit times was estimated at $\Delta\text{MTT} \sim 0.22$ years for MTTs ~ 3 years, the difference in the estimate of the 90th percentile of water ages, as metric for the presence of old ages, was with $\Delta 90^{\text{th}} \sim 0.15$ years even lower. The authors concluded that these results cast some doubt on “[...] the perception that stable isotopes systematically truncate the tails of TTDs” (Rodriguez et al., 2021). However, their interpretation was questioned by Stewart et al. (2021), who pointed out that simply no older water may be present in their study catchment.

Building on the above work of Rodriguez et al. (2021), the objective of this study is therefore to further scrutinize the notion that the use of seasonally variable tracers leads to truncated estimates of water age distributions in a systematic comparative experiment. The novel aspects of this study for the $\sim 13,000$ km² Neckar River basin in South-West Germany include that we here use (1) long-term records, i.e. > 20 years, of hydrological data as well as of seasonally variable (^{18}O) and radioactive tracers (^3H) together with (2) a **suite of lumped and** spatially semi-distributed implementations of (3) SW, CO and SAS-function based models, including a formulation of an integrated, process-based model to simultaneously reproduce hydrological and tracer response dynamics and to track temporally variable water age distributions in the system. The above points allow us to, at least partially, explore several unresolved questions how different factors may or may not contribute to the apparent underestimation of water ages by seasonally variable tracers, including potential effects of uncertainties arising from short data records, spatial aggregation and the use of oversimplified **time-invariant, lumped** models. More specifically, we here test the hypothesis that ^{18}O as tracer generally and systematically cannot detect tails in water age distributions and that this truncation leads to systematically younger water age estimates than the use of ^3H .

2 Study site

The Neckar River basin in South-West Germany has an area of $\sim 13,000$ km². The elevation in the basin ranges from 122 m at the outlet in the north to about 1019 m in the South (Fig. 1a; Table 1). Following the elevation gradient, the landscape is characterized by terrace-like elements and undulating hills with wide valleys used as grass- and croplands in lower regions, in

particular in the northern parts of the Neckar Basin, and increasingly steep and narrow forested valleys towards the southern parts (Fig. 1c). Long-term mean annual precipitation (P) reaches $\sim 909 \text{ mm yr}^{-1}$, with considerable spatial variability ranging from $\sim 660 \text{ mm yr}^{-1}$ in the lower parts of the basin to over 1500 mm yr^{-1} at high elevations in the southwest (Fig. 1b). With a long-term mean temperature of about $8.9 \text{ }^\circ\text{C}$, potential evaporation (E_p) around $\sim 870 \text{ mm yr}^{-1}$ and an aridity index (I_A) (i.e., $I_A = E_p/P$) $I_A \sim 0.98$ the basin is characterized by a temperate-humid climate, where snow cover can be present for several weeks in the winter months.

3 Data

3.1 Data

Daily hydro-meteorological data were available for the period 01/01/1970 – 31/12/2016. As the forcing data of the hydrological models, daily precipitation and daily mean air temperature were obtained from stations operated by the German Weather Service (DWD). Precipitation was recorded at 16 stations and temperature measurements were available at 12 stations (Fig. 1) in or close to the study basin. Daily mean discharge data for the period 01/01/1970 – 31/12/2016 at the outlet of the Neckar basin at Rockenau station were provided by the German Federal Institute of Hydrology (BfG). In addition, data of daily mean discharge for the same time period from three sub-catchments within the Neckar basin (Fig. 1) at the gauges Kirchentellinsfurt (C1; 2324 km^2), Calw (C2; 584 km^2) and Untergriesheim (C3; 1827 km^2) were available from the Environmental Agency of the Baden-Württemberg region (LUBW).

Long-term volume-weighted monthly $\delta^{18}\text{O}$ data in precipitation was available for the period 01/01/1978 – 31/12/2016 at the Stuttgart station. At the sampling gauge, a monthly accumulation bottle was filled with the collected daily precipitation, and all collected water was mixed together. Therefore, the water samples of precipitation reflect the volume-weighted monthly isotopic composition. Then, a monthly isotope sample bottle for stable isotope (i.e., ^{18}O) was filled with 50 ml precipitation water from the corresponding monthly accumulation bottle. All precipitation samples were tightly sealed and stored in a dark room at $\sim 4^\circ\text{C}$ before analysis. Monthly stream water samples were collected at Schwabenheim, close to the Rockenau discharge station, by the BfG for the period of 01/10/2001 – 31/12/2016 (Schmidt et al. 2020; Königer et al. 2022). Note that the available data do not represent instantaneous grab samples but bulk samples from mixed daily samples. River water was sampled automatically by samplers (SP III-XY-36, Maxx Meb- und Probenahmetechnik GmbH, Germany), which contained 36 bottles (each with a volume of 2.5 L). Every 30 minutes, 50 ml river water was pumped into one bottle (48 subsamples per day). A new bottle was filled every 24 h with the same procedure. All daily river water samples were stored in the sample compartment at $\sim 4^\circ\text{C}$ and were subsequently combined into monthly samples in the laboratory of BfG. This means the stream water samples reflect a non-flow-weighted monthly average isotopic composition. The stable isotopes ratios were analyzed with dual-inlet mass spectrometry and a laser-based cavity ring-down spectrometer (L2120-i/L2130-i, Picarro Inc.) at Helmholtz Zentrum München, Germany. When changing from dual-inlet mass spectrometry to cavity ring-down spectrometry, the long-term precision of the analytical systems ($\pm 0.15 \text{ } \%$ and $\pm 0.1 \text{ } \%$, respectively, for $\delta^{18}\text{O}$) was ensured (Stumpp et al. 2014; Reckerth

et al., 2017).

Long-term monthly ^3H data in precipitation were obtained for the period 01/01/1978 – 31/12/2016 at Stuttgart station (same station as ^{18}O data in precipitation; Schmidt et al., 2020). For the purpose of establishing robust initial conditions for the model experiment (see section 4.2) the tritium record in precipitation was reconstructed for the preceding 1970-1977 period by bias correcting data from the sampling station Vienna, available from the Global Network of Isotopes in Precipitation which is a joint database of the International Atomic Energy Agency (IAEA) and the World Meteorological Organization (WMO) (Supplementary Material Fig. S1). The precipitation for tritium data was sampled based on the same method as that for ^{18}O in precipitation which means that the precipitation samples for tritium also reflect the volume-weighted monthly isotopic composition. Stream water samples for tritium were collected based on the same method as that for as ^{18}O in stream. Therefore, tritium stream water samples also reflect non-volume-weighted monthly average isotopic compositions. The tritium stream water samples are not influenced by water release from nuclear power stations. All water samples were analyzed for tritium concentrations by the BfG Environmental Radioactivity Laboratory using liquid scintillation counters (Ultima Gold LLT) with a 2-sigma analytical uncertainty (Schmidt et al. 2020).

Land use types of the catchments are determined using the CORINE Land Cover data set of 2018 (<https://land.copernicus.eu/pan-european/corine-land-cover>). The $90\text{ m} \times 90\text{ m}$ digital elevation model of the study region (Fig. 1a) was obtained from <https://www.usgs.gov/> and used to derive the local topographic indices including height above nearest drainage (HAND) and slope.

3.2 Data pre-processing

For the subsequent model experiment (section 4.2), the study basin was stratified into four regions P1 – P4 that are characterized by distinct long-term precipitation pattern (hereafter: precipitation zones). In the following the procedure to infer these precipitation zones and to estimate the associated differences in $\delta^{18}\text{O}$ and ^3H input is described.

3.2.1 Spatial distribution of precipitation and identification of precipitation zones

To account, at least to some degree, for spatial heterogeneity in precipitation we stratified the Neckar River basin into precipitation zones that are each characterized by distinct average annual precipitation totals. Goovaerts (2000) and Lloyd (2005) showed that areal precipitation estimates informed by elevation data were often more accurate than those based on precipitation gauge observations alone. Thus, to interpolate and to estimate areal precipitation across the basin we used Co-Kriging, considering elevation, as a preliminary analysis suggested lower errors. Finally, the individual precipitation estimates for each grid cell were used with K-means clustering to establish four clusters, representing the four precipitation zones P1 – P4 (see Fig. 1b).

3.2.2 Spatial extrapolation of precipitation $\delta^{18}\text{O}$ to precipitation zones

Records of observed precipitation $\delta^{18}\text{O}$ are available at one location close to the center of the Neckar Basin (Fig. 1). However,

it is well described (e.g. Kendall and McDonnell, 2012) that precipitation $\delta^{18}\text{O}$ input can be subject to considerable spatial heterogeneity, largely controlled by topographic and meteorological influences. Stumpp et al. (2014) specifically identified latitude, elevation and temperature as the key factors controlling $\delta^{18}\text{O}$ input heterogeneity in the greater study region. To at least partially account for these effects and to locally adjust $\delta^{18}\text{O}$ input signals throughout the study basin, we made use of the sinusoidal isoscapes method (Allen et al., 2018, 2019). Briefly, this method exploits the seasonal pattern in $\delta^{18}\text{O}$ precipitation signal by fitting sine functions to observed $\delta^{18}\text{O}$ input signals for a large sample of locations:

$$\delta^{18}O_p(t) = a_p \sin(2\pi t - \varphi_p) + b_p, \quad (1)$$

With a_p [%] the amplitude of the seasonal precipitation signal, b_p [%] a constant offset and φ_p [rad] the phase of the signal. For each of the three fitting parameters, i.e., a_p , b_p and φ_p , multiple regression relationships were previously developed (Allen et al., 2018). Depending on the fitting parameter, predictor variables included a selection of latitude, longitude, elevation, range of annual temperature range and mean annual precipitation (Allen et al., 2018). The relationships defined by these predictor variables then allow to estimate a_p , b_p and φ_p , and thus the seasonal signal of $\delta^{18}\text{O}_p$ for locations where no precipitation $\delta^{18}\text{O}$ observations are available.

Here, we adopted the method as described in the following. In a first step, we estimated the sine wave parameters for the time series of precipitation $\delta^{18}\text{O}$ observed at the station Stuttgart, using the procedure described by Allen et al. (2018). Subsequently, we estimated the associated sine wave parameters a_p , b_p and φ_p in each of the four precipitation zones (P1 – P4; Supplementary Material Table S2) based on Eqs. (S1) - (S3) in the Supplement, using the above-described individual predictor variables, averaged for each precipitation zone (Supplementary Material Table S1). We then used the estimated sine wave parameters to construct an individual $\delta^{18}\text{O}_p$ sine wave for each precipitation zone (Eq.1). In a last step, we adjusted the observed $\delta^{18}\text{O}$ input for the four precipitation zones by rescaling and bias correcting the observed $\delta^{18}\text{O}$ signal according to the differences between the sine waves at the observation station and sine waves estimated for each precipitation zone, respectively (Supplementary Material Fig. S2).

3.2.3 Spatial extrapolation of precipitation ^3H to precipitation zones

As for $\delta^{18}\text{O}$, it is well documented that ^3H exhibits spatial heterogeneity that is to some extent controlled by geographical factors. It has been shown that the ^3H concentration in precipitation increases with latitude, with highest concentrations in polar regions (Rozanski et al., 1991). In addition, ^3H concentrations in precipitation increase with elevation due to the ^3H -enriched upper troposphere and isotopic exchange between liquid water and atmospheric moisture, depleting ^3H in lower tropospheric layers (Tadros et al., 2014). Considering the above effects, we established a multiple linear regression relationship between ^3H concentrations in precipitation observed at 15 multiple locations across Germany (Supplementary Material Fig. S3) as available through the WISER database (IAEA and WMO, 2022; Schmidt et al., 2020), and their corresponding elevation and latitude, respectively (Supplementary Material Fig. S4). We then used this relationship to adjust the ^3H precipitation input for the four precipitation zones according to their corresponding average latitude and elevation estimate:

$${}^3H_P(t) = -0.75(L_P - L_o) - 0.002(E_P - E_o) + {}^3H_o, \quad (2)$$

where 3H_P is the latitude- and elevation-adjusted tritium precipitation concentration for each precipitation zone (P1 – P4), 3H_o is the tritium precipitation concentration observed at the Stuttgart station, L_P and E_P are the mean latitude and elevation, respectively, of each precipitation zone and L_o and E_o are the latitude and elevation, respectively, of the Stuttgart station.

265 4 Methods

The experiment to test the hypothesis that the use of $\delta^{18}\text{O}$ data systematically leads to truncated water age distributions and associated underestimations of water ages is designed and executed in a step-wise approach. 21 different scenarios of model types and spatial implementations thereof are sequentially calibrated and tested to reproduce observed $\delta^{18}\text{O}$ and ${}^3\text{H}$ signals in stream flow. For each of these models, several metrics of water age distributions resulting from the 2 independent calibration procedures, i.e., for $\delta^{18}\text{O}$ and ${}^3\text{H}$, respectively, are then estimated and compared. As a baseline and to ensure comparability with previous studies, water ages are quantified with spatially lumped, time-invariant implementations of twelve commonly used SW/CO model scenarios (Table 2): sine-wave models using exponential (SW-EM) and gamma distributions as TTDs (SW-GM; only $\delta^{18}\text{O}$), lumped parameter convolution integral models using exponential (CO-EM) and gamma distributions as TTDs (CO-GM), two parallel reservoirs (CO-2EM), three parallel reservoirs (CO-3EM) as well as an exponential piston flow (CO-EPM) implementation. The above baseline scenarios are complemented by nine additional models on the basis of SAS-functions (Table 3). In order of increasing complexity, these include three spatially integrated formulations of a “pure” SAS-function approach with one storage component and based on observed stream flow (P-SAS), three implementations of a spatially integrated hydrological model with tracer routing based on SAS-functions (IM-SAS-L) as well as three spatially distributed implementations of the same integrated hydrological model in combination with SAS-functions (IM-SAS-D).

4.1 Models

4.1.1 Sine-wave model (SW)

As demonstrated by Małoszewski et al. (1983), sine waves fitted to $\delta^{18}\text{O}$ precipitation and stream flow signals can be used to indicatively determine water ages. More specifically, the ratio of the amplitudes of the fitted sine waves, i.e. A_s/A_p , can be used together with the assumption of a shape of the TTD to estimate the associated MTT of a system. In the case of a gamma distribution as TTD, this is done according to (Kirchner, 2016):

$$\bar{\tau} = \alpha\beta, \quad (3)$$

with

$$\beta = \frac{1}{2\pi f} \sqrt{(A_s/A_p)^{-2/\alpha} - 1}, \quad (4)$$

290 where $\bar{\tau}$ is the MTT, α is a shape parameter, β is a scale parameter and f here is the frequency for the seasonal $\delta^{18}\text{O}$ signal, i.e., $f = 1 \text{ yr}^{-1}$. Here we analyze the two cases $\alpha = 1$ (SW-EM) and 0.5 (SW-GM). Note that with $\alpha = 1$, the gamma distribution is equivalent to an exponential distribution. The sine wave model is a simplification of a convolution integral model and can be directly derived from that. For a more detailed description of the method and underlying assumptions we refer to McGuire and McDonnell (2006) and Kirchner (2016).

295 **4.1.2 Time-invariant, lumped parameter convolution integral model (CO)**

While the sine wave approach requires regular cyclic signals of tracer composition, i.e., sine waves fitted to the observations, convolution integral models make direct use of the observed tracer data (e.g. Kreft and Zuber, 1978). Tracer composition in the system output can thus be estimated based on a convolution operation of the tracer composition in the system input together with an *a priori* assumption of a TTD (e.g. Maloszewski and Zuber, 1982; Kirchner et al., 2001):

300

$$C_o(t) = \int_0^\infty g(\tau)C_i(t - \tau)e^{-\lambda\tau} d\tau, \quad (5)$$

Where $C_o(t)$ is the tracer composition of the system output (here: stream flow) at time t , $C_i(t - \tau)$ is the tracer composition of the system input (here: precipitation) at any previous time $t - \tau$, λ is the radioactive decay constant ($\lambda = 0.00015 \text{ d}^{-1}$ for ^3H and $\lambda = 0 \text{ d}^{-1}$ for stable isotopes) and $g(\tau)$ is the distribution of transit times τ . Here, we used gamma distributions as basis for a flexible and general formulation of TTDs in the different CO scenarios tested in this study:

305

$$g(\tau) = \sum_{i=1}^N \eta f_i \frac{\tau^{\alpha-1}}{\beta_i^\alpha \Gamma(\alpha)} e^{\left(\frac{-\tau}{\eta\beta_i} + \frac{1}{\eta} - 1\right)} \quad \text{for } \tau \geq \tau_m(1 - \eta), g(\tau) = 0 \text{ otherwise} \quad (6)$$

310

With the α and β_i being the shape and scale parameters, respectively, f_i the fraction of the contribution of the i^{th} reservoir, so that $\sum f_i = 1$ and η the ratio of the exponential volume to the total volume. For a single exponential TTD (CO-EM) with $\alpha = 1$, $N = 1$, $\eta = 1$ and $f_1 = 1$, β_1 was the only calibration parameter. The two parallel exponential TTD model (CO-2EM) with $\alpha = 1$, $N = 2$, $\eta = 1$ and $f_2 = 1 - f_1$, required β_1 , β_2 and f_1 as calibration parameters, while the three parallel exponential TTD model (CO-3EM) with $\alpha = 1$, $N = 3$, $\eta = 1$ and $f_3 = 1 - f_1 - f_2$, required β_1 , β_2 , β_3 as well as f_1 and f_2 as calibration parameters. The exponential piston flow model (CO-EPM) with $\alpha = 1$, $N = 1$ and $f_1 = 1$ was characterized by the two calibration parameters β_1 and η . In contrast, the Gamma distribution model (CO-GM), with $N = 1$, $\eta = 1$ and $f_1 = 1$, used both, α and β_1 as free calibration parameters.

315

The MTTs associated with the above parameters in the individual model implementations are then obtained with Eq. (7).

$$\bar{\tau} = \sum_{i=1}^N f_i \alpha \beta_i \quad (7)$$

For more detailed description of the method and the individual shapes of TTDs considered here, refer to McGuire and McDonnell (2006).

320 4.1.3 SAS-function models (P-SAS, IM-SAS)

The storage-age selection function (SAS) concept as outlined by Rinaldo et al. (2015) requires the explicit tracking of water and tracer storage volumes. The age compositions of water fluxes are then sampled from the age composition in the associated storage volume. Two alternative and frequently used approaches to account for the evolution of water storage volumes were explored here: firstly, a “pure” SAS-function model in which the observed stream flow was used to account for changes in water storage volumes (P-SAS) and secondly, an integrated process-based hydrological model that generates stream flow and other fluxes in the system (IM-SAS). Water ages, their distributions, and the associated moments thereof were then estimated by tracking water and tracer fluxes through the models.

Hydrological model

330 The hydrological component of the “pure” SAS-function model (P-SAS) was implemented as described in Benettin et al. (2017). This model consists of one single storage volume, which receives observed precipitation P as input and releases observed stream flow as output. Evaporation E_A from that storage is modelled following the simplifying assumption that there is negligible storage change over the entire 47-year study period (01/01/1970 – 31/12/2016), as expressed by:

$$E_A(t) = E_p(t) \left(\frac{\bar{P} - \bar{Q}}{\bar{E}_p} \right) \quad (8)$$

335 With \bar{P} and \bar{Q} being long-term mean daily precipitation P (mm d^{-1}) and discharge Q (mm d^{-1}), respectively, and \bar{E}_p the long-term mean daily potential evaporation E_p (mm d^{-1}).

In contrast, the water storage fluctuations and fluxes in the IM-SAS approach were modelled based on a previously developed, process-based model, based on the DYNAMIT modular modelling scheme (Hrachowitz et al., 2013, 2021). Briefly, this hydrological model consists of a suite of storage components and associated water fluxes between them. The influence of functionally different landscape elements, i.e. forest, grass-/cropland and flat valley bottoms, for brevity hereafter referred to as wetland, is represented by parallel hydrological response units (HRU), linked by a common storage component representing the groundwater system (Fig. 2), as previously implemented and successfully tested in many contrasting environments (e.g. Gao et al., 2014; Gharari et al., 2014; Euser et al., 2015; Nijzink et al., 2016; Prenner et al., 2018; Hanus et al., 2021). Briefly, precipitation P (mm d^{-1}) falling on days with temperatures below threshold temperature T_t ($^{\circ}\text{C}$), is accumulated as snow P_{snow} (mm d^{-1}) in the snow storage S_{snow} (mm). On days with temperatures higher than that, precipitation enters the system as rainfall P_{rain} (mm d^{-1}) and, based on a simple degree-day approach, water is released from S_{snow} as snow melt M_{snow} (mm d^{-1}), controlled by melt factor C_{melt} ($\text{mm d}^{-1} \text{ }^{\circ}\text{C}^{-1}$; e.g. Gao et al., 2017; Girons Lopez et al., 2020). Rain water is then routed through the interception storage S_i (mm). With E_i (mm d^{-1}) as interception evaporation at the potential evaporation rate, effective precipitation P_{re} (mm d^{-1}) generated by overflow once the maximum interception capacity ($S_{i\text{max}}$) is exceeded, together with M_{snow} , enters the unsaturated root-zone S_u (mm). From S_u water can then be released as vapor via a combined soil evaporation and transpiration flux E_a (mm d^{-1}). Drainage of liquid water from S_u can either recharge the groundwater S_s (mm) over a percolation flux R_{perc} (mm d^{-1}) and a faster preferential recharge R_{pref} (mm d^{-1}). Alternatively, it can be routed via R_{uf} (mm d^{-1})

to a faster responding component S_f (mm) from where it is directly released to the stream as Q_f (mm d⁻¹), representing lateral preferential flow. Rain and snow melt entering the wetland HRU directly reach S_u . Soil moisture levels in the wetland S_u are further sustained by a fraction of groundwater R_{cap} (mm d⁻¹) that is upwelling into S_u from S_s (e.g., Hulsman et al., 2021a). The detailed equations of the model are provided as Table S3 in the Supplementary Material.

Tracer transport model

$\delta^{18}\text{O}$ and ^3H were routed through the above-described storage components of both the P-SAS and the IM-SAS (Fig. 2) models by sampling the observed (i.e. Q in P-SAS) and modeled outflow volumes (i.e. E_a in P-SAS; all outflows in IM-SAS) that leave the individual components at each time step t (d) (e.g. M_{snow} , R_{perc} , E_a , etc.) from the individual water volumes of different age T (d) that are stored in the associated storage component (e.g. S_{snow} , S_u , etc.) at each time step according to a SAS function. The distribution of water volumes of different ages in each storage component, i.e., the residence time distribution RTD, depends on the past sequence of inflows I (mm d⁻¹) and outflows O (mm d⁻¹) and therefore varies over time. As a consequence of being sampled from RTDs that evolve over time, both, inflows I and outflows O are correspondingly characterized by water age distributions (or transit time distributions TTD) that change over time. A straightforward implementation of this SAS concept is facilitated by the formulation of age-ranked storages $S_T(T,t)$ (mm). As emphasized by Benettin et al. (2017), $S_T(T,t)$ describes “at any time t the cumulative volumes of water in a storage component as ranked by their age T ”. Correspondingly, the total inflow (I) into as well as the total outflow volumes (O) from different storages can be expressed in terms of their cumulative, age-ranked volumes $I_T(T,t)$ and $O_T(T,t)$ (mm d⁻¹). At any time, closing the resulting water age balance for each storage component j (e.g. S_{snow} , S_u , etc.) also leads to an updated age-ranked storage $S_{T,j}(T,t)$ for that component, formulated as (Benettin et al., 2015a; Botter et al., 2011; Harman, 2015; Van Der Velde et al., 2012):

$$\frac{\partial S_{T,j}(T,t)}{\partial t} + \frac{\partial S_{T,j}(T,t)}{\partial T} = \sum_{n=1}^N I_{T,n,j}(T,t) - \sum_{m=1}^M O_{T,m,j}(T,t), \quad (9)$$

Where $\partial S_T / \partial T$ is the aging process of water in storage. Here, the water age balance (Eq.7) was formulated individually for each storage reservoir j , also accounting for different numbers N of storage component inflows I (e.g. P_{rain} , M_{snow} , R_{perc}) and numbers M of outflows O (e.g., R_{perc} , R_{pref} , E_a) (Fig. 2), similar to previous studies (e.g. Hrachowitz et al., 2021). For a daily modelling time step, it can in the water age balance be assumed that precipitation $P(t)$ that is falling on day t is characterized by an age $T = 0$. This implies for the age ranked inflow $I_{T,p,j}(0,t) = P_T(0,t) = P(t)$. Note, that all other age ranked inflows $I_{T,n,j}(T,t)$ that enter a storage component are equivalent to the corresponding age ranked outflows $O_{T,m,j}(T,t)$ that leave a “higher” storage component.

Depending on the total volume of outflow $O_{m,j}(t)$ and the cumulative distribution of ages $P_{o,m,j}(T,t)$ of that flow, an age-ranked outflow $O_{T,m,j}(T,t)$ for each flux m released from each storage component j can be defined as:

$$O_{T,m,j}(T,t) = O_{m,j}(t)P_{o,m,j}(T,t), \quad (10)$$

While the outflow $O_{m,j}(t)$ from any storage component j is computed for each time step t by the hydrological model described

above, the associated $\overline{P_{o,m,j}(T,t)}$ cannot be assumed to be known as it is controlled by the temporally evolving distribution of water ages present in that storage component $S_{T,j}(T,t)$ at t . However, the temporally variable $P_{o,m,j}(T,t)$ can be inferred for each time step t by defining for each storage j and for each outflow m released from j a SAS function $\omega_{o,m,j}$ together with its cumulative form $\Omega_{o,m,j}$. These functions then describe how the water volumes of different ages, stored in component j at time t , i.e. $S_{T,j}(T,t)$, are sampled and combined into the corresponding total outflow volume $O_{m,j}(t)$:

$$P_{o,m,j}(T, t) = \Omega_{o,m,j}(S_{T,j}(T, t), t), \quad (11)$$

The probability density function $p_{o,m,j}(T,t)$ associated with the cumulative distribution of ages $P_{o,m,j}(T,t)$, then represents the transit time distribution TTD of that outflow and can be written as:

$$p_{o,m,j}(T, t) = \omega_{o,m,j}(S_{T,j}(T, t), t) \frac{\partial S_{T,j}}{\partial T}, \quad (12)$$

Conservation of mass dictates that

$$\Omega_{o,m,j}(S_{T,j}(T, t) \rightarrow S_j(t), t) = 1, \quad (13)$$

Where S_j (mm) is the total volume of water stored in component j at time t . The resulting need to rescale $\omega_{o,m,j}$ for each time step was here avoided by instead normalizing and therefore bounding the age ranked storage to the interval $[0,1]$ according to

$$S_{T,norm,j}(T, t) = \frac{S_{T,j}(T,t)}{S_j(t)}, \quad (14)$$

Note that $S_{T,norm,j}$ also represents the RTD of storage component j at time t .

For the P-SAS model implementation in this study, we used power law distributions with one parameter to sample streamflow (k_Q) and evaporation (k_E), respectively, as described by Benettin et al. (2017). In contrast, we used uniform distributions in the form of $\omega = \text{const.}$ as SAS function in each storage component in the IM-SAS model implementations as previously shown to be effective in many studies (e.g. Birkel et al., 2011; van der Velde et al., 2015; Benettin et al., 2015b, 2017; Ala-Aho et al., 2017; Kuppel et al., 2018; Rodriguez et al., 2018). The latter implies random sampling and the assumption that each storage component is fully mixed and that there is no preference for sampling younger or older water. However, note that due to distinct storage capacities and time-scales of the individual storage components, the “combined” SAS functions of all storage components will *not* lead to an overall fully mixed system response. Uniform SAS functions were here chosen over other shapes, such as beta-distributions (e.g. van der Velde et al., 2012; Hrachowitz et al., 2021), as they do not need additional model parameters and avoid the need for explicit calculation of TTDs at each model time step to route tracers through the model (Benettin et al., 2015b), thereby drastically reducing computer memory requirements and computational time (Benettin et al., 2022).

To adequately damp tracer input signals, suitable system storage volumes have to be defined as calibration parameters. In the P-SAS implementation the parameter S_{tot} is used, reflecting the initial total system storage (e.g. Benettin et al., 2017). In

contrast, the IM-SAS implementations made use of additional and hydrologically passive storage volumes (e.g. Christophersen and Wright, 1981; Birkel et al., 2010; Hrachowitz et al., 2015, 2016), which physically represents groundwater volumes below the river bed, as illustrated by Zuber (1986; Fig.1 therein). Such a passive water storage volume $S_{s,p}$ (mm), characterized by $dS_{s,p}/dt = 0$, was thus added as calibration parameter to the active groundwater storage S_s (Fig. 2). While the outflow Q_s from the groundwater storage is exclusively regulated by the temporally varying storage volume in S_s (Supplementary Material Eq. S9), the tracer and age composition of that outflow is also randomly sampled from the total groundwater storage volume $S_{s,tot} = S_s + S_{s,p}$.

The $\delta^{18}O$ and 3H concentrations were then routed through each individual storage component according to (e.g. Harman, 2015; Benettin et al., 2017):

$$C_{o,m,j}(t) = \int_0^{S_j} C_{s,j}(S_{T,j}(T, t), t) \omega_{o,m,j}(S_{T,j}(T, t), t) e^{-\lambda T} dS_T, \quad (15)$$

Where $C_{o,m,j}$ is the tracer concentration in outflow m from storage component j at time t , $C_{s,j}$ is the tracer concentration of water in storage at time t and λ is the radioactive decay constant ($\lambda = 0 \text{ d}^{-1}$ for $\delta^{18}O$ and $\lambda = 0.00015 \text{ d}^{-1}$ for 3H).

4.2 Model implementation

4.2.1 Spatially lumped model implementation

The original argument that the use of seasonally variable tracers' underestimates water ages was exclusively based on lumped, time-invariant implementations of sine-wave and convolution integral models (Stewart et al., 2010). For a baseline comparison and to check whether the above conclusion would also have been reached for our study basin using the same methods, we here similarly implemented the sine-wave (SW-EM, SW-GM) and convolution integral (CO-EM, CO-GM, CO-2EM, CO-3EM, CO-EPM) in a spatially lumped way. For this baseline case the catchment average tracer input was estimated as the spatially weighted mean from the four precipitation zones P1 – P4 as described in section 3.2. The calibration parameters of the CO implementations are shown in Table 2.

The “pure” SAS-model (P-SAS; Table 3) and the spatially lumped implementation of the integrated model (IM-SAS-L) were also forced with the same spatially averaged input. In addition, the spatial fractions of the grassland and wetland HRUs for IM-SAS-L, respectively, were set to 0 and the entire study basin therefore represented by one HRU which is equivalent to the forest HRU described in distributed model, similar to many traditional lumped formulations of process-based conceptual models (Bouaziz et al., 2021; Clark et al., 2008; Fenicia et al., 2006; Fovet et al., 2015; Seibert et al., 2010). This implementation has 11 calibration parameters (Table 3).

4.2.2 Spatially distributed model implementation

To balance the need for spatial detail to some extent with the adverse effects of increased parameter uncertainty (e.g. Beven, 2006) and computational capacity (in particular for the calculation of TTDs), we here implemented the integrated model in

parallel (IM-SAS-D) in the four precipitation zones P1 – P4 and forced it with the corresponding input (e.g. P , $\delta^{18}\text{O}$ and ^3H) for each precipitation zone as described in section 3.2. Each precipitation zone was further discretized (1) into 100 m elevation zones for a stratified representation of the snow storage S_{snow} (e.g. Mostbauer et al., 2018) and (2) into three HRUs, i.e., forest, grassland, wetland (Fig.2; e.g. Gharari et al., 2014; Hanus et al., 2021). Rain P_{rain} and melt water M_{snow} from the different elevation zones was aggregated according to their associated spatial weights in each elevation zone. This total liquid water input was then routed through the three parallel HRUs. The classification into the three HRUs was based on the metric Height-above-nearest-drainage (HAND; Gharari et al., 2011) and land cover. While landscape elements with $\text{HAND} < 5$ m were classified as wetland, all other parts of the landscape were classified as forest or grassland according to land-use data. In total, there are therefore 12 individual, parallel model components, i.e., three HRUs in each of the four precipitation zones, not counting the elevation zones for the snow module. All flux and storage variables of the 12 components are weighted according to their areal fractions. While each of the three HRUs was characterized by individual parameters (e.g. Gao et al., 2016; Prenner et al., 2018), the same parameter values were used in all four precipitation zones in distributed moisture accounting approach (e.g. Ajami et al., 2004; Euser et al., 2015; Hulsman et al., 2021b; Roodari et al., 2021). Overall, the spatially distributed implementation has 19 model parameters, including five global parameters (T_1 , C_{melt} , C_a , K_s and $S_{s,p}$) that are identical for each HRU and 14 HRU-specific parameters (Table 3; Fig.2).

4.3 Model calibration and post-calibration evaluation

The models were run at a daily time step, whereby the observed volume-weighted monthly tracer concentration in precipitation was used as model input for each day of that month together with the daily data of precipitation. Model performance was evaluated based on the Mean Square Error (MSE) as error metric. The time-invariant, lumped convolution integral models, using uniform prior parameter distributions as shown in Table 2, were individually calibrated to the observed $\delta^{18}\text{O}$ (calibration strategy $C_{\delta^{18}\text{O}}$; Table 2) and ^3H stream water concentrations ($C^3\text{H}$), respectively. In contrast, a multi-objective calibration approach was applied for the integrated IM-SAS models to simultaneously reproduce stream flow volumes and tracer concentrations thereof (e.g. ^3H and/or $\delta^{18}\text{O}$). Briefly, the model parameters were calibrated by using Borg_MOEA algorithm (Borg Multi-objective evolutionary algorithm; Hadka and Reed, 2013) and based on uniform prior distributions (Table 3). The model performances were evaluated based on the models' ability to simultaneously reproduce multiple signatures of stream flow as well as signatures of tracer dynamics as shown in Table 3. The sets of pareto optimal solutions obtained from the calibration procedures were then retained as acceptable solutions for the subsequent analysis. To compare the water age distributions (i.e., TTDs and RTDs) and thus to test the research hypothesis, different calibration strategies – $C_{\delta^{18}\text{O},Q}$, $C^3\text{H},Q$ and $C_{\delta^{18}\text{O},^3\text{H},Q}$ – were adopted (Table 3). While in strategy $C_{\delta^{18}\text{O},Q}$ the models were calibrated to simultaneously reproduce signatures of stream flow and $\delta^{18}\text{O}$, $C^3\text{H},Q$ combined the stream flow signatures with ^3H . In strategy $C_{\delta^{18}\text{O},^3\text{H},Q}$ the model was finally calibrated to simultaneously reproduce the six stream flow signatures, $\delta^{18}\text{O}$, and ^3H dynamics. For each strategy, all performance metrics were also combined into an overall performance metric based on the Euclidian distance (D_E), where $D_E = 0$ indicates a perfect fit. To find a somewhat balanced solution in absence of more detailed information all individual

performance metrics were here equally weighted (e.g., Hrachowitz et al., 2021; Hulsman et al., 2021b):

480

$$D_E = \sqrt{\frac{1}{2} \left(\frac{\sum_{n=1}^N (E_{MSE,Q,n})^2}{N} + \frac{\sum_{m=1}^M (E_{MSE,tracer,m})^2}{M} \right)}, \quad (16)$$

485

Where $N = 6$ is the number of performance metrics with respect to stream flow ($E_{MSE,Q,n}$) and M is the number of performance metrics for tracers ($E_{MSE,tracer,m}$) in each combination (e.g. $M=1$ for $C_{\delta^{18}O,Q}$, and $C_{\delta^{18}O,^3H,Q}$, $M=2$ for $C_{\delta^{18}O,^3H,Q}$). Note that the different units and thus different magnitudes of residuals introduce some subjectivity in finding the most balanced overall solution according to D_E (Eq. 16). However, a preliminary sensitivity analysis with varying weights for the individual performance metrics in D_E suggested limited influence on the overall results and is thus not further reported here.

490

After a warm-up period 01/01/1978 – 30/09/2001 the models were calibrated for the 01/10/2001 – 31/12/2009 period. The calibration period was chosen so that observations of all three calibration variables, i.e., Q , 3H and $\delta^{18}O$, are available for the entire calibration period to allow a consistent comparison. The long model warm-up period was deemed necessary to meaningfully approximate the model initial conditions due to the potential and *a priori* unknown relevance of old water in the study basin, and thus to avoid underestimation of water ages inferred from 3H data. The pareto optimal solutions (parameter sets) of the Neckar basin model were then used to test the model in the post-calibration evaluation period 01/01/2010 –

495

31/12/2016. In addition, the model was tested for its ability to represent spatial differences in the hydrological response by evaluating it against streamflow observations in three sub-catchments (C1 – C3) of the Neckar without further re-calibration whereby each one of them largely represents the hydrological response from one of the precipitation zones (Fig. 1). The water age distributions, i.e., TTDs and RTDs, extracted from the individual models and calibration strategies were then estimated based on the corresponding sets of pareto optimal solutions obtained for each calibration strategy.

5 Results

500

5.1 Model performance

505

The stream tracer responses of the lumped baseline models were found to be broadly consistent with the available observations (Table 4). For the SW models (scenarios 1, 2) in particular the sine wave fitted to the stream water $\delta^{18}O$ observations provides a robust characterization of the observed signal with $MSE_{\delta^{18}O} = 0.121$ and 0.144 ‰ for calibration and model evaluation periods, respectively (Supplementary Material Fig. S5). Similarly, the CO models (scenarios 3, 5, 7, 9, 11) reproduced the overall pattern of seasonal fluctuations and the degree of dampening of the $\delta^{18}O$ response (Supplementary Material Fig. S6). The best performing model, the CO-3EM model, was characterized by $MSE_{\delta^{18}O} = 0.171$ and 0.191 ‰ for the calibration and model evaluation periods, respectively while, in comparison, the CO-EM implementation with exhibited considerably higher errors with $MSE_{\delta^{18}O} = 0.327$ and 0.432 ‰ (Table 4). When used with 3H data (scenarios 4, 6, 8, 10, 12), the CO models do

capture the general decrease in the magnitude of stream water ^3H concentrations although fluctuations at shorter timescales are not well reproduced (Supplementary Material Fig. S7). The CO-2EM model gives the best performance with $\text{MSE}^3\text{H} = 5.171$ and 3.964 TU^2 for the calibration and evaluation periods, respectively, while the CO-EPM model resulted in $\text{MSE}^3\text{H} = 5.926$ and 5.115 TU^2 (Table 4). It is also noted that the models already mimic the ^3H response well in the 1978 – 2001 pre-calibration model warm-up period.

The P-SAS implementations (scenarios 13 – 15; Table 5; Fig. 3a – d and Fig. 4a – d) show a somewhat higher skill to reproduce the dampening of $\delta^{18}\text{O}$ response with $\text{MSE}_{\delta^{18}\text{O}} = 0.069 – 0.078 \text{ ‰}$ for the calibration and $0.215 – 0.231 \text{ ‰}$ for the evaluation periods, respectively, as well as the general decrease in the magnitude of stream water ^3H with $\text{MSE}^3\text{H} < 3 \text{ TU}^2$. In contrast to the above, the implementations of the integrated model IM-SAS (Table 5) aim to not only to reproduce the $\delta^{18}\text{O}$ or ^3H stream signals, but to additionally and simultaneously describe the hydrological response (Table 5). Both, the lumped IM-SAS-L (scenario 16; Supplementary Material Fig. S10a, b) and the distributed IM-SAS-D (scenario 19; Fig. 3e, f) reproduce the seasonal fluctuations as well as the degree of dampening of the $\delta^{18}\text{O}$ signals with $\text{MSE}_{\delta^{18}\text{O}} = 0.079 – 0.083 \text{ ‰}$ for the calibration and $0.273 – 0.332 \text{ ‰}$ for the evaluation periods similar to or better than the baseline SW/CO models. The IM-SAS models do also describe the evolution of the ^3H stream signals rather well (scenarios 17 and 20). With $\text{MSE}^3\text{H} < 3 \text{ TU}^2$, IM-SAS-L (Supplementary Material Fig. S11) and IM-SAS-D (Fig. 4e – h) do not only outperform the baseline models with respect to the overall magnitude of ^3H , but do, in spite of somewhat underestimating the magnitude of seasonal amplitudes, also provide a better representation of these intra-annual fluctuations. Similar to the SW/CO baseline models, both the P-SAS and IM-SAS implementations also very well capture the overall decline of the stream water ^3H levels in the 1978 – 2001 pre-calibration model warm-up period. The simultaneous calibration to the hydrological response and the $\delta^{18}\text{O}$ and ^3H stream signals (scenarios 18 and 21) led to a comparable model skill to reproduce the tracer signals. In addition to the tracer concentrations, all IM-SAS implementations do also reproduce the main features of the hydrological response (Table 5). More specifically, the modelled hydrographs in particular describe well the timing of peaks as well as the shape of recessions, although in some cases peak flows were underestimated and low flows overestimated as shown for scenario 21 in Figure 5 (for scenarios 16 – 20 see Supplementary Material Figs. S12 – S16). The resulting in MSE_Q remains $\leq 0.336 \text{ mm}^2 \text{ d}^{-2}$ across all IM-SAS implementations (scenarios 16 – 21). Crucially, the models also reproduce well the other observed stream flow signatures such as the flow duration curves ($\text{MSE}_{\text{FDCQ}} \leq 0.047 \text{ mm}^2 \text{ d}^{-2}$; Fig. 5d), the seasonal runoff coefficients ($\text{MSE}_{\text{RC}} \leq 0.008$; Fig. 5e) and the autocorrelation functions ($\text{MSE}_{\text{ACQ}} \leq 0.007$; Fig. 5f). The model, calibrated on the overall response of the Neckar basin, also exhibited considerable skill to represent spatial differences in the hydrological response by reproducing observed stream flow in the three sub-catchments (C1 – C3) similarly well (Fig.6) without any further re-calibration.

5.2 Model parameters

Parameters of the SW/CO baseline models (scenarios 1 – 12) directly define the shapes of parametric TTDs and thus the associated metrics of water age, such as MTT following Eqs. (3 – 7). The CO models representing ^3H signals (scenarios 4, 6, 8, 10, 12) are characterized by values of parameters β_1 , β_2 and β_3 that are by a factor of up to ~ 10 higher than the same

parameters of models calibrated to $\delta^{18}\text{O}$ signals (Table 2). For example, $\beta_1 = 513$ d for the CO-EM in scenario 3 and 3795 d in scenario 4.

The individual parameters of the P-SAS and IM-SAS model implementations (scenarios 13 – 21), in contrast, do not directly define parametric TTDs nor can they be readily and directly be linked to water ages. However, it has been previously shown that the sizes of water storage volumes is an important control on water ages (e.g. Harman, 2015) and that in particular total storage volumes, represented by parameter S_{tot} in P-SAS, and the hydrologically passive storage volumes, represented by parameter $S_{\text{s,p}}$ in IM-SAS models, are key to regulate in particular older water ages in many systems (e.g. Hrachowitz et al., 2016). Calibration of P-SAS to $\delta^{18}\text{O}$ in scenario 13 suggested $S_{\text{tot}} \sim 15595$ mm while calibration of the lumped IM-SAS-L to $\delta^{18}\text{O}$ and stream flow ($C_{\delta^{18}\text{O},\text{Q}}$) in scenario 16 led to a moderately well identifiable range of this parameter $S_{\text{s,p}} \sim 4107 - 10029$ mm across all pareto optimal solutions and in the same order of magnitude as P-SAS (Fig. 7a, Table 3). Reflecting the water storage capacity in the unsaturated root zone, which is an important control on younger water ages (Hrachowitz et al., 2021), the parameter S_{umaxF} was found to range between $\sim 314 - 415$ mm (Fig. 7b, Table 3) for the same IM-SAS-L scenario. The calibration of the same models to ^3H (scenarios 14, 17) resulted in a similar parameter ranges for $S_{\text{tot}} \sim 16638$ mm, $S_{\text{s,p}} \sim 3924 - 9339$ mm (Fig. 7a) as well as, albeit slightly lower, $S_{\text{umaxF}} \sim 236 - 355$ mm (Fig. 7b). The similarities between these two scenarios are also reflected in the parameter ranges obtained from the simultaneous calibration to $\delta^{18}\text{O}$ and ^3H ($C_{\delta^{18}\text{O},^3\text{H},\text{Q}}$) in scenarios 15 and 18. The calibration of the distributed IM-SAS-D model following all the three calibration strategies in scenarios 19 – 21, resulted in values for $S_{\text{s,p}} \sim 3270 - 9011$ mm (Fig. 7c) that are broadly in the similar ranges as for IM-SAS-L ($S_{\text{s,p}} \sim 3924 - 13676$ mm). In contrast, the distinction into the individual HRUs led to clear differences between S_{umaxF} , S_{umaxG} and S_{umaxW} (Figs. 7d-f), reflective of the different hydrological functioning of these HRUs. Nevertheless, the area-weighted average of these parameters comes close to the equivalent parameter from the lumped model implementation (S_{umaxF}). The general consistency of these parameters obtained from the different calibration strategies is exacerbated by the limited differences in the most balanced solutions (smallest D_{E}) between the different scenarios. For example the most balanced solutions of $S_{\text{s,p}}$ fall between $\sim 4000 - 5000$ mm for all IM-SAS scenarios 16 – 21 (Fig. 7a, c). All other parameters, which are less clearly related to water ages, exhibit different levels of variation across the individual scenarios yet not following any clear and systematic pattern (Table 3).

5.3 Water age distributions

Based on a $\delta^{18}\text{O}$ amplitude ratio $A_s/A_p = 0.21$ (Table 2), the results of the SW models (scenarios 1, 2) suggest a system that is characterized by rather young stream water with MTT $\sim 0.7 - 1.8$ yr, depending on the choice of TTD (Table 6; Fig. 8). The TTDs obtained from the CO models calibrated to $\delta^{18}\text{O}$ (scenarios 3, 5, 7, 9, 11) are broadly consistent with that, suggesting MTT $\sim 1.4 - 2.4$ yr. These TTDs suggest mean water ages that are up to ~ 9 yr lower than estimates from CO models calibrated to ^3H (scenarios 4, 6, 8, 10, 12) with MTT $\sim 9.4 - 10.4$ yr (Table 6; Fig. 8). For higher percentiles the differences in water ages can even reach more than 20 years (Table 6). Correspondingly, the fractions of water younger than 3 months, $F(T < 3 \text{ m})$, exhibit considerable differences of $-2 - 22\%$ points between $\delta^{18}\text{O}$ and ^3H inferred estimates, which further increase to

575 differences of 30 – 64% for $F(T < 3 \text{ yr})$.

In contrast, from the implementations of the P-SAS and IM-SAS models in scenarios 13 – 21, it can be clearly seen that the stream water ages inferred from $\delta^{18}\text{O}$ are across most percentiles by a factor of around 10 higher than those from SW and CO models, resulting in volume-weighted average MTT $\sim 11 - 17$ yr over the modelling period (Table 7; Fig. 9). Similarly, all water fractions below 20 years are substantially lower for the P-SAS and IM-SAS models than for SW and CO models. The most pronounced difference is observed at $F(T < 5 \text{ yr})$ that reaches 38 – 57% for SAS-functions models and 91 – 100% for SW and CO, which equals to a difference of more than 50%. As such, these water age estimates from $\delta^{18}\text{O}$ in SAS-function models (scenarios 13, 16, 19) are not only very similar to the estimates from ^3H in these models (scenarios 14, 17, 20) but $\delta^{18}\text{O}$ suggests, against the expectations, even slightly *older* water than ^3H does. More specifically, while $\delta^{18}\text{O}$ results in stream water MTT 11 -17 yr (scenarios 13, 16, 19), the ^3H -based estimates reach MTT $\sim 11 - 13$ yr (scenarios 14, 17, 20) and thus up to 585 five years younger (Table 7; Fig. 9). The differences between $\delta^{18}\text{O}$ and ^3H water ages from individual P-SAS and IM-SAS model implementations (scenarios 13 – 21) are similar over all percentiles with $\Delta\text{TT}_{\delta^{18}\text{O},^3\text{H}}$, on average, ~ 1.4 yr and not exceeding ~ 5.5 yr. Accordingly, the fractions of water of any given age up to $T < 20$ years is $\sim 1 - 8$ % higher for ^3H than for $\delta^{18}\text{O}$, suggesting higher fractions of old water modelled with $\delta^{18}\text{O}$ (Table 7). Equivalent pattern and comparable magnitudes are found for the combined use of $\delta^{18}\text{O}$ and ^3H in scenarios 15, 18 and 21.

590 An explicit comparison between the lumped IM-SAS-L (scenarios 16 – 18) and the distributed IM-SAS-D (scenarios 19 – 21) also suggests a good correspondence between the respective inferred water ages for both tracers. While IM-SAS-L generates MTT $\sim 11.2 - 17.4$ years, the MTT obtained from IM-SAS-D reach $\sim 12.8 - 15.6$ years (Table 7, Fig. 9). Besides the MTT, also the differences in water ages across all percentiles is minor and reaches a maximum of 4.6 years at the 75th percentile. Accordingly, the fractions of water with ages $T < 20$ yr exhibit only marginal differences between the lumped (IM-SAS-L) and 595 distributed model (IM-SAS-D) implementations. It is noted that these overall water ages from IM-SAS-D for the entire Neckar basin emerge from the aggregation of TTDs of the four individual precipitation zones P1 – P4 (Supplementary Material Figure S31-33 and Table S6), which are characterized by pronounced differences with MTT ranging from $\sim 8 - 10$ years in P4 and $\sim 18 - 22$ years in P2, depending on the scenario.

The consistency between water ages inferred from $\delta^{18}\text{O}$ and ^3H , respectively, in all SAS-function model scenarios is further 600 illustrated by the direction and magnitude of change in water age distributions as a consequence of changing wetness conditions. In particular during wet-up and wet periods, a marked variability of daily TTDs can be observed, with young water fractions $F(T < 3 \text{ m})$ ranging between $\sim 20 - 65\%$ for $\delta^{18}\text{O}$ -based estimates and $\sim 25 - 70\%$ for ^3H (Fig. 10a, b, e, f). Less variability in daily TTDs is found under drying and dry conditions with generally $F(T < 3 \text{ m})$ in the range of $\sim 1 - 20\%$, with only very few outliers $> 30\%$. Overall, the volume-weighted average TTDs for wet conditions suggest slightly older water inferred from $\delta^{18}\text{O}$ 605 with a median water age of ~ 3 year and $F(T < 3 \text{ m}) \sim 30\%$, for wet conditions than from ^3H , for which a median age of ~ 1 year and $F(T < 3 \text{ m}) \sim 40\%$ were found (Fig. 10d, h). This is in opposite to dry conditions for which the differences between $\delta^{18}\text{O}$ and ^3H -derived water age estimates become mostly negligible (Fig. 10d, h).

With P-SAS and IM-SAS models, not only MTT/TTD in streams can be derived but also in any fluxes/storages (i.e.,

transpiration flux E_a , ground water storage). An even more pronounced young water variability in daily TTDs was found for the transpiration flux E_a leaving the unsaturated root zone storage S_u in the IM-SAS models (scenarios 16 – 21). As shown in Figure 11a, the transpiration TTDs inferred from $\delta^{18}\text{O}$ suggest a median transpiration age during wet conditions of $\sim 2 - 40$ days and $F(T < 3 \text{ m}) \sim 60 - 100\%$. This variability shifts to median ages between $\sim 30 - 100$ days and $F(T < 3 \text{ m}) \sim 30 - 95\%$ for dry conditions. This pattern of variability in daily TTDs in wet and dry periods is very closely matched by the estimates based on ^3H (Fig. 11b). Overall, the volume-weighted average TTDs of transpiration suggest median ages of around 14 days for wet conditions and between 35 days (^3H) and 70 days ($\delta^{18}\text{O}$) for dry conditions (Fig. 11d).

The modelled groundwater, in comparison, was found to be characterized by substantially less temporal variability in TTDs and older water ages (Fig. 12). The TTDs inferred from both, $\delta^{18}\text{O}$ and ^3H , are similar and characterized by a median age of ~ 10 years under both, wet and dry conditions. While $F(T < 3 \text{ m})$ of the groundwater largely remains $< 1\%$, around 20 – 25 % of the groundwater is older than 20 years.

6 Implications, limitations and unresolved questions

What can we learn from the above? We believe the results obtained in this study have several implications for the utility of different tracer and model types, as described in detail below.

6.1 The individual roles of the choices of tracers and models for underestimation of water ages

The overall magnitude of water ages here estimated from time-invariant, lumped SW and CO models in combination with $\delta^{18}\text{O}$ reach MTTs of ~ 2 years (Table 6, Fig. 8). These values fall within the age ranges reported for comparable model experiments with seasonally variable tracers in many other catchments world-wide (see McGuire and McDonnell, 2006; Godsey et al., 2009; Hrachowitz et al., 2009; Stewart et al., 2010 and references therein). Similarly, the water ages estimated with the same CO models in combination with ^3H are with MTTs ~ 10 yrs by a factor of ~ 5 higher (Table 6, Fig. 8), and also well reflect the findings of previous studies, many of which suggest ^3H -inferred catchment MTTs of $\sim 10 - 15\text{yr}$ (Stewart et al., 2010 and references therein). This suggests that the Neckar basin does not exhibit unusual or unexpected water age characteristics. By themselves, these results would therefore lend further supporting evidence for the interpretation provided by Stewart et al. (2010) and, crucially, lead us to the same conclusion, that the use of $\delta^{18}\text{O}$ and comparable seasonally variable tracers truncate stream water ages.

However, and in stark contrast, the estimates of water age obtained from all P-SAS and IM-SAS model implementations in this study, i.e., scenarios 13 – 21, are similar to each other irrespective of the tracer used. Water ages estimated from $\delta^{18}\text{O}$ are, with $\text{MTT} > 11.4 \text{ yr}$, not only substantially older than those inferred from the SW and CO models (scenarios 1 – 3, 5, 7, 9, 11), but, most importantly, similar to those inferred from ^3H in P-SAS and IM-SAS models, which reach $\text{MTT} \sim 11 - 13 \text{ yr}$ (Table 7, Fig. 9). These water ages highlight the importance of old water in the Neckar basin, similar to what is suggested by the use of ^3H in CO models (scenarios 4, 6, 8, 10, 12).

640 It is important to note that the IM-SAS and, to a lesser degree, P-SAS models can simultaneously reproduce several signatures of the hydrological response together with the $\delta^{18}\text{O}$ and ^3H stream water signals. They therefore provide a more holistic description of physical transport processes in the system (Table 7, Fig. 3 – 5) than the SW and CO models, which mimic one single tracer signal and thus one isolated variable at a time. In addition, the P-SAS and IM-SAS model parameters that are most linked to tracer circulation, e.g. S_{tot} , $S_{\text{s,p}}$ and S_{umax} (Fig. 7), exhibit little difference when obtained from calibration to $\delta^{18}\text{O}$ or ^3H , respectively. This implies that both, $\delta^{18}\text{O}$ and ^3H , provide similar information about how tracers are routed through the model and how water is stored in and released from the system. As a consequence, also the *simultaneous* representation of all three types of variables under consideration, i.e., the hydrological response as well as the $\delta^{18}\text{O}$ and ^3H stream signals, in these models is consistent with the observed data (scenarios 18, 21).

645 The above is further corroborated by how water ages in the Neckar basin respond to changing wetness conditions. Although not identical, $\delta^{18}\text{O}$ and ^3H -inferred daily TTDs exhibit nevertheless broad agreement in the directions and magnitudes of change in response to changing wetness conditions (Fig. 10). Changes in stream flow TTDs in IM-SAS are not primarily caused by changes of water ages within individual storage components. In particular, the modelled water age distributions in the groundwater S_s show limited sensitivity to changing wetness conditions, with MTT varying between ~ 18 years in dry periods and ~ 17 years in wet periods (Fig. 12). The TTDs in the transpiration flux E_a , which are reflective of the water ages in the unsaturated root zone S_u , exhibit with MTTs between ~ 0.20 and 0.12 years in dry and wet periods (Fig. 11), respectively, magnitudes and fluctuations over time that are similar to what has been previously reported in other studies (e.g., Hrachowitz et al., 2015; Soulsby et al., 2016; Visser et al., 2019; Birkel et al., 2020; Kuppel et al., 2020). However, the level of these age fluctuations alone is insufficient to explain the magnitude of change in stream flow TTDs, which can vary by several years. Instead, the temporal variability of stream flow TTDs is largely controlled by switches in the relative contributions of individual storage components to stream flow under different wetness conditions. Under increasingly wet conditions, considerably increasing proportions of comparably young water from S_U contribute over shallow preferential flow pathways (S_F) to stream flow, while the relative proportion of groundwater contributing to stream flow under such conditions is reduced (Hrachowitz et al., 2013). Both tracers, $\delta^{18}\text{O}$ and ^3H , generate these patterns in a corresponding way.

655 Altogether, this suggests that the P-SAS and IM-SAS models and the resulting estimates of water ages inferred from both, $\delta^{18}\text{O}$ and ^3H , provide plausible descriptions of transport processes and thus water ages in the Neckar basin. Clearly, with current observation technology, it is impossible to know the real water age distribution at river basin scale. However, the water ages and their temporal variability inferred from both, $\delta^{18}\text{O}$ and ^3H using P-SAS and IM-SAS models are widely consistent. This is suggestive that it is not the use of $\delta^{18}\text{O}$ *per se* that leads to truncation of TTDs, but rather that time-invariant, lumped convolution integral models are incapable of extracting sufficient information from $\delta^{18}\text{O}$ signals. These results mirror anecdotal evidence from several previous studies (e.g., Hrachowitz et al., 2015, 2021; Ala-aho et al., 2017; Buzacott et al., 2020; Yang et al, 2021). Although no direct comparison with ^3H data is provided in these studies, they demonstrated the potential of $\delta^{18}\text{O}$ in SAS-based model approaches to estimate water age distributions with considerable fractions of water older than 5 – 10 years and Birkel et al. (2020) explicitly estimated MTTs of up to 18 years. Our results also strongly support the findings and general

675 conclusions of Rodriguez et al. (2021), who undertook a direct comparison of water ages inferred from $\delta^{18}\text{O}$ and ^3H . In their study for a small catchment and based on shorter tracer time series, i.e., 2 years, and a system that is characterized by rather low MTT of ~ 3 years, they found that although ^3H led to higher MTTs than $\delta^{18}\text{O}$, the absolute difference between these ages estimates was with 0.2 years limited and even decreasing for higher percentiles of the water age distributions.

We therefore argue that the evidence emerging from our results and the above considerations is strong enough to reject the hypothesis that $\delta^{18}\text{O}$ as a tracer generally and systematically “cannot see water older than about 4 years” (Stewart et al., 2010, 680 2012) and the corresponding tails in water age distributions, leading to underestimations of water ages. We further argue that previous underestimations of water ages are rather a consequence of the use of **time-invariant**, lumped parameter convolution integral model techniques that cannot resolve the information contained $\delta^{18}\text{O}$ signals in a meaningful way for catchments with transient flow conditions. **In contrast, the combined information using hydrological and tracer data and thus the consideration of transient flow conditions results in similar MTTs**, independent of the used tracer. **Note, that for this reason, time-variant implementations of convolution integral models that can describe transient conditions may hold the potential to similarly generate water age estimates from $\delta^{18}\text{O}$ signals that reflect the results of the P-SAS and IM-SAS models tested here.**

685 However, and notwithstanding the rejection of the above hypothesis it is important to note that overall and in spite of the similarity between $\delta^{18}\text{O}$ and ^3H inferred water ages in the study basin on the basis of **P-SAS and** IM-SAS models, there may be no general equivalence between $\delta^{18}\text{O}$ and ^3H tracers. Instead, it is plausible to assume that differences will gradually increase with higher water ages. In systems characterized by water older than the water in the Neckar study basin, and where the amplitudes of the $\delta^{18}\text{O}$ stream signal are attenuated to below the analytical precision, the water age estimates from $\delta^{18}\text{O}$ will indeed become subject to increasing uncertainty up to the point where further attenuation and thus older water ages cannot be discerned anymore independent of modelling approaches. The specific magnitude of such a water age threshold remains difficult to quantify with the available data. However, given the results in the Neckar study basin, the question raised by Stewart et al. (2021), if $\delta^{18}\text{O}$ allows to see “the full range of travel times”, can to some extent be answered: it can be assumed that, 695 when used with a suitable model, $\delta^{18}\text{O}$ contains sufficient information for a meaningful characterization of water ages in systems characterized by MTTs of at least $\sim 15 - 20$ years, which encompasses the vast majority of river basins so far analyzed in literature (see Stewart et al., 2010 and references therein). As a step forward, the original hypothesis above can, for future research, be reformulated into: $\delta^{18}\text{O}$ -inferred water age estimates are subject to increasing uncertainty and bias when compared to ^3H -inferred estimates when stream water MTTs of $\sim 15 - 20$ years are exceeded in systems characterized by increasingly 700 old water.

6.2 The role of spatial aggregation on underestimation of water ages

In addition to the above, Kirchner (2016) demonstrated that the use of seasonally variable tracers with **time-invariant**, lumped parameter model approaches, i.e., SW and CO, has considerable potential to underestimate water ages due to **spatial aggregation of heterogeneous MTTs in systems characterized by large spatial contrasts in MTTs**. We could here not reproduce that exact experiment, as stream observations were available only at one location for each tracer. However, in the distributed

implementation of the IM-SAS-D model (scenarios 19 – 21), we nevertheless explicitly accounted, albeit to a limited degree, for heterogeneity in the system input variables as well as for potential differences in landscape types, as expressed by the three model HRUs. This resulted in different TTDs for the individual precipitation zones (Supplementary Material Figures S31-S33 and Table S6) and elevation zones and HRUs therein (not shown). The comparison between the lumped IM-SAS-L (scenarios 16 – 18) and the distributed IM-SAS-D models does not show major differences in their ability to reproduce the various hydrological signatures nor the $\delta^{18}\text{O}$ and ^3H stream signals (Table 5). Against evidence from various previous studies (e.g., Euser et al., 2015; Gao et al., 2016; Nijzink et al., 2016; Nguyen et al., 2022), this reflects to some degree the conclusion by Loritz et al. (2021), who found in a comparative analysis that distributed model implementations do not necessarily improve a model's ability to reproduce the hydrological response as compared to spatially lumped formulations. In addition, the contrasts in water ages between the discretized model components, with MTTs reaching from ~ 8 to ~ 22 yrs in the individual precipitation zones, may not be sufficient to significantly affect basin overall MTTs. As a consequence, the results of IM-SAS-L and IM-SAS-D also do not show major differences in the associated water age estimates, with MTTs ~ 11 – 17 yrs and 12 – 16 yrs, respectively (Table 7, Fig. 9).

How can this be interpreted? If significantly older ages were inferred from the distributed IM-SAS-D implementation, this would have provided strong supporting evidence for the role and effect of spatial heterogeneity on water ages as demonstrated by Kirchner (2016). However, the similar water ages inferred from the spatially lumped and distributed implementations, respectively, allow two possible but mutually contradicting interpretations. Either, it could indicate that the aggregation of spatial heterogeneity does not have any discernible effect on water ages inferred from the IM-SAS model in the study basin or, on the contrary, the spatial contrasts in water ages, limited by the spatial resolution of the model and the available data, were not sufficient to detect any significant differences. The evidence found here therefore remains inconclusive and further research is required to describe the role of the aggregation of spatial heterogeneity for estimates of water ages using IM-SAS type of models.

For any estimates of water ages in this study – as in any other study – it is important to bear in mind that they are conditional on the available data and models used. Uncertainties can and do arise from both, data and from decisions taken in the modelling process (e.g., Beven, 2006; Kirchner, 2006). One challenge in this study was that precipitation $\delta^{18}\text{O}$ and ^3H compositions were only available at rather coarse spatial and temporal resolutions. We have used the best available information to spatially extrapolate the tracer precipitation data from the individual sampling stations to estimate their spatial variation across the Neckar basin including stations outside the study basin. The monthly $\delta^{18}\text{O}$ and ^3H distribution in precipitation within South-Germany is generally similar (Stumpp et al. 2014; Schmidt et al. 2020); still, regional correction for $\delta^{18}\text{O}$ might not be sufficient to explain local differences in $\delta^{18}\text{O}$ precipitation data. A similar limitation applies to the temporal resolution of tracer composition in precipitation as only monthly information was available. However, as the available data nevertheless reflect the seasonal variation in $\delta^{18}\text{O}$ and ^3H precipitation input, the uncertainties arising can be assumed to largely affect the short-term dynamics of tracers in the stream and thus rather young water ages, whereas the objective of our analysis was focused on the right tail of the water age distributions and thus on old ages. Notwithstanding these uncertainties, the overall model

performances with respect to the hydrological and tracer responses, suggest that the choice of input data and the model formulations led to model results that are largely consistent with the observed responses in the stream. The observation that there is little ambiguity in the results further suggests that the remaining uncertainties are unlikely to affect the overall interpretation and conclusions of this study.

745 7 Conclusions

$\delta^{18}\text{O}$ and ^3H are frequently used as tracers in environmental sciences to estimate age distributions of water. However, it has previously been argued that seasonally variable tracers, such as $\delta^{18}\text{O}$, fail to detect the tails of water age distributions and therefore substantially underestimate water ages as compared to radioactive tracers, such as ^3H . In this study for the Neckar River basin in central Europe and based on a >20-year record of hydrological, $\delta^{18}\text{O}$ and ^3H data we systematically scrutinized the above postulate by comparing water age distributions inferred from $\delta^{18}\text{O}$ and ^3H with a total of 21 different model implementations. The main findings of our analysis are the following:

(1) Water ages inferred from $\delta^{18}\text{O}$ with commonly used time-invariant, sine wave (SW) and lumped parameter convolution integral models (CO) are with MTTs $\sim 1 - 2$ years substantially lower than those obtained from ^3H with the same models, reaching MTTs ~ 10 years.

755 (2) In contrast, the concept of SAS-functions in combination with hydrological models (P-SAS, IM-SAS) did not only allow simultaneous representations of water storage fluctuations together with $\delta^{18}\text{O}$ and ^3H stream signals, but water ages inferred from $\delta^{18}\text{O}$ were with MTTs $\sim 11 - 17$ years much higher and even higher than inferred from ^3H , which suggested MTTs $\sim 11 - 13$ years.

760 (3) Constraining P-SAS and IM-SAS model implementations individually with $\delta^{18}\text{O}$ and ^3H observations resulted in similar values for parameters that control water ages, such as the total storage S_{tot} (P-SAS) or passive groundwater volumes $S_{\text{s,p}}$ (IM-SAS). In addition, $\delta^{18}\text{O}$ and ^3H -constrained models both exhibited limited differences in the magnitudes of water ages in different parts of the models as well as in the temporal variability of TTDs in response to changing wetness conditions. This suggests that both tracers lead to comparable descriptions of how water is routed through the system.

765 (4) Based on the points above, we reject the hypothesis that $\delta^{18}\text{O}$ as a tracer generally and systematically “cannot see water older than about 4 years” (Stewart et al., 2010, 2012) and that it truncates the corresponding tails in water age distributions, leading to underestimations of water ages.

(5) Instead, our results provide evidence of broad equivalence of $\delta^{18}\text{O}$ and ^3H as age tracers for systems characterized by MTTs of at least 15 – 20 years.

770 (6) The question to which degree aggregation of spatial heterogeneity can further adversely affect estimates of water ages remains unresolved as the lumped and distributed implementations of the IM-SAS model provided similar and thus inconclusive results.

Overall, this study demonstrates that previously reported underestimations of water ages are most likely not a result of the use

of $\delta^{18}\text{O}$ or other seasonally variable tracers *per se*. Rather, these underestimations can be largely attributed to the choices of model approaches which rely on assumptions not frequently met in catchment hydrology. Given the vulnerability of lumped, time-invariant parameter convolution integral approaches in combination with $\delta^{18}\text{O}$ to substantially underestimate water ages due to transient flow conditions, spatial aggregation and potentially other, still unknown effects, we therefore strongly advocate to avoid the use of this model type in combination with seasonally variable tracers and to instead adopt SAS-based or other model formulations that allow for the representation of transient conditions.

Code availability. The model codes underlying this paper will be available online in the 4TU data repository (DOI: 10.4121/b75c9108-c5b8-4266-9b82-1ad08c76adcc). The equations used in the model are described in supplement.

Data availability. The meteorological and hydrological data used in this study can be obtained from German Weather Service (DWD) and the German Federal Institute of Hydrology (BfG). Both $\delta^{18}\text{O}$ and ^3H input data used in this study can be obtained from the WISER database portal of the International Atomic Energy Agency (http://www-naweb.iaea.org/naweb/ih/IHS_resources_gnip.html). Both $\delta^{18}\text{O}$ and ^3H output data used in this study can be made available by Christine Stumpp upon request.

Author contributions. SW, MH and GS designed the study, SW executed the experiments, all authors contributed to general idea, the discussion and writing of the manuscript.

Competing interests. Some authors are members of the editorial board of the HESS journal. The peer-review process was guided by an independent editor, and the authors have also no other competing interests to declare.

Disclaimer. Publisher's note: Copernicus Publications remains neutral with regard to jurisdictional claims in published maps and institutional affiliations.

Acknowledgements. We thank Dr. Axel Schmidt of BAFG for valuable assistance with and information on tritium data. We gratefully acknowledge financial support from China Scholarship Council (CSC). We would like to thank the editor and two reviewers for providing a list of critical and very valuable comments that helped to considerably improve the manuscript.

References

Ajami, N. K., Gupta, H., Wagener, T., and Sorooshian, S.: Calibration of a semi-distributed hydrologic model for streamflow estimation along a river system, *J. Hydrol.*, 298, 112–135, <https://doi.org/10.1016/j.jhydrol.2004.03.033>, 2004.

Ala-Aho, P., Tetzlaff, D., McNamara, J. P., Laudon, H., and Soulsby, C.: Using isotopes to constrain water flux and age

- 805 estimates in snow-influenced catchments using the STARR (Spatially distributed Tracer-Aided Rainfall–Runoff) model, *Hydrol. Earth Syst. Sci.*, 21, 5089-5110, <https://doi.org/10.5194/hess-21-5089-2017>, 2017.
- Allen, S. T., Kirchner, J. W., and Goldsmith, G. R.: Predicting spatial patterns in precipitation isotope ($\delta^2\text{H}$ and $\delta^{18}\text{O}$) seasonality using sinusoidal isoscapes, *Geophysical Research Letters*, 45, 4859-4868, <https://doi.org/10.1029/2018GL077458>, 2018.
- 810 Allen, S. T., Jasechko, S., Berghuijs, W. R., Welker, J. M., Goldsmith, G. R., and Kirchner, J. W.: Global sinusoidal seasonality in precipitation isotopes, *Hydrol. Earth Syst. Sci.*, 23, 3423-3436, <https://doi.org/10.5194/hess-23-3423-2019>, 2019.
- Asadollahi, M., Stumpp, C., Rinaldo, A., and Benettin, P.: Transport and water age dynamics in soils: A comparative study of spatially integrated and spatially explicit models, *Water Resour. Res.*, 56, e2019WR025539, <https://doi.org/10.1029/2019WR025539>, 2020.
- 815 Barnes, C. and Bonell, M.: Application of unit hydrograph techniques to solute transport in catchments, *Hydrological Processes*, 10, 793-802, [https://doi.org/10.1002/\(SICI\)1099-1085\(199606\)10:6<793::AID-HYP372>3.0.CO;2-K](https://doi.org/10.1002/(SICI)1099-1085(199606)10:6<793::AID-HYP372>3.0.CO;2-K), 1996.
- Begemann, F. and Libby, W. F.: Continental water balance, ground water inventory and storage times, surface ocean mixing rates and world-wide water circulation patterns from cosmic-ray and bomb tritium, *Geochimica et Cosmochimica Acta*, 12, 277-296, [https://doi.org/10.1016/0016-7037\(57\)90040-6](https://doi.org/10.1016/0016-7037(57)90040-6), 1957.
- 820 Benettin, P., Kirchner, J. W., Rinaldo, A., and Botter, G.: Modeling chloride transport using travel time distributions at Plynlimon, Wales, *Water Resour. Res.*, 51, 3259-3276, <https://doi.org/10.1002/2014WR016600>, 2015a.
- Benettin, P., Soulsby, C., Birkel, C., Tetzlaff, D., Botter, G., and Rinaldo, A.: Using SAS functions and high-resolution isotope data to unravel travel time distributions in headwater catchments, *Water Resour. Res.*, 53, 1864-1878, <https://doi.org/10.1002/2016WR020117>, 2017.
- 825 Benettin, P., Nehemy, M. F., Asadollahi, M., Pratt, D., Bensimon, M., McDonnell, J. J., and Rinaldo, A.: Tracing and closing the water balance in a vegetated lysimeter, *Water Resour. Res.*, 57, e2020WR029049, <https://doi.org/10.1029/2020WR029049>, 2021.
- Benettin, P., Bailey, S. W., Campbell, J. L., Green, M. B., Rinaldo, A., Likens, G. E., McGuire, K. J., and Botter, G.: Linking water age and solute dynamics in streamflow at the Hubbard Brook Experimental Forest, NH, USA, *Water Resour. Res.*, 51, 9256-9272, <https://doi.org/10.1002/2015WR017552>, 2015b
- 830 Benettin, P., Rodriguez, N. B., Sprenger, M., Kim, M., Klaus, J., Harman, C. J., Van Der Velde, Y., Hrachowitz, M., Botter, G., McGuire, K. J., Kirchner, J. W., Rinaldo, A., McDonnell, J. J.: Transit time estimation in catchments: Recent developments and future directions, *Water Resour. Res.*, <https://doi.org/10.1029/2022WR033096>, 2022
- Bergström, S., Carlsson, B., Sandberg, G., and Maxe, L.: Integrated modelling of runoff, alkalinity, and pH on a daily basis, *Hydrology Research*, 16, 89-104, <https://doi.org/10.2166/nh.1985.0008>, 1985.
- 835 Beven, K.: Searching for the Holy Grail of scientific hydrology: $Q_t = (S, R, \Delta t) A$ as closure, *Hydrol. Earth Syst. Sci.*, 10, 609-618, <https://doi.org/10.5194/hess-10-609-2006>, 2006.
- Birkel, C., Soulsby, C., and Tetzlaff, D.: Modelling catchment-scale water storage dynamics: Reconciling dynamic storage

- with tracer-inferred passive storage, *Hydrol. Process.*, 25, 3924-3936, <https://doi.org/10.1002/hyp.8201>, 2011.
- 840 Birkel, C., Soulsby, C., and Tetzlaff, D.: Conceptual modelling to assess how the interplay of hydrological connectivity, catchment storage and tracer dynamics controls nonstationary water age estimates, *Hydrol. Process.*, 29, 2956-2969, <https://doi.org/10.1002/hyp.10414>, 2015.
- Birkel, C., Dunn, S., Tetzlaff, D., and Soulsby, C.: Assessing the value of high-resolution isotope tracer data in the stepwise development of a lumped conceptual rainfall-runoff model, *Hydrol. Process.*, 24, 2335-2348, <https://doi.org/10.1002/hyp.7763>,
845 2010.
- Birkel, C., Duvert, C., Correa, A., Munksgaard, N. C., Maher, D. T., and Hutley, L. B.: Tracer-aided modeling in the low-relief, wet-dry tropics suggests water ages and DOC export are driven by seasonal wetlands and deep groundwater, *Water Resour. Res.*, 56, e2019WR026175, <https://doi.org/10.1029/2019WR026175>, 2020.
- Bolin, B. and Rodhe, H.: A note on the concepts of age distribution and transit time in natural reservoirs, *Tellus*, 25, 58-62, <https://doi.org/10.1111/j.2153-3490.1973.tb01594.x>, 1973.
- 850 Botter, G., Bertuzzo, E., and Rinaldo, A.: Catchment residence and travel time distributions: The master equation, *Geophys. Res. Lett.*, 38, <https://doi.org/10.1029/2011GL047666>, 2011.
- Bouaziz, L. J., Fenicia, F., Thirel, G., de Boer-Euser, T., Buitink, J., Brauer, C. C., De Niel, J., Dewals, B. J., Drogue, G., and Grelier, B.: Behind the scenes of streamflow model performance, *Hydrol. Earth Syst. Sci.*, 25, 1069-1095, <https://doi.org/10.5194/hess-25-1069-2021>, 2021.
- 855 Buzacott, A. J., van Der Velde, Y., Keitel, C., and Vervoort, R. W.: Constraining water age dynamics in a south-eastern Australian catchment using an age-ranked storage and stable isotope approach, *Hydrol. Process.*, 34, 4384-4403, <https://doi.org/10.1002/hyp.13880>, 2020.
- Christophersen, N., Seip, H. M., and Wright, R. F.: A model for streamwater chemistry at Birkenes, Norway, *Water Resources Research*, 18, 977-996, <https://doi.org/10.1029/WR018i004p00977>, 1982.
- 860 Christophersen, N. and Wright, R. F.: Sulfate budget and a model for sulfate concentrations in stream water at Birkenes, a small forested catchment in southernmost Norway, *Water Resources Research*, 17, 377-389, <https://doi.org/10.1029/WR017i002p00377>, 1981.
- Clark, M. P., Rupp, D. E., Woods, R. A., Zheng, X., Ibbitt, R. P., Slater, A. G., Schmidt, J., and Uddstrom, M. J.: Hydrological data assimilation with the ensemble Kalman filter: Use of streamflow observations to update states in a distributed hydrological model, *Adv. Water Resour.*, 31, 1309-1324, <https://doi.org/10.1016/j.advwatres.2008.06.005>, 2008.
- 865 De Grosbois, E., Hooper, R. P., and Christophersen, N.: A multisignal automatic calibration methodology for hydrochemical models: a case study of the Birkenes model, *Water Resources Research*, 24, 1299-1307, <https://doi.org/10.1029/WR024i008p01299>, 1988.
- 870 DeWalle, D., Edwards, P., Swistock, B., Aravena, R., and Drimmie, R.: Seasonal isotope hydrology of three Appalachian forest catchments, *Hydrol. Process.*, 11, 1895-1906, [https://doi.org/10.1002/\(SICI\)1099-1085\(199712\)11:15<1895::AID-HYP538>3.0.CO;2-%23](https://doi.org/10.1002/(SICI)1099-1085(199712)11:15<1895::AID-HYP538>3.0.CO;2-%23), 1997.

- Dincer, T., Payne, B., Florkowski, T., Martinec, J., and Tongiorgi, E.: Snowmelt runoff from measurements of tritium and oxygen-18, *Water Resour. Res.*, 6, 110-124, <https://doi.org/10.1029/WR006i001p00110>, 1970.
- 875 Duvert, C., Stewart, M., Cendón, D., and Raiber, M.: Time series of tritium, stable isotopes and chloride reveal short-term variations in groundwater contribution to a stream, *Hydrol. Earth Syst. Sci.*, 20, 257-277, <https://doi.org/10.5194/hess-20-257-2016>, 2016.
- Eriksson, E.: The possible use of tritium' for estimating groundwater storage, *Tellus*, 10, 472-478, <https://doi.org/10.3402/tellusa.v10i4.9265>, 1958.
- 880 Euser, T., Hrachowitz, M., Winsemius, H. C., and Savenije, H. H.: The effect of forcing and landscape distribution on performance and consistency of model structures, *Hydrol. Process.*, 29, 3727-3743, <https://doi.org/10.1002/hyp.10445>, 2015.
- Fenicia, F., Savenije, H., Matgen, P., and Pfister, L.: Is the groundwater reservoir linear? Learning from data in hydrological modelling, *Hydrol. Earth Syst. Sci.*, 10, 139-150, <https://doi.org/10.5194/hess-10-139-2006>, 2006.
- Fenicia, F., Wrede, S., Kavetski, D., Pfister, L., Hoffmann, L., Savenije, H. H., and McDonnell, J. J.: Assessing the impact of
885 mixing assumptions on the estimation of streamwater mean residence time, *Hydrol. Process.*, 24, 1730-1741, <https://doi.org/10.1002/hyp.7595>, 2010.
- Fovet, O., Ruiz, L., Hrachowitz, M., Faucheux, M., and Gascuel-Oudou, C.: Hydrological hysteresis and its value for assessing process consistency in catchment conceptual models, *Hydrol. Earth Syst. Sci.*, 19, 105-123, <https://doi.org/10.5194/hess-19-105-2015>, 2015.
- 890 Gallart, F., Roig-Planasdemunt, M., Stewart, M. K., Llorens, P., Morgenstern, U., Stichler, W., Pfister, L., and Latron, J.: A GLUE-based uncertainty assessment framework for tritium-inferred transit time estimations under baseflow conditions, *Hydrol. Process.*, 30, 4741-4760, <https://doi.org/10.1002/hyp.10991>, 2016.
- Gao, H., Ding, Y., Zhao, Q., Hrachowitz, M., and Savenije, H. H.: The importance of aspect for modelling the hydrological response in a glacier catchment in Central Asia, *Hydrol. Process.*, 31, 2842-2859, <https://doi.org/10.1002/hyp.11224>, 2017.
- 895 Gao, H., Hrachowitz, M., Fenicia, F., Gharari, S., and Savenije, H.: Testing the realism of a topography-driven model (FLEX-Topo) in the nested catchments of the Upper Heihe, China, *Hydrol. Earth Syst. Sci.*, 18, 1895-1915, <https://doi.org/10.5194/hess-18-1895-2014>, 2014.
- Gao, H., Hrachowitz, M., Sriwongsitanon, N., Fenicia, F., Gharari, S., and Savenije, H. H.: Accounting for the influence of vegetation and landscape improves model transferability in a tropical savannah region, *Water Resour. Res.*, 52, 7999-8022, <https://doi.org/10.1002/2016WR019574>, 2016.
- 900 Gharari, S., Hrachowitz, M., Fenicia, F., and Savenije, H.: Hydrological landscape classification: investigating the performance of HAND based landscape classifications in a central European meso-scale catchment, *Hydrol. Earth Syst. Sci.*, 15, 3275-3291, <https://doi.org/10.5194/hess-15-3275-2011>, 2011.
- Gharari, S., Hrachowitz, M., Fenicia, F., Gao, H., and Savenije, H.: Using expert knowledge to increase realism in
905 environmental system models can dramatically reduce the need for calibration, *Hydrol. Earth Syst. Sci.*, 18, 4839-4859, <https://doi.org/10.5194/hess-18-4839-2014>, 2014.

- Girons Lopez, M., Vis, M. J., Jenicek, M., Griessinger, N., and Seibert, J.: Assessing the degree of detail of temperature-based snow routines for runoff modelling in mountainous areas in central Europe, *Hydrol. Earth Syst. Sci.*, 24, 4441-4461, <https://doi.org/10.5194/hess-24-4441-2020>, 2020.
- 910 Godsey, S. E., Kirchner, J. W., and Clow, D. W.: Concentration–discharge relationships reflect chemostatic characteristics of US catchments, *Hydrol. Process.*, 23, 1844-1864, <https://doi.org/10.1002/hyp.7315>, 2009.
- Godsey, S. E., Aas, W., Clair, T. A., De Wit, H. A., Fernandez, I. J., Kahl, J. S., Malcolm, I. A., Neal, C., Neal, M., and Nelson, S. J.: Generality of fractal 1/f scaling in catchment tracer time series, and its implications for catchment travel time distributions, *Hydrol. Process.*, 24, 1660-1671, <https://doi.org/10.1002/hyp.7677>, 2010.
- 915 Goovaerts, P.: Geostatistical approaches for incorporating elevation into the spatial interpolation of rainfall, *J. Hydrol.*, 228, 113-129, [https://doi.org/10.1016/S0022-1694\(00\)00144-X](https://doi.org/10.1016/S0022-1694(00)00144-X), 2000.
- Hadka, D. and Reed, P.: Borg: An auto-adaptive many-objective evolutionary computing framework, *Evolutionary computation*, 21, 231-259, https://doi.org/10.1162/EVCO_a_00075, 2013.
- Hanus, S., Hrachowitz, M., Zekollari, H., Schoups, G., Vizcaino, M., and Kaitna, R.: Future changes in annual, seasonal and monthly runoff signatures in contrasting Alpine catchments in Austria, *Hydrol. Earth Syst. Sci.*, 25, 3429-3453, <https://doi.org/10.5194/hess-25-3429-2021>, 2021.
- 920 Harman, C. J.: Time-variable transit time distributions and transport: Theory and application to storage-dependent transport of chloride in a watershed, *Water Resour. Res.*, 51, 1-30, <https://doi.org/10.1002/2014WR015707>, 2015.
- Harms, P. A., Visser, A., Moran, J. E., and Esser, B. K.: Distribution of tritium in precipitation and surface water in California, *J. Hydrol.*, 534, 63-72, <https://doi.org/10.1016/j.jhydrol.2015.12.046>, 2016.
- 925 Hooper, R. P., Stone, A., Christophersen, N., de Grosbois, E., and Seip, H. M.: Assessing the Birkenes model of stream acidification using a multisignal calibration methodology, *Water Resources Research*, 24, 1308-1316, <https://doi.org/10.1029/WR024i008p01308>, 1988.
- Hrachowitz, M., Fovet, O., Ruiz, L., and Savenije, H. H.: Transit time distributions, legacy contamination and variability in biogeochemical 1/f α scaling: how are hydrological response dynamics linked to water quality at the catchment scale?, *Hydrol. Process.*, 29, 5241-5256, <https://doi.org/10.1002/hyp.10546>, 2015.
- 930 Hrachowitz, M., Savenije, H., Bogaard, T., Tetzlaff, D., and Soulsby, C.: What can flux tracking teach us about water age distribution patterns and their temporal dynamics?, *Hydrol. Earth Syst. Sci.*, 17, 533-564, <https://doi.org/10.5194/hess-17-533-2013>, 2013.
- 935 Hrachowitz, M., Soulsby, C., Tetzlaff, D., Dawson, J. J. C., and Malcolm, I.: Regionalization of transit time estimates in montane catchments by integrating landscape controls, *Water Resour. Res.*, 45, <https://doi.org/10.1029/2008WR007496>, 2009a.
- Hrachowitz, M., Soulsby, C., Tetzlaff, D., Malcolm, I., and Schoups, G.: Gamma distribution models for transit time estimation in catchments: Physical interpretation of parameters and implications for time-variant transit time assessment, *Water Resour. Res.*, 46, <https://doi.org/10.1029/2010WR009148>, 2010a.

- 940 Hrachowitz, M., Soulsby, C., Tetzlaff, D., & Speed, M. Catchment transit times and landscape controls—does scale matter? *Hydrological Processes: An International Journal*, 24(1), 117-125, <https://onlinelibrary.wiley.com/doi/pdf/10.1002/hyp.7510>, 2010b.
- Hrachowitz, M., Soulsby, C., Tetzlaff, D., Dawson, J. J. C., Dunn, S., and Malcolm, I.: Using long-term data sets to understand transit times in contrasting headwater catchments, *J. Hydrol.*, 367, 237-248, <https://doi.org/10.1016/j.jhydrol.2009.01.001>,
945 2009b.
- Hrachowitz, M., Stockinger, M., Coenders-Gerrits, M., van der Ent, R., Bogena, H., Lücke, A., and Stumpp, C.: Reduction of vegetation-accessible water storage capacity after deforestation affects catchment travel time distributions and increases young water fractions in a headwater catchment, *Hydrol. Earth Syst. Sci.*, 25, 4887-4915, <https://doi.org/10.5194/hess-25-4887-2021>, 2021.
- 950 Hrachowitz, M., Benettin, P., Van Breukelen, B. M., Fovet, O., Howden, N. J., Ruiz, L., Van Der Velde, Y., and Wade, A. J.: Transit times—The link between hydrology and water quality at the catchment scale, *WIREs Water*, 3, 629-657, <https://doi.org/10.1002/wat2.1155>, 2016.
- Hulsman, P., Hrachowitz, M., and Savenije, H. H.: Improving the representation of long-term storage variations with conceptual hydrological models in data-scarce regions, *Water Resour. Res.*, 57, e2020WR028837,
955 <https://doi.org/10.1029/2020WR028837>, 2021a.
- Hulsman, P., Savenije, H. H., and Hrachowitz, M.: Learning from satellite observations: increased understanding of catchment processes through stepwise model improvement, *Hydrol. Earth Syst. Sci.*, 25, 957-982, <https://doi.org/10.5194/hess-25-957-2021>, 2021b.
- IAEA/WMO. Global Network of Isotopes in Precipitation. The GNIP Database. Accessible at: <https://nucleus.iaea.org/wiser>,
960 2022.
- Kendall, C. and McDonnell, J. J.: *Isotope tracers in catchment hydrology*, Elsevier, 2012.
- Kim, M., Volkmann, T. H., Wang, Y., Meira Neto, A. A., Matos, K., Harman, C. J., and Troch, P. A.: Direct Observation of Hillslope Scale StorAge Selection Functions in Experimental Hydrologic Systems: Geomorphologic Structure and Preferential Discharge of Old Water, *Water Resour. Res.*, 58, e2020WR028959, <https://doi.org/10.1029/2020WR028959>, 2022.
- 965 Kirchner, J. W.: Getting the right answers for the right reasons: Linking measurements, analyses, and models to advance the science of hydrology, *Water Resour. Res.*, 42, <https://doi.org/10.1029/2005WR004362>, 2006.
- Kirchner, J. W.: Aggregation in environmental systems—Part 1: Seasonal tracer cycles quantify young water fractions, but not mean transit times, in spatially heterogeneous catchments, *Hydrol. Earth Syst. Sci.*, 20, 279-297, <https://doi.org/10.5194/hess-20-279-2016>, 2016.
- 970 Kirchner, J. W., Feng, X., and Neal, C.: Catchment-scale advection and dispersion as a mechanism for fractal scaling in stream tracer concentrations, *J. Hydrol.*, 254, 82-101, [https://doi.org/10.1016/S0022-1694\(01\)00487-5](https://doi.org/10.1016/S0022-1694(01)00487-5), 2001.
- Kirchner, J. W., Tetzlaff, D., and Soulsby, C.: Comparing chloride and water isotopes as hydrological tracers in two Scottish catchments, *Hydrol. Process.*, 24, 1631-1645, <https://doi.org/10.1002/hyp.7676>, 2010.

- 975 Koeniger P, Stumpp C, Schmidt A.: Stable isotope patterns of German rivers with aspects on scales, continuity and network status, *Isotopes in Environmental and Health Studies*, 1-17, <https://doi.org/10.1080/10256016.2022.2127702>, 2022.
- Kreft, A. and Zuber, A.: On the physical meaning of the dispersion equation and its solutions for different initial and boundary conditions, *Chemical Engineering Science*, 33, 1471-1480, [https://doi.org/10.1016/0009-2509\(78\)85196-3](https://doi.org/10.1016/0009-2509(78)85196-3), 1978.
- 980 Kuppel, S., Tetzlaff, D., Maneta, M. P., and Soulsby, C.: EcH 2 O-iso 1.0: Water isotopes and age tracking in a process-based, distributed ecohydrological model, *Geoscientific Model Development*, 11, 3045-3069, <https://doi.org/10.5194/gmd-11-3045-2018>, 2018.
- Kuppel, S., Tetzlaff, D., Maneta, M. P., and Soulsby, C.: Critical zone storage controls on the water ages of ecohydrological outputs, *Geophys. Res. Lett.*, 47, e2020GL088897, <https://doi.org/10.1029/2020GL088897>, 2020.
- Lloyd, C.: Assessing the effect of integrating elevation data into the estimation of monthly precipitation in Great Britain, *J. Hydrol.*, 308, 128-150, <https://doi.org/10.1016/j.jhydrol.2004.10.026>, 2005.
- 985 Loritz, R., Hrachowitz, M., Neuper, M., and Zehe, E.: The role and value of distributed precipitation data in hydrological models. *Hydrol. Earth Syst. Sci.*, 25, 147-167, <https://doi.org/10.5194/hess-25-147-2021>, 2021.
- Lundquist, D.: Hydrochemical modelling of drainage basins. SNSF-project, Norwegian Institute for Water Research, Oslo, Rep. IR, 31, 27, 1977.
- Małozewski, P. and Zuber, A.: Determining the turnover time of groundwater systems with the aid of environmental tracers: 990 1. Models and their applicability, *J. Hydrol.*, 57, 207-231, [https://doi.org/10.1016/0022-1694\(82\)90147-0](https://doi.org/10.1016/0022-1694(82)90147-0), 1982.
- Małozewski, P., Rauert, W., Stichler, W., and Herrmann, A.: Application of flow models in an alpine catchment area using tritium and deuterium data, *J. Hydrol.*, 66, 319-330, [https://doi.org/10.1016/0022-1694\(83\)90193-2](https://doi.org/10.1016/0022-1694(83)90193-2), 1983.
- McDonnell, J. J. and Beven, K.: Debates—The future of hydrological sciences: A (common) path forward? A call to action aimed at understanding velocities, celerities and residence time distributions of the headwater hydrograph, *Water Resour. Res.*, 995 50, 5342-5350, <https://doi.org/10.1002/2013WR015141>, 2014.
- McGuire, K. J. and McDonnell, J. J.: A review and evaluation of catchment transit time modeling, *J. Hydrol.*, 330, 543-563, <https://doi.org/10.1016/j.jhydrol.2006.04.020>, 2006.
- 1000 Michel, R. L., Aggarwal, P., Araguas-Araguas, L., Kurttas, T., Newman, B. D., and Vitvar, T.: A simplified approach to analysing historical and recent tritium data in surface waters, *Hydrol. Process.*, 29, 572-578, <https://doi.org/10.1002/hyp.10174>, 2015.
- Morgenstern, U., Stewart, M. K., and Stenger, R.: Dating of streamwater using tritium in a post nuclear bomb pulse world: continuous variation of mean transit time with streamflow, *Hydrol. Earth Syst. Sci.*, 14, 2289-2301, <https://doi.org/10.5194/hess-14-2289-2010>, 2010.
- 1005 Mostbauer, K., Kaitna, R., Prenner, D., and Hrachowitz, M.: The temporally varying roles of rainfall, snowmelt and soil moisture for debris flow initiation in a snow-dominated system, *Hydrol. Earth Syst. Sci.*, 22, 3493-3513, <https://doi.org/10.5194/hess-22-3493-2018>, 2018.
- Nguyen, T. V., Kumar, R., Musolff, A., Lutz, S. R., Sarrazin, F., Attinger, S., & Fleckenstein, J. H.: Disparate seasonal nitrate**

- 1010 Nijzink, R., Hutton, C., Pechlivanidis, I., Capell, R., Arheimer, B., Freer, J., Han, D., Wagener, T., McGuire, K., and Savenije, H.: The evolution of root-zone moisture capacities after deforestation: a step towards hydrological predictions under change?, *Hydrol. Earth Syst. Sci.*, 20, 4775-4799, <https://doi.org/10.5194/hess-20-4775-2016>, 2016.
- Niemi, A. J.: Residence time distributions of variable flow processes, *The International Journal of Applied Radiation and Isotopes*, 28, 855-860, [https://doi.org/10.1016/0020-708X\(77\)90026-6](https://doi.org/10.1016/0020-708X(77)90026-6), 1977.
- 1015 Nir, A.: Tracer relations in mixed lakes in non-steady state, *Journal of Hydrology*, 19, 33-41, [https://doi.org/10.1016/0022-1694\(73\)90091-7](https://doi.org/10.1016/0022-1694(73)90091-7), 1973.
- Pfister, L., Martínez-Carreras, N., Hissler, C., Klaus, J., Carrer, G. E., Stewart, M. K., and McDonnell, J. J.: Bedrock geology controls on catchment storage, mixing, and release: A comparative analysis of 16 nested catchments, *Hydrol. Process.*, 31, 1828-1845, <https://doi.org/10.1002/hyp.11134>, 2017.
- 1020 Prenner, D., Kaitna, R., Mostbauer, K., and Hrachowitz, M.: The value of using multiple hydrometeorological variables to predict temporal debris flow susceptibility in an alpine environment, *Water Resour. Res.*, 54, 6822-6843, <https://doi.org/10.1029/2018WR022985>, 2018.
- Rank, D., Wyhlidal, S., Schott, K., Weigand, S., and Oblin, A.: Temporal and spatial distribution of isotopes in river water in Central Europe: 50 years experience with the Austrian network of isotopes in rivers, *Isotopes in Environmental and Health Studies*, 54, 115-136, <https://doi.org/10.1080/10256016.2017.1383906>, 2018.
- 1025 Reckerth, A., Stichler, W., Schmidt, A., and Stumpp, C.: Long-term data set analysis of stable isotopic composition in German rivers, *J. Hydrol.*, 552, 718-731, <https://doi.org/10.1016/j.jhydrol.2017.07.022>, 2017.
- Rinaldo, A., Benettin, P., Harman, C. J., Hrachowitz, M., McGuire, K. J., Van Der Velde, Y., Bertuzzo, E., and Botter, G.: Storage selection functions: A coherent framework for quantifying how catchments store and release water and solutes, *Water Resour. Res.*, 51, 4840-4847, <https://doi.org/10.1002/2015WR017273>, 2015.
- 1030 Rodriguez, N. B. and Klaus, J.: Catchment travel times from composite StorAge Selection functions representing the superposition of streamflow generation processes, *Water Resour. Res.* 55, 9292-9314, <https://doi.org/10.1029/2019WR024973>, 2019.
- Rodriguez, N. B., McGuire, K. J., and Klaus, J.: Time-varying storage–water age relationships in a catchment with a Mediterranean climate, *Water Resour. Res.*, 54, 3988-4008, <https://doi.org/10.1029/2017WR021964>, 2018.
- 1035 Rodriguez, N. B., Pfister, L., Zehe, E., and Klaus, J.: A comparison of catchment travel times and storage deduced from deuterium and tritium tracers using StorAge Selection functions, *Hydrol. Earth Syst. Sci.*, 25, 401-428, <https://doi.org/10.5194/hess-25-401-2021>, 2021.
- Roodari, A., Hrachowitz, M., Hassanpour, F., and Yaghoobzadeh, M.: Signatures of human intervention—or not? Downstream intensification of hydrological drought along a large Central Asian river: the individual roles of climate variability and land use change, *Hydrol. Earth Syst. Sci.*, 25, 1943-1967, <https://doi.org/10.5194/hess-25-1943-2021>, 2021.
- 1040

- Rozanski, K., Gonfiantini, R., and Araguas-Araguas, L.: Tritium in the global atmosphere: Distribution patterns and recent trends, *Journal of Physics G: Nuclear and Particle Physics*, 17, S523, 1991.
- Schmidt, A., Frank, G., Stichler, W., Duester, L., Steinkopff, T., and Stumpp, C.: Overview of tritium records from precipitation and surface waters in Germany, *Hydrol. Process.*, 34, 1489-1493, <https://doi.org/10.1002/hyp.13691>, 2020.
- 1045 Seeger, S. and Weiler, M.: Reevaluation of transit time distributions, mean transit times and their relation to catchment topography, *Hydrol. Earth Syst. Sci.*, 18, 4751-4771, <https://doi.org/10.5194/hess-18-4751-2014>, 2014.
- Seibert, J., McDonnell, J. J., and Woodsmith, R. D.: Effects of wildfire on catchment runoff response: a modelling approach to detect changes in snow-dominated forested catchments, *Hydrology research*, 41, 378-390,
- 1050 <https://doi.org/10.2166/nh.2010.036>, 2010.
- Seip, H. M., Seip, R., Dillon, P. J., and Grosbois, E. d.: Model of sulphate concentration in a small stream in the Harp Lake catchment, Ontario, *Canadian Journal of Fisheries and Aquatic Sciences*, 42, 927-937, <https://doi.org/10.1139/f85-117>, 1985.
- Shaw, S. B., Harpold, A. A., Taylor, J. C., and Walter, M. T.: Investigating a high resolution, stream chloride time series from the Biscuit Brook catchment, Catskills, NY, *J. Hydrol.*, 348, 245-256, <https://doi.org/10.1016/j.jhydrol.2007.10.009>, 2008.
- 1055 Soulsby, C., Birkel, C., and Tetzlaff, D.: Characterizing the age distribution of catchment evaporative losses, *Hydrol. Process.*, 30, 1308-1312, <https://doi.org/10.1002/hyp.10751>, 2016.
- Sprenger, M., Stumpp, C., Weiler, M., Aeschbach, W., Allen, S. T., Benettin, P., Dubbert, M., Hartmann, A., Hrachowitz, M., and Kirchner, J. W.: The demographics of water: A review of water ages in the critical zone, *Reviews of Geophysics*, 57, 800-834, <https://doi.org/10.1029/2018RG000633>, 2019.
- 1060 Stewart, M. and Thomas, J.: A conceptual model of flow to the Waikoropupu Springs, NW Nelson, New Zealand, based on hydrometric and tracer (^{18}O , Cl, ^3H and CFC) evidence, *Hydrol. Earth Syst. Sci.*, 12, 1-19, <https://doi.org/10.5194/hess-12-1-2008>, 2008.
- Stewart, M., Morgenstern, U., McDonnell, J., and Pfister, L.: The 'hidden streamflow' challenge in catchment hydrology: a call to action for stream water transit time analysis, *Hydrol. Process.*, 26, 2061-2066, <https://doi.org/10.1002/hyp.9262>, 2012.
- 1065 Stewart, M. K. and Morgenstern, U.: Importance of tritium-based transit times in hydrological systems, *WIREs Water*, 3, 145-154, <https://doi.org/10.1002/wat2.1134>, 2016.
- Stewart, M. K., Mehlhorn, J., and Elliott, S.: Hydrometric and natural tracer (oxygen-18, silica, tritium and sulphur hexafluoride) evidence for a dominant groundwater contribution to Pukemanga Stream, New Zealand, *Hydrol. Process.*, 21, 3340-3356, <https://doi.org/10.1002/hyp.6557>, 2007.
- 1070 Stewart, M. K., Morgenstern, U., and McDonnell, J. J.: Truncation of stream residence time: how the use of stable isotopes has skewed our concept of streamwater age and origin, *Hydrol. Process.*, 24, 1646-1659, <https://doi.org/10.1002/hyp.7576>, 2010.
- Stewart, M. K., Morgenstern, U., and Cartwright, I.: Comment on "A comparison of catchment travel times and storage deduced from deuterium and tritium tracers using StorAge Selection functions" by Rodriguez et al.(2021), *Hydrology and*
- 1075 *Earth System Sciences*, 25, 6333-6338, <https://doi.org/10.5194/hess-25-6333-2021>, 2021.

Stumpp, C., Klaus, J., and Stichler, W.: Analysis of long-term stable isotopic composition in German precipitation, *J. Hydrol.*, 517, 351-361, <https://doi.org/10.1016/j.jhydrol.2014.05.034>, 2014.

Tadros, C. V., Hughes, C. E., Crawford, J., Hollins, S. E., and Chisari, R.: Tritium in Australian precipitation: A 50 year record, *J. Hydrol.*, 513, 262-273, <https://doi.org/10.1016/j.jhydrol.2014.03.031>, 2014.

1080 Uhlenbrook, S., Frey, M., Leibundgut, C., and Maloszewski, P.: Hydrograph separations in a mesoscale mountainous basin at event and seasonal timescales, *Water Resour. Res.*, 38, 31-31-31-14, <https://doi.org/10.1029/2001WR000938>, 2002.

Van Der Velde, Y., Torfs, P., Van Der Zee, S., and Uijlenhoet, R.: Quantifying catchment-scale mixing and its effect on time-varying travel time distributions, *Water Resour. Res.*, 48, <https://doi.org/10.1029/2011WR011310>, 2012.

1085 Van Der Velde, Y., Heidebüchel, I., Lyon, S. W., Nyberg, L., Rodhe, A., Bishop, K., and Troch, P. A.: Consequences of mixing assumptions for time-variable travel time distributions, *Hydrol. Process.*, 29, 3460-3474, <https://doi.org/10.1002/hyp.10372>, 2015.

Visser, A., Thaw, M., Deinhard, A., Bibby, R., Safeeq, M., Conklin, M., Esser, B., and Van der Velde, Y.: Cosmogenic isotopes unravel the hydrochronology and water storage dynamics of the Southern Sierra Critical Zone, *Water Resour. Res.*, 55, 1429-1450, <https://doi.org/10.1029/2018WR023665>, 2019.

1090 Vitvar, T. and Balderer, W.: Estimation of mean water residence times and runoff generation by ^{180}m measurements in a Pre-Alpine catchment (Rietholzbach, Eastern Switzerland), *Applied Geochemistry*, 12, 787-796, [https://doi.org/10.1016/S0883-2927\(97\)00045-0](https://doi.org/10.1016/S0883-2927(97)00045-0), 1997.

Yang, D., Yang, Y., and Xia, J.: Hydrological cycle and water resources in a changing world: A review, *Geography and Sustainability*, 2, 115-122, <https://doi.org/10.1016/j.geosus.2021.05.003>, 2021.

1095

1100

1105

1110

Table1. Characteristics of the Neckar catchment in Germany

Characteristics	
latitude (N)	48°02'00"-49°33'45"
longitude (E)	8°18'45"-10°18'45"
Area (km ²)	13,041
Average annual precipitation (mm yr ⁻¹)	909
Average annual temperature (°C)	8.9
Elevation range (m)	122-1019
Mean elevation (m)	569
Slope range (°)	0-53
Mean slope (°)	5.1
Forest dominated land (%)	38.1
Grass dominated land (%)	51.2
Wetland (%)	10.7

1115

1120

Table 2. The 12 time-invariant, lumped SW/CO model scenarios here implemented for the Neckar study basin together with the associated calibration strategies, the individual calibration performance metric, the type of models as well as the prior parameter ranges and the optimal parameter value from calibration. SW indicates sine-wave models, CO indicates time-invariant, lumped parameter convolution integral models. EM represents an exponential TTD and GM indicates a gamma distribution TTD. 2EM indicates a two parallel linear reservoir model, 3EM indicates a three parallel linear reservoir model and EPM indicates an exponential piston flow model. The calibration strategies show which variable a model was calibrated to using the Mean Square Error (MSE) with $C_{\delta^{18}O}$ calibration to the observed stream water $\delta^{18}O$ signal and C_{δ^3H} calibration to observed stream water δ^3H . *) Note, that for SW models calibration involves least-square fits of sine waves to both, the precipitation and stream flow signals available. †) fixed to a value of 1.

Scenario		1	2	3	4	5	6	7	8	9	10	11	12
Model		SW-EM	SW-GM	CO-EM	CO-GM	CO-2EM	CO-3EM	CO-2EM	CO-3EM	CO-3EM	CO-3EM	CO-EPM	CO-EPM
Signature	Calibration strategy → Performance metric ↓	$C_x^*)$	$C_x^*)$	$C_{\delta^{18}O}$	C_{δ^3H}	$C_{\delta^{18}O}$	C_{δ^3H}	$C_{\delta^{18}O}$	C_{δ^3H}	$C_{\delta^{18}O}$	C_{δ^3H}	$C_{\delta^{18}O}$	C_{δ^3H}
Times series $\delta^{18}O$	$MSE_{\delta^{18}O}$	•	•	•	-	•	-	•	-	•	-	•	-
Time series δ^3H	MSE_{δ^3H}	-	-	-	•	-	•	-	•	-	•	-	•
Parameter	Prior range	Optimal parameter value											
A_p (‰)	- ^{†)}	2.69											
A_s (‰)	- ^{†)}	0.57											
α (-)	0.1 – 2	-	-	1 ^{†)}	1 ^{†)}	0.44	0.58	1 ^{†)}	1 ^{†)}	1 ^{†)}	1 ^{†)}	1 ^{†)}	1 ^{†)}
β_1 (d)	1 – 15000	-	-	513	3795	2048	6086	16	84	11	66	662	3665
β_2 (d)	1 – 15000	-	-	-	-	-	-	832	5388	12	112	-	-
β_3 (d)	1 – 15000	-	-	-	-	-	-	-	-	963	5299	-	-
f_1 (-)	0 – 1			1 ^{†)}	1 ^{†)}	1 ^{†)}	1 ^{†)}	0.18	0.36	0.06	0.02	1 ^{†)}	1 ^{†)}
f_2 (-)	0 – 1			-	-	-	-	-	-	0.12	0.34	-	-
η (-)	1 – 3	-	-	1 ^{†)}	1 ^{†)}	1 ^{†)}	1 ^{†)}	1 ^{†)}	1 ^{†)}	1 ^{†)}	1 ^{†)}	1.91	1.01

1125

1130

1135

1140

Table 3. The 9 P-SAS and IM-SAS model scenarios here implemented for the Neckar study basin together with the associated calibration strategies, the individual calibration performance metrics and the type of spatial implementation (lumped or distributed) as well as the associated prior parameter ranges and the ranges of the pareto optimal solutions from calibration. P-SAS indicates the model with one compartment as described in Benettin et al. (2017), and IM-SAS indicates the integrated hydrological model based on SAS-functions. The symbols L and D indicate lumped and distributed model implementations, respectively. The calibration strategies show which variables/signatures a model was simultaneously calibrated to using the Mean Square Error (MSE) with $C_{\delta^{18}\text{O},\text{O}_2}$ simultaneous calibration to $\delta^{18}\text{O}$ and six signatures of stream flow Q; $C_{\text{H}_2\text{O}}^3$ simultaneous calibration to ^3H and the signatures of Q; $C_{\delta^{18}\text{O},\text{O}_2,^3\text{H}}$ the simultaneous calibration to $\delta^{18}\text{O}$, ^3H and the signatures of Q. †) fixed to a value of 1.

Scenario		13	14	15	16	17	18	19	20	21
Model		P-SAS			IM-SAS-L			IM-SAS-D		
Implementation		Lumped						Distributed		
Signature	Calibration strategy → Performance metric ↓	$C_{\delta^{18}\text{O}}$	$C_{^3\text{H}}$	$C_{\delta^{18}\text{O},^3\text{H}}$	$C_{\delta^{18}\text{O},\text{O}_2}$	$C_{\text{H}_2\text{O}}^3$	$C_{\delta^{18}\text{O},^3\text{H},\text{O}_2}$	$C_{\delta^{18}\text{O},\text{O}_2}$	$C_{^3\text{H},\text{O}_2}$	$C_{\delta^{18}\text{O},^3\text{H},\text{O}_2}$
Times series $\delta^{18}\text{O}$	$MSE_{\delta^{18}\text{O}}$	•	-	•	•	-	•	•	-	•
Time series ^3H	$MSE_{^3\text{H}}$	-	•	•	-	•	•	-	•	•
Time series of stream flow (Q)	MSE_Q	-	-	-	•	•	•	•	•	•
Time series of log(Q)	$MSE_{\log(Q)}$	-	-	-	•	•	•	•	•	•
Flow duration curve of Q (FDC _Q)	MSE_{FDC_Q}	-	-	-	•	•	•	•	•	•
Flow duration curve log(Q) (FDC _{log(Q)})	$MSE_{FDC_{\log(Q)}}$	-	-	-	•	•	•	•	•	•
Seasonal runoff coefficient (RC)	MSE_{RC}	-	-	-	•	•	•	•	•	•
Autocorrelation function of Q (AC _Q)	MSE_{AC_Q}	-	-	-	•	•	•	•	•	•
Parameter	Prior range	Optimal parameter value								
k_E	0.1-1.0	† ¹⁾	† ¹⁾	† ¹⁾	-	-	-	-	-	-
k_Q	0.1-1.0	0.34	0.28	0.29-0.33	-	-	-	-	-	-
S_{sat} (mm)	100-20000	15595	16638	7414-18245	-	-	-	-	-	-
T_f (°C)	-2.5-2.5	-	-	-	-0.94-2.08	-0.88-1.75	-2.15-1.57	-1.84-1.81	-1.74-0.16	-1.92-1.54
C_{melt} (mm°C ⁻¹ d ⁻¹)	1-5	-	-	-	2.32-4.42	1.67-3.96	1.79-3.77	2.30-4.89	1.56-3.25	1.23-4.10
S_{maxF} (mm)	0.1-5	-	-	-	1.53-3.73	1.35-4.39	0.55-4.10	3.18-4.03	2.94-4.98	2.04-4.39
S_{maxG} (mm)	0.1-5	-	-	-	-	-	-	0.30-0.60	0.46-0.70	0.38-1.39
C_a (-)	0.1-0.7	-	-	-	0.24-0.43	0.35-0.55	0.33-0.62	0.30-0.66	0.38-0.52	0.30-0.56
S_{maxF} (mm)	50-500	-	-	-	314-415	236-355	233-464	355-438	301-441	352-485
S_{maxG} (mm)	50-500	-	-	-	-	-	-	161-199	152-287	173-297
S_{maxW} (mm)	50-500	-	-	-	-	-	-	56-149	89-149	85-148
γ_F (-)	0.1-5	-	-	-	0.93-1.68	0.61-1.01	0.57-2.03	0.99-4.59	2.04-3.98	0.76-4.94
γ_G (-)	0.1-5	-	-	-	-	-	-	0.15-0.26	0.23-0.53	0.11-0.52
γ_W (-)	0.1-5	-	-	-	-	-	-	0.14-3.64	0.12-0.32	0.10-2.88
D (-)	0-1	-	-	-	0.30-0.77	0.41-0.81	0.30-0.69	0.03-0.35	0.06-0.33	0.03-0.33
C_{pmaxF} (mm d ⁻¹)	0.1-4	-	-	-	1.04-2.03	0.98-1.83	1.05-2.62	0.91-3.19	0.94-3.66	1.37-3.72
C_{pmaxG} (mm d ⁻¹)	0.1-4	-	-	-	-	-	-	0.74-1.80	0.22-1.17	0.93-2.13
C_{max} (mm d ⁻¹)	0-4	-	-	-	-	-	-	0.00-0.31	0.02-1.06	0.01-0.98
K_{off} (d ⁻¹)	0.2-5	-	-	-	0.27-2.99	0.24-1.52	0.31-3.79	0.21-3.03	0.21-0.70	0.50-4.21
K_{offG} (d ⁻¹)	0.2-5	-	-	-	-	-	-	0.21-4.04	0.25-0.41	0.25-3.66
K_s (d ⁻¹)	0.002-0.2	-	-	-	0.04-0.19	0.05-0.18	0.05-0.18	0.05-0.17	0.03-0.14	0.05-0.17
S_{sp} (mm)	100-20000	-	-	-	4107-10029	3924-9339	4078-13676	4278-9011	3270-4622	4150-8568

1145

1150

1155

Table 4. Performance metrics of the 12 time-invariant, lumped SW/CO model implementations for the 2001 – 2009 calibration period (cal.) and the 2010 – 2016 model evaluation period (val.). For brevity only the values for the most balanced solution are shown here. *) The MSE values provided for C_x describe the sine wave fits of both, the precipitation and stream flow $\delta^{18}\text{O}$ signals, respectively.

Scenario	1	2	3	4	5	6	7	8	9	10	11	12
Model	SW-EM	SW-GM	CO-EM	CO-GM	CO-2EM	CO-3EM	CO-2EM	CO-3EM	CO-3EM	CO-3EM	CO-EPM	CO-EPM
Calibration strategy → Performance metric ↓	C_x	C_x	$C_{\delta^{18}\text{O}}$	$C^3\text{H}$	$C_{\delta^{18}\text{O}}$	$C^3\text{H}$	$C_{\delta^{18}\text{O}}$	$C^3\text{H}$	$C_{\delta^{18}\text{O}}$	$C^3\text{H}$	$C_{\delta^{18}\text{O}}$	$C^3\text{H}$
$MSE_{\delta^{18}\text{O}}$	cal.	3.850/0.121*)	0.327	-	0.204	-	0.171	-	0.171	-	0.254	-
	val.	5.208/0.144*)	0.432	-	0.192	-	0.192	-	0.191	-	0.683	-
$MSE^3\text{H}$	cal.	-	-	5.903	-	5.791	-	5.171	-	5.170	-	5.926
	val.	-	-	5.155	-	4.597	-	3.964	-	4.000	-	5.115

1160

Table 5. Performance metrics of the 9 P-SAS and IM-SAS model scenarios for the 2001 – 2009 calibration period (cal.) and the 2010 – 2016 model evaluation period (val.). For brevity only the values for the most balanced solution, i.e., lowest D_E (Eq. 16) are shown here. The ranges of all performance metrics for the full set of pareto optimal solutions for the multi-objective calibration cases (Scenarios 15 – 21) are provided in the Table S5 in supplement.

Scenario	13	14	15	16	17	18	19	20	21	
Model	P-SAS			IM-SAS-L			IM-SAS-D			
Implementation	Lumped						Distributed			
Calibration strategy → Performance metric ↓	$C_{\delta^{18}\text{O}}$	$C^3\text{H}$	$C_{\delta^{18}\text{O},^3\text{H}}$	$C_{\delta^{18}\text{O},\text{Q}}$	$C^3\text{H},\text{Q}$	$C_{\delta^{18}\text{O},^3\text{H},\text{Q}}$	$C_{\delta^{18}\text{O},\text{Q}}$	$C^3\text{H},\text{Q}$	$C_{\delta^{18}\text{O},^3\text{H},\text{Q}}$	
$MSE_{\delta^{18}\text{O}}$	cal.	0.069	-	0.078	0.083	-	0.118	0.079	-	0.114
	val.	0.231	-	0.215	0.332	-	0.273	0.273	-	0.475
$MSE^3\text{H}$	cal.	-	2.828	2.847	-	2.972	2.823	-	2.920	2.981
	val.	-	1.717	1.710	-	2.389	2.285	-	2.357	2.450
MSE_Q	cal.	-	-	-	0.202	0.299	0.308	0.228	0.263	0.317
	val.	-	-	-	0.224	0.297	0.329	0.251	0.283	0.336
$MSE_{\log(Q)}$	cal.	-	-	-	0.120	0.158	0.174	0.130	0.171	0.161
	val.	-	-	-	0.120	0.148	0.150	0.127	0.201	0.165
MSE_{FDC_Q}	cal.	-	-	-	0.058	0.024	0.073	0.022	0.017	0.025
	val.	-	-	-	0.103	0.022	0.142	0.043	0.065	0.059
$MSE_{FDC_{\log(Q)}}$	cal.	-	-	-	0.011	0.011	0.047	0.006	0.019	0.009
	val.	-	-	-	0.015	0.009	0.047	0.009	0.050	0.018
MSE_{RC}	cal.	-	-	-	0.004	0.005	0.007	0.003	0.006	0.003
	val.	-	-	-	0.004	0.004	0.005	0.003	0.008	0.003
MSE_{AC_Q}	cal.	-	-	-	0.003	0.002	0.003	0.002	0.001	0.001
	val.	-	-	-	0.008	0.002	0.001	0.005	0.002	0.007

1170

1175

1180

Table 6. Metrics of stream flow TTDs derived from the 12 SW/CO model scenarios with the different associated calibration strategies based on different, where $C_{\delta^{18}\text{O}}$ indicates calibration to $\delta^{18}\text{O}$, $C_{^3\text{H}}$ calibration to ^3H . The TTD metrics represent the best fits of the respective time-invariant TTD. The water fractions are shown as the fractions of below a specific age T, i.e. $F(T < \text{age})$. The columns with absolute difference Δ summarize the differences in TTDs from the same models calibrated to $\delta^{18}\text{O}$ and ^3H , respectively. The subscripts indicate the scenarios that are compared (e.g., $\Delta_{3,4}$ compares scenarios 3 and 4). *Note that the fraction of water younger than 3 months $F(T < 3\text{m})$ is comparable to the fraction of young water as suggested by Kirchner (2016)

1185

Scenario	1	2	3	4	5	6	7	8	9	10	11	12	$\Delta_{3,4}$	$\Delta_{5,6}$	$\Delta_{7,8}$	$\Delta_{9,10}$	$\Delta_{11,12}$	
Model	SW-EM	SW-GM	CO-EM	CO-GM	CO-2EM	CO-3EM	CO-EPM	Absolute difference										
Calibration strategy → TTD metrics ↓	C_x	C_x	$C_{\delta^{18}\text{O}}$	$C_{^3\text{H}}$	$C_{\delta^{18}\text{O}}$	$C_{^3\text{H}}$	$C_{\delta^{18}\text{O}}$	$C_{^3\text{H}}$	$C_{\delta^{18}\text{O}}$	$C_{^3\text{H}}$	$C_{\delta^{18}\text{O}}$	$C_{^3\text{H}}$	$\Delta TT_{\delta^{18}\text{O}, ^3\text{H}}$ $\Delta F(T < x)_{\delta^{18}\text{O}, ^3\text{H}}$					
Percentiles (yr)	Mean (yr)	0.7	1.8	1.4	10.4	2.4	9.7	1.9	9.5	2.1	9.4	1.8	10	-9.0	-7.3	-7.6	-7.3	-8.2
	10 th	0.1	<0.1	0.1	1.1	<0.1	0.3	<0.1	<0.1	<0.1	0.9	1.0	1.1	-1.0	-0.2	0.0	-0.8	-0.1
	25 th	0.2	0.2	0.4	3.0	0.2	1.3	0.2	0.3	0.2	2.8	1.1	2.9	-2.6	-1.1	-0.1	-2.6	-1.8
	50 th (median)	0.5	0.8	1.0	7.2	1.0	5.0	1.1	3.6	1.3	7.3	1.5	7	-6.2	-4.0	-2.5	-6.0	-5.5
	75 th	1.0	2.3	1.9	14.4	3.2	13.1	2.7	13.8	3.1	15.0	2.2	13.9	-12.5	-9.9	-11.1	-11.9	-11.7
	90 th	1.7	4.8	3.2	26.3	6.8	25.4	4.8	27.3	5.6	25.6	3.0	23.1	-23.1	-18.6	-22.5	-20.0	-20.1
Water fractions (%)	F(T<3 m)*	29	29	16	2	28	10	26	25	25	3	0	2	14	18	1	22	-2
	F(T<6 m)	49	41	30	5	38	14	34	34	32	6	0	5	25	24	0	26	-5
	F(T<1 yr)	74	55	51	9	50	21	47	40	44	10	13	9	42	29	7	34	4
	F(T<3 yr)	98	81	88	25	74	39	78	48	74	26	90	26	63	35	30	48	64
	F(T<5 yr)	100	91	97	38	85	50	91	55	88	38	99	39	59	35	36	50	60
	F(T<10 yr)	100	98	100	62	95	68	99	68	98	60	100	63	38	27	31	38	37
	F(T<20 yr)	100	100	100	85	100	85	100	84	100	84	100	86	15	15	16	16	14

Table 7. Metrics of stream flow TTDs derived from the 9 P-SAS and IM-SAS model scenarios with the different associated calibration strategies, where $C_{\delta^{18}\text{O}}$ indicates calibration to $\delta^{18}\text{O}$, $C_{^3\text{H}}$ calibration to ^3H , while $C_{\delta^{18}\text{O}, Q}$, $C_{^3\text{H}, Q}$ and $C_{\delta^{18}\text{O}, ^3\text{H}, Q}$ indicate multi-objective, i.e. simultaneous calibration to combinations of $\delta^{18}\text{O}$, ^3H and stream flow. The TTD metrics represent the mean of all volume-weighted daily streamflow TTDs for the modelling period 01/10/2001 – 31/12/2016 from the most balanced solutions (i.e. lowest D_E). The values in brackets indicate the 5th/95th percentiles of TTDs representing the pareto optimal solutions. The mean TT was estimated by fitting Gamma distributions to the volume-weighted mean TTDs of each scenario. The water fractions are shown as the fractions of below a specific age T, i.e. $F(T < \text{age})$. The columns with absolute difference Δ summarize the differences in TTDs from the most balanced solutions of the same models calibrated to $\delta^{18}\text{O}$ and ^3H , respectively. The subscripts indicate the scenarios that are compared (e.g., $\Delta_{13,14}$ compares scenarios 13 and 14). *Note that the fraction of water younger than 3 months $F(T < 3\text{m})$ is comparable to the fraction of young water suggested by Kirchner (2016).

1190

1195

Scenario	13	14	15	16	17	18	19	20	21	$\Delta_{13,14}$	$\Delta_{16,17}$	$\Delta_{19,20}$	
Model	P-SAS			IM-SAS-L			IM-SAS-D			Absolute difference			
Calibration strategy → TTD metrics ↓	$C_{\delta^{18}\text{O}}$	$C_{^3\text{H}}$	$C_{\delta^{18}\text{O}, ^3\text{H}}$	$C_{\delta^{18}\text{O}, Q}$	$C_{^3\text{H}, Q}$	$C_{\delta^{18}\text{O}, ^3\text{H}, Q}$	$C_{\delta^{18}\text{O}, Q}$	$C_{^3\text{H}, Q}$	$C_{\delta^{18}\text{O}, ^3\text{H}, Q}$	$\Delta TT_{\delta^{18}\text{O}, ^3\text{H}}$ $\Delta F(T < x)_{\delta^{18}\text{O}, ^3\text{H}}$			
Percentiles (yr)	Mean (yr)	11.4	11.0	11.0	17.4 (16.9/21.1)	11.9 (11.5/21.3)	11.2 (9.9/16.8)	15.6 (12.0/19.9)	13.2 (13.2/21.1)	12.8 (11.1/18.6)	0.4	5.5	2.4
	10 th	0.0	0.0	0.0	0.5 (0.0/0.1)	0.5 (0.0/0.1)	0.4 (0.0/0.1)	0.3 (0.0/0.0)	0.3 (0.0/0.0)	0.3 (0.0/0.1)	0.0	0.0	0.0
	25 th	0.4	0.2	0.2	2.1 (0.1/0.4)	1.9 (0.1/1.2)	1.5 (0.1/1.7)	2.1 (0.1/0.2)	1.5 (0.1/0.2)	1.4 (0.2/0.4)	0.2	0.2	0.6
	50 th (median)	3.2	2.4	2.5	9.0 (9.8/15.9)	6.5 (3.6/11.7)	5.7 (4.8/11.6)	8.6 (4.7/10.9)	6.7 (1.6/5.8)	6.6 (5.4/12.3)	0.7	2.5	1.9
	75 th	13.7	12.5	12.5	22.2 (25.1/28.3)	17.6 (17.1/27.7)	16.3 (14.7/25.0)	20.8 (18.0/26.9)	18.8 (14.3/18.0)	17.8 (16.4/26.7)	1.2	4.6	2.0
	90 th	33.4	33.4	32.7	31.3 (32.0/34.0)	29.2 (27.3/33.8)	28.6 (25.2/31.8)	31.1 (28.2/33.1)	30.4 (26.3/28.9)	29.9 (27.1/32.9)	0.0	2.1	0.7
Water fractions (%)	F(T<3 m)*	22	26	26	18 (23/29)	23 (19/38)	21 (15/33)	16 (28/36)	22 (26/43)	23 (20/29)	-5	-5	-6
	F(T<6 m)	27	32	32	21 (25/31)	29 (22/43)	30 (18/36)	27 (30/38)	27 (30/47)	27 (23/32)	-5	-8	-7
	F(T<1 yr)	34	39	39	24 (26/33)	32 (24/44)	35 (19/37)	22 (31/39)	30 (33/49)	29 (25/35)	-5	-8	-8
	F(T<3 yr)	49	53	52	31 (31/37)	39 (31/49)	42 (22/43)	30 (34/45)	37 (40/53)	37 (31/42)	-4	-8	-7
	F(T<5 yr)	57	60	60	38 (33/41)	46 (35/53)	49 (24/51)	38 (38/51)	44 (47/58)	44 (36/48)	-3	-8	-6
	F(T<10 yr)	69	71	71	52 (41/50)	59 (41/62)	62 (46/64)	53 (46/62)	58 (60/68)	58 (46/62)	-2	-7	-5
	F(T<20 yr)	82	83	83	71 (55/65)	77 (52/78)	79 (65/78)	74 (59/78)	76 (75/81)	77 (61/79)	-1	-6	-2

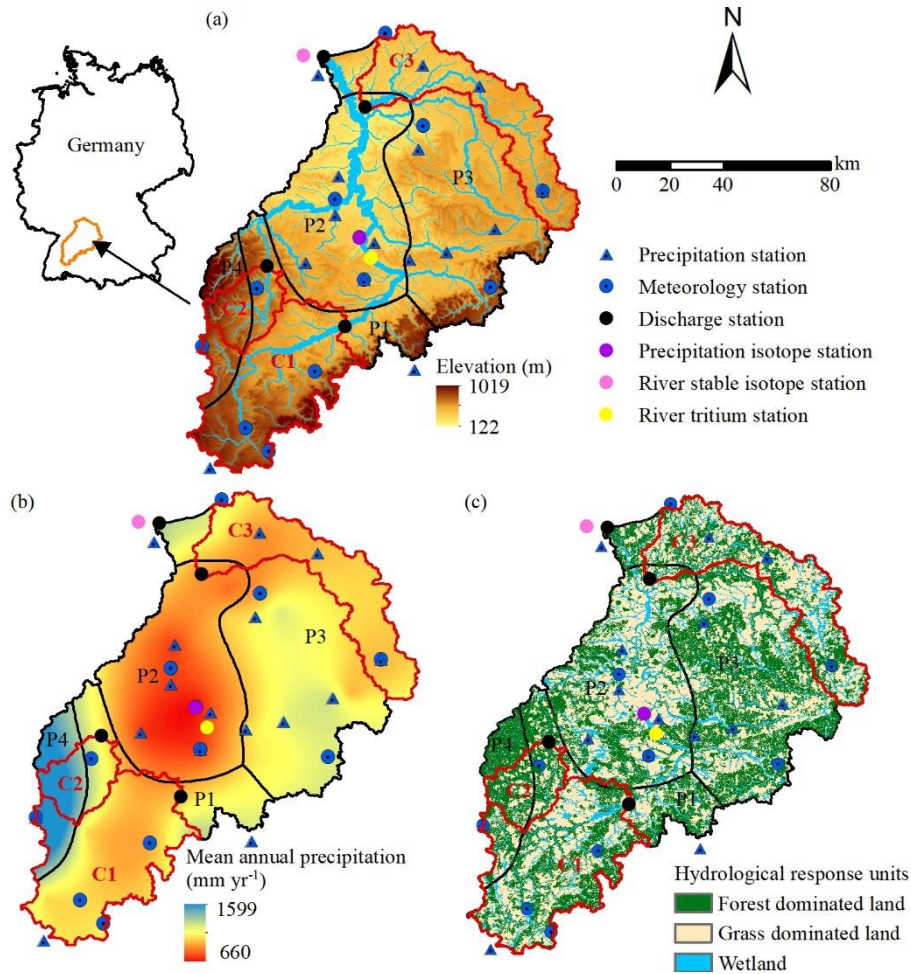


Figure 1. (a) Elevation of the Neckar catchment with discharge and hydro-meteorological stations as well as the water sampling locations used in this study, (b) the spatial distribution of long-term mean annual precipitation in the Neckar catchment and the stratification into four distinct precipitation zones P1 – P4 (black outline), and the red outlines indicate three sub-catchments (C1: Kirchentellinsfurt, C2: Calw, and C3: Untergriesheim) within the Neckar basin, (c) hydrological response units classified according to their land-cover and topographic characteristics.

1200

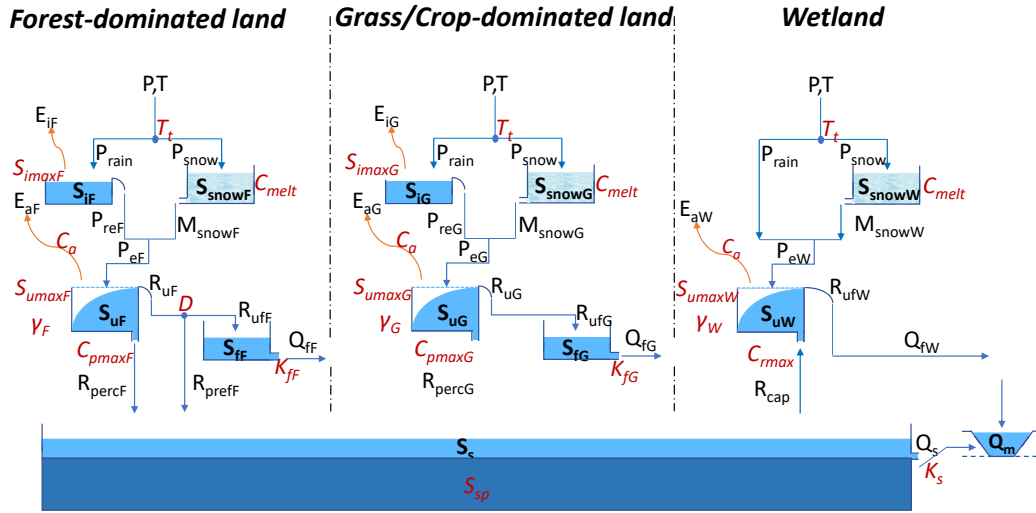


Figure 2. Model structure of the integrated model, discretized into three parallel hydrological response units HRU, i.e. forest, grassland and wetland in each precipitation zone P1 – P4. The light blue boxes indicate the hydrologically active individual storage volumes. The dark blue box indicates the hydrologically passive storage volume $S_{s,p}$. The arrow lines indicate water fluxes and model parameters are shown in red. All symbols are described in Table S4 in the Supplementary Material.

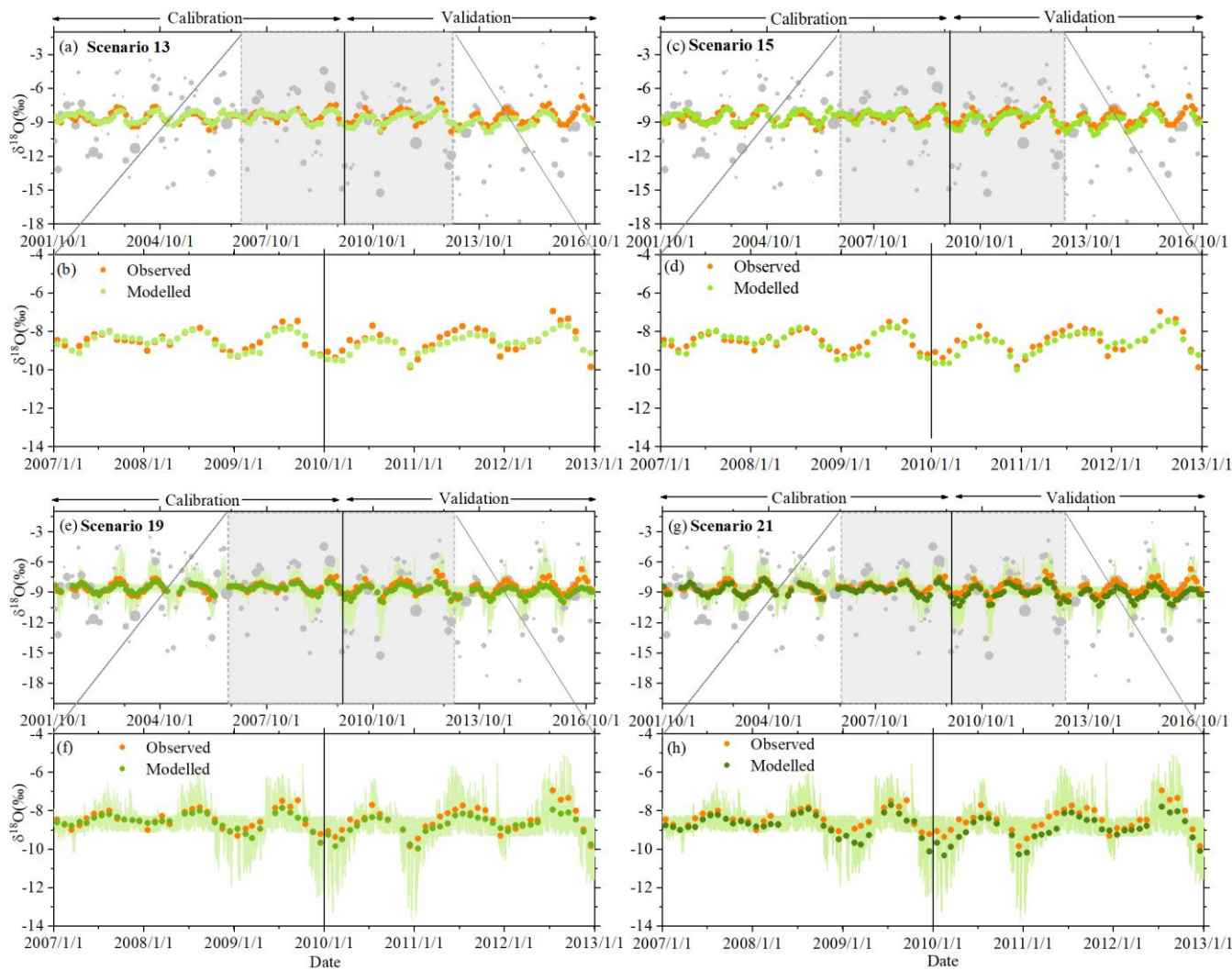


Figure 3 The time series of stream $\delta^{18}\text{O}$ reproduced by models P-SAS (scenarios 13 and 15) and IM-SAS-D (scenarios 19 and 21) based on different calibration strategies. IM-SAS-D model based on simultaneous calibration to $\delta^{18}\text{O}$ and the streamflow signatures, i.e. calibration strategy $C_{\delta^{18}\text{O},Q}$ (scenario 19) and $C_{\delta^{18}\text{O},^3\text{H}_O}$ (scenario 21), for the model calibration and evaluation periods. (a) Observed $\delta^{18}\text{O}$ signals in precipitation (light grey dots; size of dots indicates the precipitation volume) and observed stream $\delta^{18}\text{O}$ signals (orange dots) as well as the most balanced modelled $\delta^{18}\text{O}$ signal in the stream (light green dots) for scenario 13 from calibration strategy $C_{\delta^{18}\text{O}}$, (b) zoom-in of observed and modelled $\delta^{18}\text{O}$ signals in the stream for the 01/01/2007 – 31/12/2012 period for scenario 13, (c) Observed $\delta^{18}\text{O}$ signals in precipitation and in stream same as (a), and the modelled stream $\delta^{18}\text{O}$ signals (relatively darker green dots) for scenario 15 from calibration strategy $C_{\delta^{18}\text{O},^3\text{H}_O}$, (d) zoom-in of observed and modelled $\delta^{18}\text{O}$ signals in the stream for the 01/01/2007 – 31/12/2012 period for scenario 15, (e) Observed $\delta^{18}\text{O}$ signals in precipitation and in stream same as (a), and the modelled stream $\delta^{18}\text{O}$ signals (relatively darker green dots) for scenario 19 and the 5th/95th percentile of all retained pareto optimal solutions obtained from calibration strategy $C_{\delta^{18}\text{O},Q}$ (light green shaded area), (f) zoom-in of observed and modelled $\delta^{18}\text{O}$ signals in the stream for the 01/01/2007 – 31/12/2012 period for scenario 19, (g) Observed $\delta^{18}\text{O}$ signals in precipitation and in stream same as (a), and the modelled stream $\delta^{18}\text{O}$ signals (relatively darker green dots) for scenario 21 and the 5th/95th percentile of all retained pareto optimal solutions obtained from calibration strategy $C_{\delta^{18}\text{O},^3\text{H}_O}$ (light green shaded area), (h) zoom-in of observed and modelled $\delta^{18}\text{O}$ signals in the stream for the 01/01/2007 – 31/12/2012 period for scenario 21.

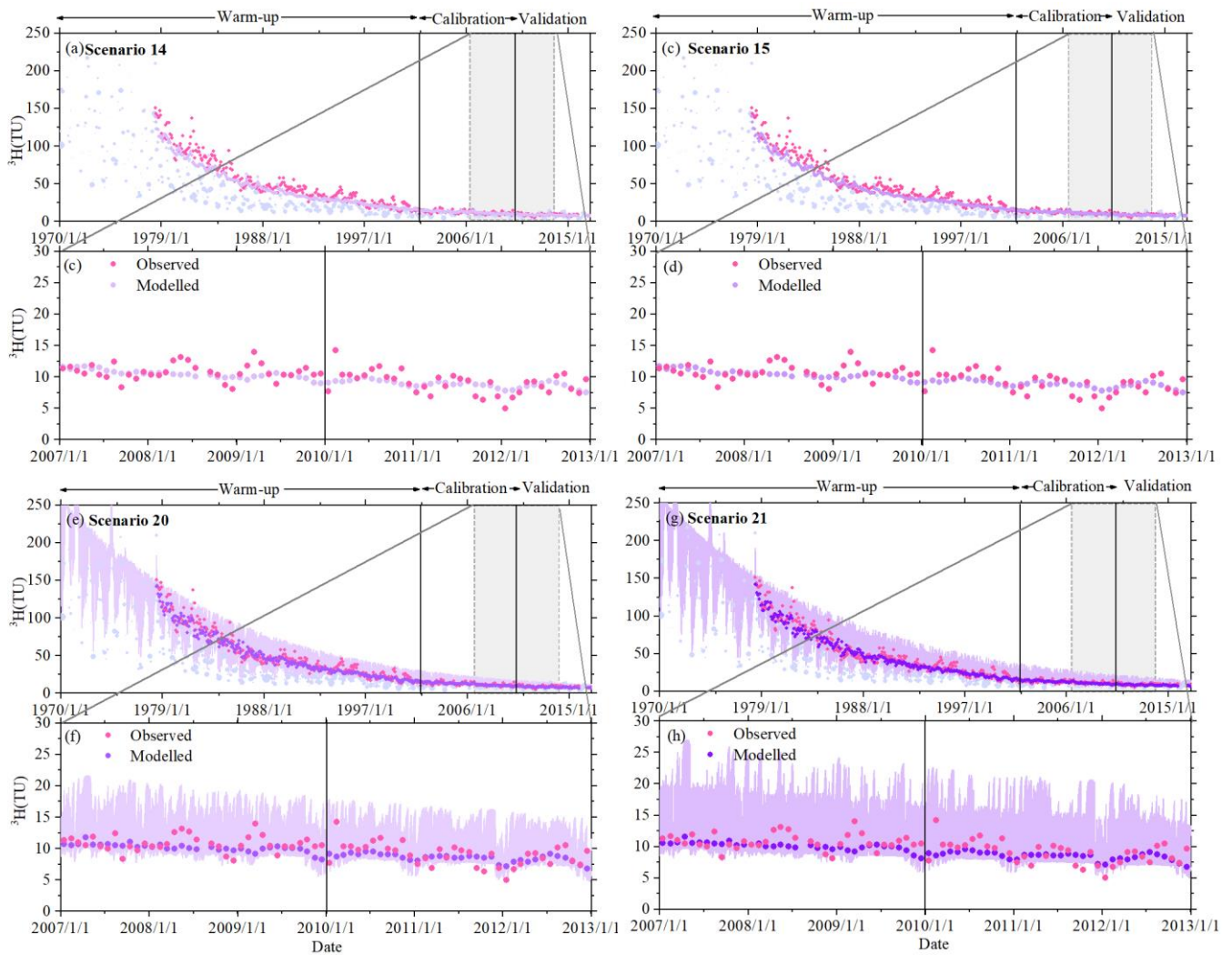


Figure 4. The time series of stream ^3H reproduced by models P-SAS (scenarios 14 and 15) and IM-SAS-D (scenarios 20 and 21) based on different calibration strategies. IM-SAS-D model based on simultaneous calibration to ^3H and the streamflow signatures, i.e. calibration strategy $C_{^3\text{H},\text{O}}$ (scenario 20 and $C_{\delta^{18}\text{O},^3\text{H},\text{O}}$ (scenario 21), for the model calibration and evaluation periods. (a) Observed ^3H signals in precipitation (light blue-purple dots; size of dots indicates the precipitation volume) and observed stream ^3H signals (pink dots) as well as the most balanced modelled ^3H signal in the stream (light purple dots) for scenario 14 from calibration strategy $C_{^3\text{H}}$, (b) zoom-in of observed and modelled ^3H signals in the stream for the 01/01/2007 – 31/12/2012 period for scenario 14, (c) Observed ^3H signals in precipitation and in stream same as (a), and the modelled stream ^3H signals (relatively darker purple dots) for scenario 15 from calibration strategy $C_{\delta^{18}\text{O},^3\text{H}}$, (d) zoom-in of observed and modelled ^3H signals in the stream for the 01/01/2007 – 31/12/2012 period for scenario 15. (e) Observed ^3H signals in precipitation and in stream same as (a), and the modelled stream ^3H signals (relatively darker purple dots) for scenario 20 and the 5th/95th percentile of all retained Pareto optimal solutions obtained from calibration strategy $C_{^3\text{H},\text{O}}$ (light purple shaded area), (f) zoom-in of observed and modelled ^3H signals in the stream for the 01/01/2007 – 31/12/2012 period for scenario 20, (g) Observed ^3H signals in precipitation and in stream same as (a), and the modelled stream ^3H signals (relatively darker green dots) for scenario 21 and the 5th/95th percentile of all retained Pareto optimal solutions obtained from calibration strategy $C_{\delta^{18}\text{O},^3\text{H},\text{O}}$ (light green shaded area), (h) zoom-in of observed and modelled ^3H signals in the stream for the 01/01/2007 – 31/12/2012 period for scenario 21.

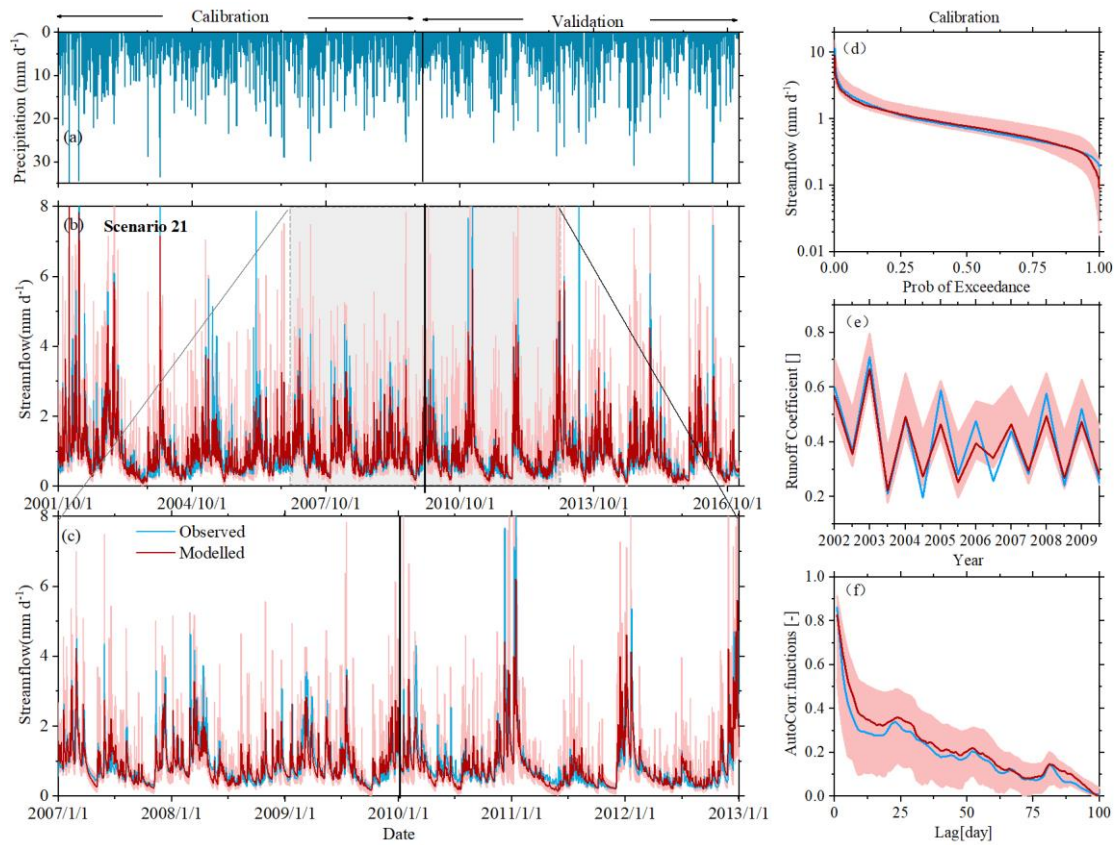


Figure 5. Hydrograph and selected hydrological signatures reproduced by IM-SAS-D, following a simultaneous calibration to the hydrological response, $\delta^{18}\text{O}$ and ^3H ($\text{C}_6^{18}\text{O}_3\text{H}_2\text{O}$; scenario 21). (a) Time series of observed daily precipitation; observed and modelled (b) daily stream flow (Q), where the red line indicates the most balanced solution, i.e., lowest D_E , and the red shaded area the 5th/95th inter-quantile range obtained from all pareto optimal solutions; (c) stream flow zoomed-in to the 01/01/2007 – 31/12/2012 period; (d) flow duration curves (FDC_Q), (e) seasonal runoff coefficients (RC_Q) and (f) autocorrelation functions of stream flow (AC_Q) for the calibration period. Blue lines indicate values based on observed streamflow (Q_o), red lines are values based on modelled stream flow (Q_m) representing the most balanced solutions, i.e., lowest D_E and the red shaded areas show the 5th/95th inter-quantile ranges obtained from all pareto optimal solutions.

1245

1250

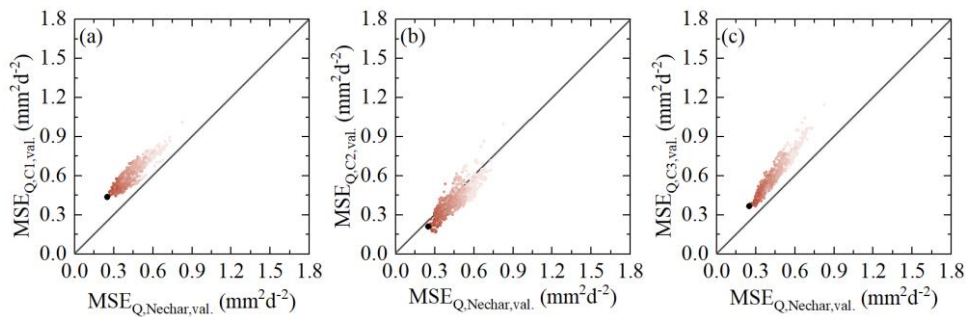


Figure 6. Selected model performances in the 01/01/2010 – 31/12/2016 validation period of the overall Neckar basins against the model performance in uncalibrated sub-catchment (a) Kirchentellinsfurt (C1), (b) Calw (C2) and (c) Untergriesheim (C3) based on Scenario 19. The dots indicate all Pareto-optimal solutions in the multi-objective model performance space. The shades from dark to light indicate the overall model performance based on the Euclidean Distance D_E , with the black solutions representing the overall better solutions (i.e. smaller D_E)

1255

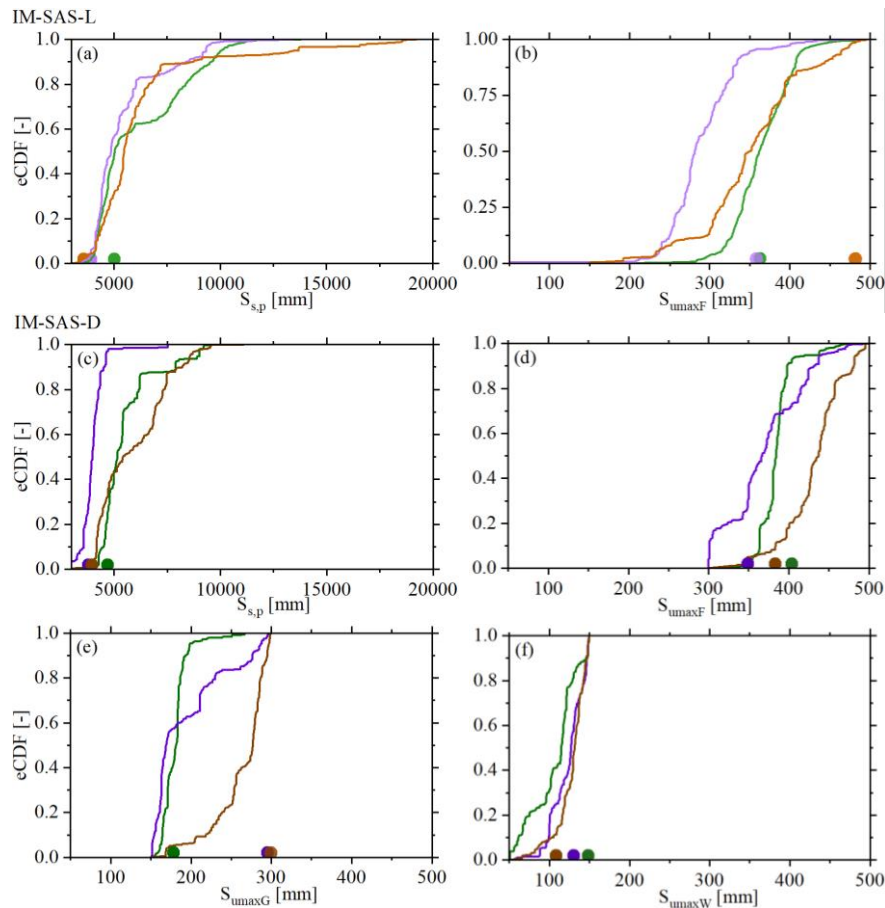
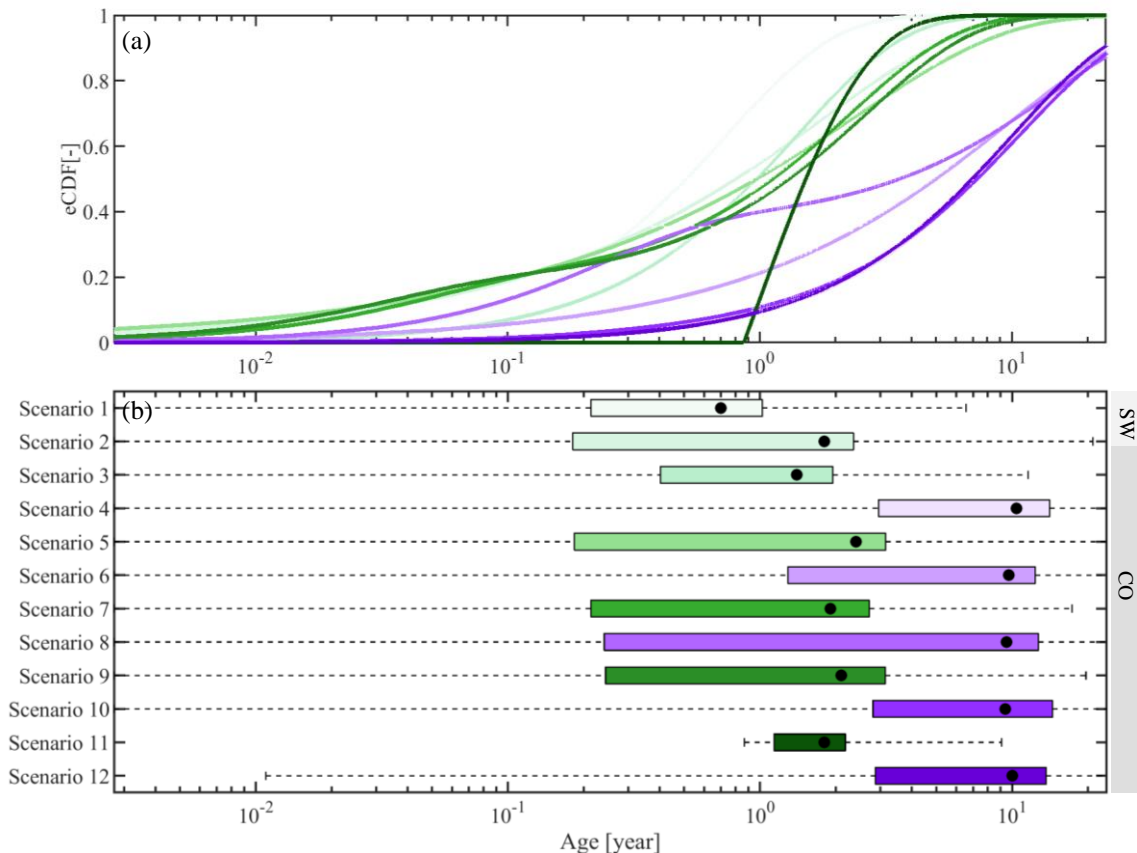


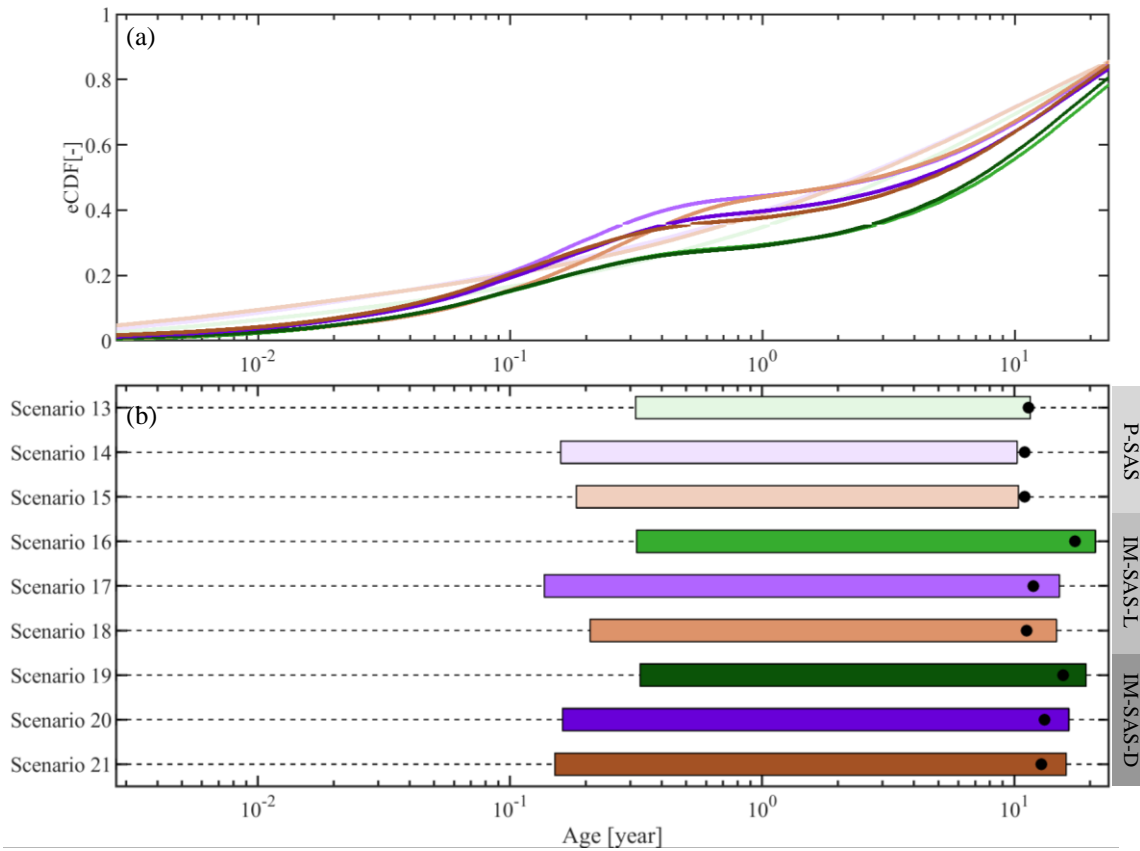
Figure 7 Pareto-optimal distributions of selected parameters of the IM-SAS models (i.e., IM-SAS-L, IM-SAS-D) shown as the associated empirical cumulative distribution functions (lines). Light green shades indicate scenario 16, light purple shades indicate scenario 17 and light brown shades indicate scenario 18 in (a) and (b); relatively darker green shades indicate scenario 19, relatively darker purple shades indicate scenario 20 and relatively darker brown shades indicate scenario 21 in (c) - (f). The dots indicate the parameter values associated with the most balanced solution, i.e. lowest D_E .

1260



1270

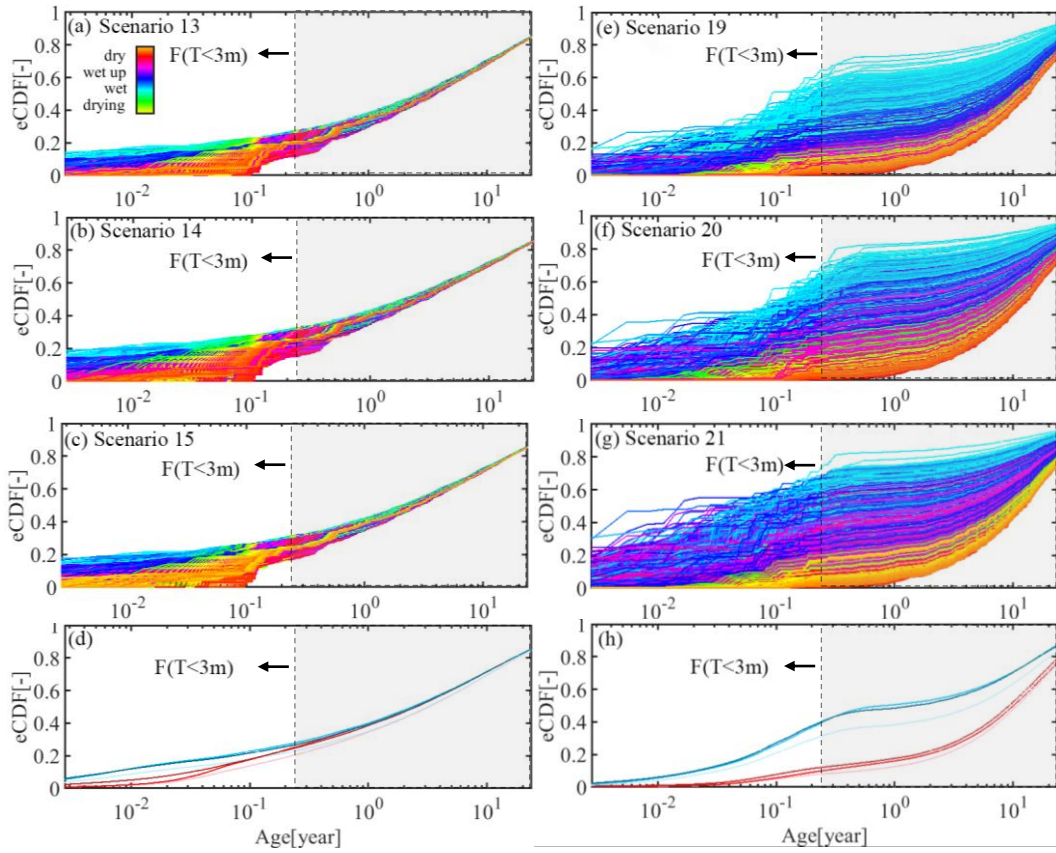
Figure 8. Stream flow TTDs derived from the 12 SW/CO model scenarios with the different associated calibration strategies based on different lumped, time-invariant models. The TTDs represent the best fits of the respective time-invariant TTD. Green shades represent the TTDs inferred from $\delta^{18}\text{O}$ (from lighter to darker for scenarios 1, 2, 3, 5, 7, 9, 11) in (a) and (b); the purple shades represent TTDs inferred from ^3H (from lighter to darker for scenario 4, 6, 8, 10 and 12); the black dots in (b) indicate the mean transit time for each model scenario.



1275

Figure 9. Stream flow TTDs derived from the 9 model scenarios with the different associated calibration strategies of P-SAS (scenarios 13 – 15), IM-SAS-L scenarios 16 – 18) and IM-SAS-D model implementations (scenarios 19 – 21). The TTDs represent the volume weighted average daily TTDs for the modelling period 01/10/2001 – 31/12/2016. Green shades represent the TTDs inferred from $\delta^{18}\text{O}$ (from lighter to darker for scenario 13, 16, 19), the purple shades represent TTDs inferred from ^3H (from lighter to darker for scenario 14, 17, 20), the brown lines represent TTDs inferred from combined $\delta^{18}\text{O}$ and ^3H (brown shades from lighter to darker for scenario 15, 18, 21); the black dots in (b) indicate the mean transit time for each model scenario. Note that the mean transit time was estimated by fitting Gamma distributions to the volume-weighted mean TTDs of each individual scenario.

1280



1285

1290

1295

Figure 10. Daily streamflow (Q) TTDs extracted from the most balanced model solutions of P-SAS (scenarios 13 – 15) based on (a) calibration strategy $C_{\delta^{18}O}$ (scenario 13), (b) calibration strategy C^3_{H} (scenario 14) and (c) calibration strategy $C_{\delta^{18}O,^3H}$ (scenario 15), and the IM-SAS-D implementations (scenarios 19 – 21), based on (a) calibration strategy $C_{\delta^{18}O,Q}$ (scenario 19), (b) calibration strategy $C^3_{H,Q}$ (scenario 20) and (c) calibration strategy $C_{\delta^{18}O,^3H,Q}$ (scenario 21). The line colors represent the transition between dry and wet periods. Panel (d) shows the volume weighted average TTDs for the wet and dry periods respectively for P-SAS model, the light shades represent calibration strategy $C_{\delta^{18}O}$ (scenario 13), the intermediate shades indicate calibration strategy C^3_{H} (scenario 14) and the dark shades are calibration strategy $C_{\delta^{18}O,^3H}$ (scenario 15). Panel (h) shows the volume weighted average TTDs for the wet and dry periods, respectively. The light shades represent calibration strategy $C_{\delta^{18}O,Q}$ (scenario 19), the intermediate shades indicate calibration strategy $C^3_{H,Q}$ (scenario 20) and the dark shades are calibration strategy $C_{\delta^{18}O,^3H,Q}$ (scenario 21). For illustrative purposes, also the fraction of water younger than 3 months $F(T < 3m)$ is indicated.

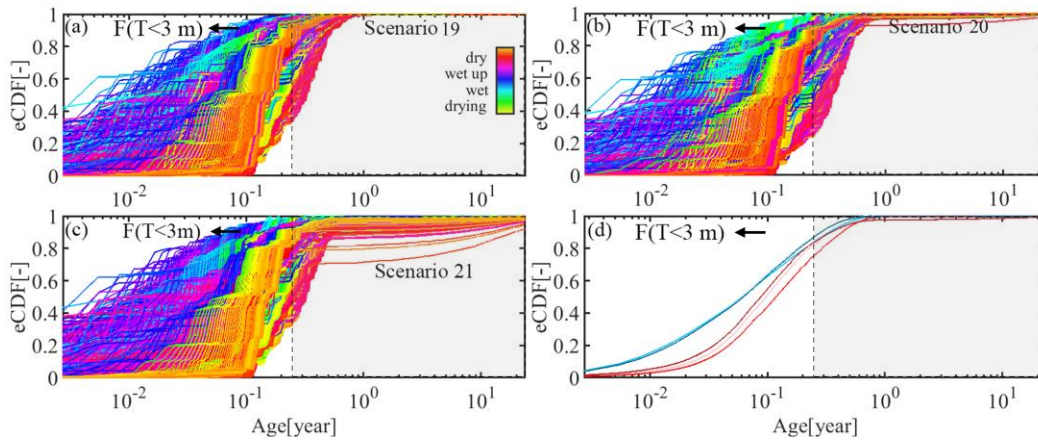


Figure 11. Daily transpiration (E_a) TTDs extracted from the most balanced model solutions of the IM-SAS-D implementations (scenarios 19–21), based on (a) calibration strategy $C_{\delta^{18}O, Q}$ (scenario 19), (b) calibration strategy $C^3_{H, Q}$ (scenario 20) and (c) calibration strategy $C_{\delta^{18}O, ^3H, Q}$ (scenario 21). The line colors represent the transition between dry and wet periods. Panel (d) shows the volume weighted average TTDs for the wet and dry periods, respectively. The light shades represent calibration strategy $C_{\delta^{18}O, Q}$ (scenario 19), the intermediate shades indicate calibration strategy $C^3_{H, Q}$ (scenario 20) and the dark shades are calibration strategy $C_{\delta^{18}O, ^3H, Q}$ (scenario 21). For illustrative purposes, also the fraction of water younger than 3 months $F(T < 3 \text{ m})$ is indicated.

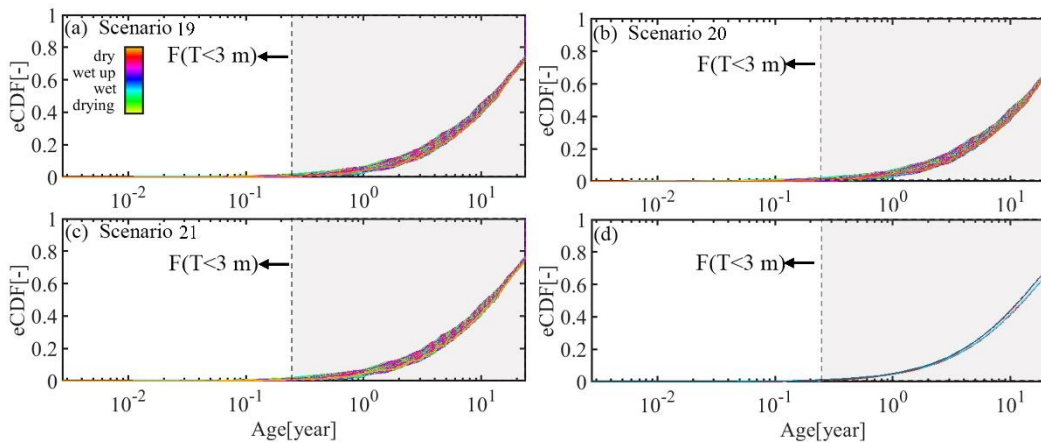


Figure 12. Daily groundwater (S_g) RTDs extracted from the most balanced model solutions of the IM-SAS-D implementations (scenarios 19–21), based on (a) calibration strategy $C_{\delta^{18}O, Q}$ (scenario 19), (b) calibration strategy $C^3_{H, Q}$ (scenario 20) and (c) calibration strategy $C_{\delta^{18}O, ^3H, Q}$ (scenario 21). The line colors represent the transition between dry and wet periods. Panel (d) shows the volume weighted average RTDs for the wet and dry periods, respectively. The light shades represent calibration strategy $C_{\delta^{18}O, Q}$ (scenario 19), the intermediate shades indicate calibration strategy $C^3_{H, Q}$ (scenario 20) and the dark shades are calibration strategy $C_{\delta^{18}O, ^3H, Q}$ (scenario 21). For illustrative purposes, also the fraction of water younger than 3 months $F(T < 3 \text{ m})$ is indicated.